



# Politecnico di Bari

Repository Istituzionale dei Prodotti della Ricerca del Politecnico di Bari

Finite element analysis of heat transfer in double U-tube borehole heat exchangers

This is a PhD Thesis

*Original Citation:*

Finite element analysis of heat transfer in double U-tube borehole heat exchangers / Jahanbin, Aminhossein. -  
ELETTRONICO. - (2018). [10.6092/unibo/amsdottorato/7844]

*Availability:*

This version is available at <http://hdl.handle.net/11589/268732> since: 2024-04-15

*Published version*

<http://hdl.handle.net/11589/268732>  
DOI: 10.6092/unibo/amsdottorato/7844

*Terms of use:*

Altro tipo di accesso

(Article begins on next page)

**ALMA MATER STUDIORUM – UNIVERSITÀ DI BOLOGNA**

**SCUOLA DI INGEGNERIA E ARCHITETTURA**

**DOTTORATO DI RICERCA IN**

**MECCANICA E SCIENZE AVANZATE DELL'INGEGNERIA**

**Ciclo XXX**

**Settore Concorsuale di afferenza: 09/C2**

**Settore Scientifico disciplinare: ING-IND/10**

**TITOLO TESI:**

**Finite element analysis of heat transfer in  
double U-tube borehole heat exchangers**

**Presentata da: Aminhossein Jahanbin**

**Coordinatore Dottorato:**

**Prof. Marco Carricato**

**Relatore:**

**Prof. Enzo Zanchini**

**Esame finale anno 2018**



# *Abstract*

---

The present Ph.D. dissertation deals with the finite element analysis of the heat transfer processes in double U-tube Borehole Heat Exchangers, called BHEs. As the main outline of this study, it can be pointed out to the analysis of the working fluid temperature distribution, proposing correlations to determine the mean fluid temperature, and the analysis of the thermal resistance and effects of the temperature distribution on it, for double U-tube BHEs. In the evaluation of thermal response tests (TRTs), in the design of the BHE fields, and in the dynamic simulation of ground-coupled heat pumps (GCHPs), the mean temperature  $T_m$  of the working fluid in a BHE, is usually approximated by the arithmetic mean of inlet and outlet temperatures. In TRTs, this approximation causes an overestimation of the thermal resistance of the heat exchanger. In the dynamic simulation of GCHPs, this approximation introduces an error in the evaluation of the outlet temperature from the ground heat exchangers. In the present thesis, by means of 3D finite element simulations, firstly, the analysis of the fluid temperature distribution is carried out, then, correlations are proposed to determine the mean fluid temperature, for double U-tube BHEs. Tables of a dimensionless coefficient are provided that allows an immediate evaluation of  $T_m$  in any working condition, with reference to double U-BHEs with a typical geometry. These tables allow a more accurate estimation of the borehole thermal resistance by TRTs and a more accurate evaluation of the outlet temperature in dynamic simulations of GCHP systems. Criteria for the extension of the results to other geometries are also provided. In addition, the effects of the surface temperature distribution on the thermal resistance of a double U-tube BHE are investigated. It is shown that the thermal resistance of a BHE cross section (2D) is not influenced by the bulk-temperature difference between pairs of tubes, but is influenced by the thermal conductivity of the ground when the shank spacing is high. Then it is shown that, if the real mean values of the bulk fluid temperature and of the BHE external surface are considered, the 3D thermal resistance of the BHE coincides with the thermal resistance of a BHE cross section, provided that the latter is invariant along the BHE. Eventually, the difference between the BHE thermal resistance (2D or 3D) and the effective BHE thermal resistance, defined by replacing the real mean temperature of the fluid with the average of inlet and outlet temperatures, is evaluated in relevant cases.



# *Sommario*

---

La presente Tesi di Dottorato tratta dell'analisi agli elementi finite dei processi di trasmissione del calore in scambiatori verticali con il terreno detti "Borehole Heat Exchangers", BHEs, con riferimento a BHEs a doppio tubo a U. Lo studio è incentrato sull'analisi della distribuzione della temperatura del fluido operatore e degli effetti che questa distribuzione ha sulla resistenza termica dello scambiatore. I risultati principali sono costituiti da correlazioni che consentono di determinare la temperatura media del fluido nello scambiatore e dallo studio degli effetti della distribuzione di temperatura sulla resistenza termica dello scambiatore. Nella valutazione di Test di Risposta Termica (TRTs), per il progetto di campi di BHEs, e nella simulazione dinamica di pompe di calore accoppiate al terreno (Ground-Coupled Heat Pumps, GCHPs), la temperatura media  $T_m$  del fluido operatore in un BHE è abitualmente approssimata dalla media aritmetica della temperatura in ingresso e di quella in uscita del fluido. Nei TRT, questa approssimazione causa una sovrastima della resistenza termica dello scambiatore. Nella simulazione dinamica delle GCHPs, questa approssimazione introduce un errore nel calcolo della temperatura in uscita dallo scambiatore di calore. In questa Tesi, la distribuzione di temperatura del fluido nello scambiatore viene studiata mediante accurate simulazioni 3D agli elementi finiti, quindi vengono proposte semplici correlazioni adimensionali che consentono di determinare la temperatura media  $T_m$  del fluido in qualsiasi condizione operativa, date le temperature in entrata e in uscita e la portata in volume del fluido e la conducibilità termica della malta sigillante. Le correlazioni si riferiscono a BHEs a doppio tubo a U con una geometria tipica. Sono forniti anche criteri per l'estensione dei risultati ad altre geometrie. Vengono inoltre analizzati gli effetti della distribuzione di temperatura superficiale dello scambiatore sulla resistenza termica dello stesso. Si mostra che la resistenza termica 2D di una sezione trasversale non è influenzata dalla differenza della temperatura di bulk fra coppie di tubi, ma è influenzata dalla conducibilità termica del terreno circostante se l'interasse fra i tubi è elevato. Si mostra anche che, se vengono considerati i veri valori della temperatura media di bulk del fluido e della temperatura alla superficie esterna dello scambiatore, la resistenza termica 3D dello scambiatore coincide con quella 2D di una sezione trasversale, a condizione che questa possa essere considerata invariante lungo lo scambiatore. Infine, viene calcolata in alcuni casi rilevanti la differenza fra la vera resistenza termica dello scambiatore (2D o 3D) e la resistenza termica detta "effettiva", che si ottiene approssimando la temperatura media di bulk del fluido con la media aritmetica delle temperature in entrata e in uscita.



I would like to express my sincere gratitude to my supervisor Professor Enzo Zanchini for his support and priceless guidance throughout my doctoral course.





*A mia madre e mio padre*



# *Contents*

---

<b>Abstract</b>	I
<b>Contents</b>	IX
<b>List of figures</b>	XI
<b>List of tables</b>	XV
<b>Nomenclature</b>	XVII
<b>1 Preface</b>	1
<b>2 An introduction on Ground-Coupled Heat Pump (GCHP) systems</b>	7
2.1 Ground-Source Heat Pumps (GSHPs) and their categories	11
2.2 Ground-Coupled Heat Pumps (GCHPs)	13
2.3 BHE field design methods	15
2.3.1 Analytical models	16
2.3.2 Numerical models	22
2.3.3 Analytical models vs. numerical models	24
2.4 Fluid-to-ground thermal resistance	24
2.5 Hybrid GCHP systems	26
<b>3 Heat transfer analysis of U-tube BHEs</b>	29
3.1 Heat transfer models for the BHE thermal resistance	34
3.2 Estimation of the BHE thermal resistance	40
3.3 Convective heat transfer inside tubes	42
<b>4 Numerical method</b>	49
4.1 Finite element analysis	51
4.2 Numerical model	53
4.3 Model validation & grid independence	61

<b>5</b>	<b>Analysis of the fluid temperature distribution</b>	65
<b>6</b>	<b>Correlations to determine the mean fluid temperature</b>	75
6.1	Model validation	80
6.2	Results for quasi-stationary regime	83
6.3	Results for the first two hours	88
6.4	Possible applications	91
<b>7</b>	<b>Effects of the temperature distribution on the thermal resistance</b>	95
7.1	Thermal resistance of the cross section of a double U-tube BHE	99
7.2	Relations between $R_{b,eff}$ , $R_{b,3D}$ and $R_{b,2D}$ for double U-tube BHEs	104
7.2.1	A theorem on the relation between $R_{b,3D}$ and $R_{b,2D}$	105
7.2.2	Results of computational analysis	106
<b>8</b>	<b>Conclusions &amp; prospective</b>	113
	<b>References</b>	119
	<b>Appendix - List of publications</b>	127

## List of figures

---

2.1	U.S. annual primary energy consumption by source from 1950 to 2015, data according to EIA [1].	10
2.2	Europe final energy consumption percentage by sector in 2015, data according to Eurostat [5].	11
2.3	Iceland's Nesjavellir geothermal power station. Geothermal plants account for more than 25 percent of the electricity produced in Iceland. Photo: Gretar Ívarsson [8].	12
2.4	Schematic of a GSHP system in heating/cooling mode, reported by EPA [12].	13
2.5	The installed capacity and annual utilization of geothermal heat pumps from 1995 to 2015 [15].	14
2.6	A vertical closed-loop GCHP system [18].	15
2.7	Fourier / $G$ -factor graph for ground thermal resistance [9].	20
2.8	Earth Energy Designer - EED [40].	22
2.9	A BHE cross section.	25
2.10	Thermal resistive network for a single U-tube BHE.	26
2.11	Schematic diagram of a HGCHP system with solar collector, presented in reference [44].	27
3.1	Temperature distribution in a double U-tube BHE and the surrounding ground.	33
3.2	Cross section of a double U-tube BHE.	34
4.1	COMSOL Multiphysics desktop environment.	53
4.2	Sketch of the BHE cross section considered.	54
4.3	3D mesh of the BHE and the surrounding ground.	56
4.4	Mesh of the BHE for a 2D simulation case.	60
4.5	3D mesh of the BHE and the surrounding ground.	60
4.6	Convergence plot for a time-dependent solver.	61
4.7	Plot of fluid temperature distribution along the vertical coordinate $z$ , compared with that yielded by the method of Zeng et al. [70], for $k_{gr} = 1.6 \text{ W/(mK)}$ and volume flow rate 12 L/min.	62
4.8	Mesh independence check for modified code (Code II), plots of $T_{ave} - T_m$ versus time.	63
5.1	Illustration of the BHE cross section.	68
5.2	Power per unit length extracted from the ground: water with inlet temperature 4 °C.	69
5.3	Power per unit length extracted from the ground: water-glycol with inlet temperature -2 °C.	70
5.4	$T_m$ , $T_{ave}$ and $T_{m, MP}$ versus time for the volume flow rate 12 L/min: water with inlet temp. 4 °C.	71

5.5	$T_m$ , $T_{ave}$ and $T_{m, MP}$ versus time for the volume flow rate 12 L/min: water-glycol with inlet temperature $-2\text{ }^\circ\text{C}$ .	72
5.6	Fluid temperature distribution versus height $z$ (m) for the volume flow rate 24 L/min: water with inlet temperature $4\text{ }^\circ\text{C}$ .	72
6.1	Enthalpy balance of the fluid heating tank.	79
6.2	Time evolution of $T_{ave} - T_m$ obtained numerically and through the analytical model by Zeng et al. [70], for $k_{gt} = 1.6\text{ W/(mK)}$ , $k_g = 1.8\text{ W/(mK)}$ , flow rate 12 L/min.	81
6.3	Time evolution of $T_{ave} - T_m$ obtained numerically and through the analytical model by Zeng et al. [70], for $k_{gt} = 1.6\text{ W/(mK)}$ , $k_g = 1.8\text{ W/(mK)}$ , flow rate 24 L/min.	82
6.4	Comparison between the experimental time evolution of $T_{in\_exp}$ and that obtained through equation (6.5), denoted by $T_{in\_num}$ , for a TRT performed at Fiesso d'Artico (Venice) [96].	83
6.5	Time evolution of $\Omega$ for $k_{gt} = 1.6\text{ W/(mK)}$ , $k_g = 1.8\text{ W/(mK)}$ , flow rates 12 and 24 L/min.	84
6.6	Linear interpolations of $T_{ave} - T_m$ as a function of $(T_{in} - T_{out})/\dot{V}$ , for $k_{gt} = 0.9, 1.2, 1.6\text{ W/(mK)}$ .	85
6.7	Effects of different values of $k_g$ , namely 1.4 and 2.2 W/(mK), for $k_{gt} = 0.9\text{ W/(mK)}$ .	86
6.8	Effects of different values of $k_g$ , namely 1.4 and 2.2 W/(mK), for $k_{gt} = 1.6\text{ W/(mK)}$ .	86
6.9	Effects of different values of the BHE diameter, for $k_{gt} = 1.2\text{ W/(mK)}$ and $k_g = 1.8\text{ W/(mK)}$ .	87
6.10	Effects of different working conditions, for $k_{gt} = 1.6\text{ W/(mK)}$ and $k_g = 1.8\text{ W/(mK)}$ .	87
6.11	Plots of $\varphi/\varphi_\infty$ versus $t^*$ , for $k_{gt} = 0.9$ and $k_{gt} = 1.6\text{ W/(mK)}$ , with flow rate 12 L/min, in the range $1/120 \leq t^* \leq 0.6$ .	89
6.12	Plots of $\varphi/\varphi_\infty$ versus $t^*$ , for $k_{gt} = 0.9$ and $k_{gt} = 1.6\text{ W/(mK)}$ , with flow rate 18 L/min, in the range $1/120 \leq t^* \leq 0.6$ .	89
6.13	Plots of $\varphi_{mean1}/\varphi_\infty$ versus $\dot{V}/\dot{V}_0$ , for $k_{gt} = 0.9, 1.2$ and $1.6\text{ W/(mK)}$ .	90
6.14	Plots of $\varphi/\varphi_\infty$ versus $t^*$ for TRTs with $k_{gt} = 1.6$ and $k_g = 1.8\text{ W/(mK)}$ : flow rate 12 L/min, power 50 W/m, $8/120 \leq t^* \leq 1$ ; flow rate 24 L/min, power 80 W/m, $4/120 \leq t^* \leq 1$ .	91
7.1	Illustration of the definition of thermal resistance: the lateral surfaces are tangent to the heat flux density vector $\mathbf{q}$ .	99
7.2	Cross section of the BHE considered, with shank spacing 85 mm (left) and 120 mm (right).	100

7.3	Temperature distribution on the BHE surface versus the angular distance from the upper point of figure 7.2, with $d = 85$ mm and $d = 120$ mm, for $k_{gt} = 0.9$ W/(mK) and $k_g = 1.4$ W/(mK), scheme 4. ....	104
7.4	Plot of $T_f$ versus the vertical coordinate $z$ , compared with that yielded by the method of Zeng et al. [70], $T_{f,z}$ , for $k_{gt} = 1.6$ W/(mK) and volume flow rate 12 L/min. ....	106
7.5	Plot of $T_{f,in} - T_{f,out}$ versus time, compared with that yielded by the method of Zeng et al. [70], $(T_{f,in} - T_{f,out})_Z$ , for $k_{gt} = 0.9$ W/(mK) and volume flow rate 12 L/min. ....	107
7.6	Plot of $T_{f,in} - T_{f,out}$ versus time, compared with that yielded by the method of Zeng et al. [70], $(T_{f,in} - T_{f,out})_Z$ , for $k_{gt} = 0.9$ W/(mK) and volume flow rate 24 L/min. ....	108
7.7	Plot of $T_{f,in} - T_{f,out}$ versus time, compared with that yielded by the method of Zeng et al. [70], $(T_{f,in} - T_{f,out})_Z$ , for $k_{gt} = 1.6$ W/(mK) and volume flow rate 12 L/min. ....	109
7.8	Plot of $T_{f,in} - T_{f,out}$ versus time, compared with that yielded by the method of Zeng et al. [70], $(T_{f,in} - T_{f,out})_Z$ , for $k_{gt} = 1.6$ W/(mK) and volume flow rate 24 L/min. ....	109
7.9	Plots of $R_{b,eff}$ and of $R_{b,3D}$ versus time, compared with the steady-state value $(R_{b,eff})_Z$ yielded by the method of Zeng et al. [70], for $k_{gt} = 0.9$ W/(mK) and volume flow rate 12 L/min. ....	110
7.10	Plots of $R_{b,eff}$ and of $R_{b,3D}$ versus time, compared with the steady-state value $(R_{b,eff})_Z$ yielded by the method of Zeng et al. [70], for $k_{gt} = 1.6$ W/(mK) and volume flow rate 12 L/min. ....	111





## List of tables

---

3.1	Shape factors for three different patterns of the shank spacing [66]. . . . .	35
3.2	Thermophysical properties and fluid flow characteristics in a simulation performed in the present study. . . . .	46
4.1	The thermophysical properties adopted in Code I, taken from reference [91]. . . . .	56
4.2	Values of water thermophysical properties and flow characteristics [91]. . . . .	57
4.3	Mesh independence check for the first code employed (Code I). . . . .	62
4.4	Mesh independence check for modified code (Code II). . . . .	63
5.1	Values of $T_{out}$ , $T_m$ , $T_{ave}$ , $T_m - T_{ave}$ and $(T_m - T_{ave})_{MP}$ for water, with $T_{in} = 4$ °C. . . . .	70
5.2	Values of $T_{out}$ , $T_m$ , $T_{ave}$ , $T_m - T_{ave}$ and $(T_m - T_{ave})_{MP}$ for water-glycol, with $T_{in} = -2$ °C. . . . .	71
6.1	Values of $\varphi_\infty$ and of the coefficients $a$ and $b$ of equation (6.16). . . . .	88
6.2	Values of $\varphi_{mean1}/\varphi_\infty$ as a function of $k_{gt}$ and of $\dot{V}/\dot{V}_0$ . . . . .	90
7.1	Values of the 2D thermal resistance for shank spacing 85 mm (figure 7.1, left), obtained by different calculation schemes. . . . .	102
7.2	Values of the 2D thermal resistance for shank spacing 120 mm (figure 7.1, right), obtained by schemes 1, 3, 5 and equation (7.8). . . . .	103
7.3	Values of $T_{f,in} - T_{f,out}$ after 100 hours of operation, compared with those yielded by the method of Zeng et al. [70]. . . . .	108
7.4	Values of $(R_{b,eff})_Z$ , asymptotic values of $R_{b,eff}$ and $R_{b,3D}$ , and steady values of $R_{b,2D}$ . . . . .	111
7.5	Percent difference between $(R_{b,eff})_Z$ and $R_{b,eff}$ , $R_{b,eff}$ and $R_{b,3D}$ , $R_{b,3D}$ and $R_{b,2D}$ . . . . .	111



## *Nomenclature*

---

$a, b$	dimensionless coefficients
$A$	pipe cross section area ( $\text{m}^2$ )
$C_w$	heat capacity at constant pressure of a fluid tank ( $\text{J K}^{-1}$ )
$c_p$	specific heat capacity at constant pressure ( $\text{J kg}^{-1} \text{K}^{-1}$ )
$d$	distance between centers of opposite tubes (shank spacing) (m)
$D$	diameter (m)
$\text{erfc}$	complementary error function
$f$	dimensionless parameter
$fr$	friction factor
$F_{sc}$	short circuiting heat loss factor
$Fo$	Fourier number
$g$	<i>g-function</i>
$G$	<i>G factor</i>
$\bar{g}$	gravity ( $\text{m s}^{-2}$ )
$Gr$	Grashof number
$h$	heat transfer coefficient ( $\text{W m}^{-2} \text{K}^{-1}$ )
$J_n$	Bessel function of first kind with order $n$
$k$	thermal conductivity ( $\text{W m}^{-1} \text{K}^{-1}$ )
$\tilde{k}$	$= k/100$ , reduced thermal conductivity ( $\text{W m}^{-1} \text{K}^{-1}$ )
$L$	length (m)
$\dot{m}$	mass flow rate ( $\text{kg s}^{-1}$ )
$n$	number of pipes
$Nu$	Nusselt number
$p$	real coefficient
$PLF$	part-load factor
$Pr$	Prandtl number
$\mathbf{q}$	flux density vector (W)
$q$	thermal load / heat flux (W)

$q_l$	heat flux per unit length ( $\text{W m}^{-1}$ )
$q_a$	heat flux per unit area ( $\text{W m}^{-2}$ )
$Q$	heat source/sink (W)
$r$	radial coordinate, radius (m)
$R$	BHE thermal resistance ( $\text{m K W}^{-1}$ )
$R_{b,2D}$	thermal resistance of a BHE cross section ( $\text{m K W}^{-1}$ )
$R_{b,3D}$	3D BHE thermal resistance ( $\text{m K W}^{-1}$ )
$R_{b,eff}$	effective BHE thermal resistance ( $\text{m K W}^{-1}$ )
$R_{11}$	thermal resistances between the fluid and the BHE external surface ( $\text{m K W}^{-1}$ )
$R_{12}$	thermal resistances between two adjoining tubes ( $\text{m K W}^{-1}$ )
$R_{13}$	thermal resistances between two opposite tubes ( $\text{m K W}^{-1}$ )
$Re$	Reynolds number
$S_1, S_2$	Boundary surfaces ( $\text{m}^2$ )
$t$	time (s)
$T$	temperature (K)
$\mathbf{u}$	velocity field ( $\text{m s}^{-1}$ )
$u$	velocity ( $\text{m s}^{-1}$ )
$\tilde{u}$	$= u/10$ , reduced fluid velocity ( $\text{m s}^{-1}$ )
$V$	volume ( $\text{m}^3$ )
$\dot{V}$	volume flow rate ( $\text{m}^3 \text{s}^{-1}$ )
$W$	system power input (W)
$x, y$	horizontal coordinates (m)
$Y_n$	Bessel function of second kind with order $n$
$z$	vertical coordinate (m)
$\tilde{z}$	$= z/10$ , reduced vertical coordinate (m)
$Z$	$= z/L$ , dimensionless vertical coordinate

### ***Greek symbols***

$\alpha$	thermal diffusivity ( $\text{m}^2 \text{s}^{-1}$ )
$\beta$	thermal expansion coefficient ( $\text{K}^{-1}$ )

$\Theta$	dimensionless fluid temperature
$\lambda$	non-dimensional geometrical parameter
$\mu$	dynamic viscosity (Pa s)
$\nu$	kinematic viscosity ( $\text{m}^2 \text{s}^{-1}$ )
$\rho$	density ( $\text{kg m}^{-3}$ )
$(\rho c)$	specific heat capacity per unit volume ( $\text{J m}^{-3} \text{K}^{-1}$ )
$\sigma$	dimensionless parameter
$\Sigma_1, \Sigma_{12}$	dimensionless parameters
$\varphi$	dimensionless parameter
$\Omega$	dimensionless parameter

### ***Subscripts / Superscripts***

*	dimensionless quantity
0	reference value
12	of volume flow rate 12 L/min
16	of volume flow rate 16 L/min
24	of volume flow rate 24 L/min
$\infty$	quasi-stationary regime / asymptotic value
<i>anl</i>	annual
<i>ave</i>	average
<i>b</i>	of BHE
<i>c</i>	cooling
<i>cond</i>	conductive heat transfer
<i>conv</i>	convective heat transfer
<i>d</i>	of fluid going down
<i>Darcy</i>	refers to Darcy friction factor
<i>des</i>	refers to building design
<i>dly</i>	daily
<i>e</i>	refers to external radius/diameter of pipe
<i>eff</i>	effective

<i>exp</i>	experimental
<i>f</i>	of fluid
<i>g</i>	of ground
<i>g<sub>0</sub></i>	refers to undisturbed ground
<i>gt</i>	of grout
<i>h</i>	heating
<i>hyd</i>	hydraulic
<i>i</i>	refers to internal radius/diameter of pipe
<i>i-th</i>	<i>i</i> <sup>th</sup>
<i>in</i>	refers to inlet
<i>l</i>	refers to laminar flow regime
<i>lc</i>	refers to laminar flow at $Re=2100$
<i>m</i>	mean value
<i>mean1</i>	mean value during the first hour
<i>mly</i>	monthly
MP	obtained by the method of Marcotte and Pasquier [66]
<i>num</i>	numerical
<i>out</i>	refers to outlet
<i>p</i>	of pipe, of polyethylene
<i>pen</i>	refers to temperature penalty for interference of adjacent bores
<i>pf</i>	at the surface between pipe and fluid
<i>ref</i>	reference
<i>s</i>	of BHE external surface
<i>t</i>	refers to turbulent flow regime
<i>tot</i>	total value
<i>tr</i>	refers to transient flow regime
<i>th</i>	thermal
<i>u</i>	of fluid going up
<u>Z</u>	obtained by the method of Zeng et al. [70]

# *Chapter 1*

---

## *Preface*





1

*Preface*

---

Adoption of renewable energy sources, and particularly geothermal energy, is an optimal way to shift from fossil-based development to sustainable development. Ground-Source Heat Pump (GSHP) systems are becoming increasingly a rather widely used technology for building heating, cooling, and also for Domestic Hot Water (DHW) production while incurring low maintenance cost. Many reports have shown that GSHP systems are more economically advantageous and eco-friendly than the traditional heating systems. In particular, Ground-Coupled Heat Pumps (GCHPs) appear as the most promising kind of GSHPs for the future developments, due to their applicability and possibility of installation in almost every ground. The most diffuse GCHP systems utilize vertical ground heat exchangers, called Borehole Heat Exchangers (BHEs). A vertical BHE is typically composed of pipes in high-density polyethylene, inserted in a drilled hole which is sealed with grouting materials. The pipe configurations within the borehole may be a single U-tube, double U-tube or coaxial arrangement. The length of the BHE is usually between 50 and 150 m, and the most common diameter is about 15 cm. The cases under study in this thesis are double U-tube BHEs commonly employed in Northern Italy.

The design of a BHE field requires the knowledge of the undisturbed ground temperature, of the thermal conductivity and thermal diffusivity of the ground, as well as of the thermal resistance per unit length of the BHE. These parameters can be determined through a Thermal Response Test (TRT) which is performed by a procedure recommended by ASHRAE (the American Society of Heating, Refrigerating and Air-conditioning Engineers) and usually evaluated by the infinite line-source approximation model. In this evaluation method, the mean fluid temperature is approximated by the arithmetic mean of inlet and outlet temperatures, that we call it average temperature. Some authors pointed out that, on account of the thermal short-circuiting between the descending and the ascending flow, a significant difference between the real mean fluid

temperature and that obtained by average of inlet and outlet temperatures can occur. This error yields an overestimation of the BHE thermal resistance that is determined by the infinite line-source evaluation of a TRT. Hence, a correct estimation of the mean fluid temperature plays an important role in the evaluation of the TRT.

The hourly simulation of the GCHP systems is another technical problem in which the knowledge of the relation between inlet, outlet and mean fluid temperature is useful. In the dynamic simulation of GCHPs, an error in the estimation of the mean fluid temperature yields an error in the evaluation of the outlet temperature from ground heat exchangers, and as a consequence, of the heat pump efficiency. Therefore, precise correlations to evaluate the mean fluid temperature would allow a more accurate estimation of the BHE thermal resistance by a TRT and of the outlet fluid temperature in the dynamic simulation of GCHP systems.

The scope of this study is to analyze the thermal characteristics of double U-tube vertical ground heat exchangers by means of finite element simulations. In particular, the main objectives of this thesis can be classified as:

- Analysis of the fluid temperature distribution over the length of tubes
- Proposing correlations to determine the mean fluid temperature
- Evaluation of the effects of the temperature distribution on the BHE thermal resistance

A brief description of the chapters is presented in the following.

After preface, the second chapter of this thesis presents an introduction on Ground-Coupled Heat Pump (GCHP) systems. A review on employing the renewable energy sources, particularly geothermal energy, is carried out and the Ground-Source Heat Pump (GSHP) systems and their categories are studied. In addition, a classification of the various methods for BHE field design is provided and differences between these methods are stressed, where it is relevant.

Heat transfer processes in U-tube BHEs are investigated in chapter 3. Internal heat transfer mechanism, theories and different definitions for the thermal resistance of U-tube BHEs, and convective heat transfer inside the tubes are presented.

The numerical approaches employed in this study are presented in chapter 4. This chapter contains a review on finite element analysis method and explanations regarding the software utilized, mathematical modeling, model validation, and boundary and working conditions. Finally, it renders some explanatory notes on the program solver, convergence results, meshes employed and grid independence.

In chapter 5, the fluid temperature distribution is analyzed by means of the finite element method, for a typical double U-tube BHE, under various unsteady working conditions. The difference between the mean fluid temperature and the arithmetic mean of inlet and outlet temperatures is determined and validated by an analytical method.

New correlations to determine the mean fluid temperature of double U-tube BHE are proposed in chapter 6. By means of 3D simulations, tables of a dimensionless coefficient are provided which allow an immediate evaluation of the mean fluid temperature of BHEs in any

working condition, including TRTs. In addition, the applicability of the correlations to different BHE geometries are investigated.

Chapter 7 is devoted to the study of the thermal resistance of double U-tube BHEs and of the effects of temperature distribution on it. In this chapter, different definitions of the BHE thermal resistance, presented in chapter 3, are considered. Furthermore, the accuracy of approximate analytical models to estimate the thermal resistance is checked by comparison with the results of various 2D and 3D finite element simulations. The parameters that may affect the thermal resistance of double U-tube BHEs are evidenced.

Finally, chapter 8 reports the conclusion of the present thesis and points out potential opportunities for future studies.



## *Chapter 2*

---

*An introduction on Ground-Coupled  
Heat Pump (GCHP) systems*



## ***An introduction on Ground-Coupled Heat Pump (GCHP) systems***

---

Due to the industrial development, improved living standards, urbanization, and population growth, the rate of world energy demand is still rising. As a consequence, the use of primary energy is increasing and fossil fuels, particularly conventional fossil fuels (oil, coal and natural gas), play a key-role as a world primary energy source. Based on EIA (US Energy Information Administration) data [1], the world annual primary energy consumption in 2015 was more than 571 EJ, which was more than 49% higher than of that in 1995. In particular, almost 86% of the world total primary energy use in 2015 was due to the conventional fossil-based energy sources. For the United States, consumption of conventional fossil fuels was 81% of the total primary energy consumption in 2015. The United States annual primary energy consumption by source, from 1950 to 2015, is illustrated in figure 2.1.

However, meeting the today's ever increasing demand for fossil fuels has become a cause of concern due to the adverse effects of the use of fossil fuels on our planet. Reducing emission of greenhouse gases (GHG), mainly CO<sub>2</sub>, causing the climate change called *global warming*, and preserving the fossil fuel sources are important challenges to be faced. Such challenges can be met via reducing the consumption of fossil fuels and exploiting alternative green energy sources.

Incremental adoption of the renewable energy sources is considered as an optimal way to shift from fossil-based development to sustainable development. Consequently, the utilization of renewable energy sources is becoming widely popular and all around the world, governments attempt to move towards a sustainable development. According to the world energy assessment



reported by United Nation (UN) in 2000 [2], at the turn of the century, renewable sources supplied almost 14% of the total world energy demand and is expected to reach 50% by 2040 [3,4].

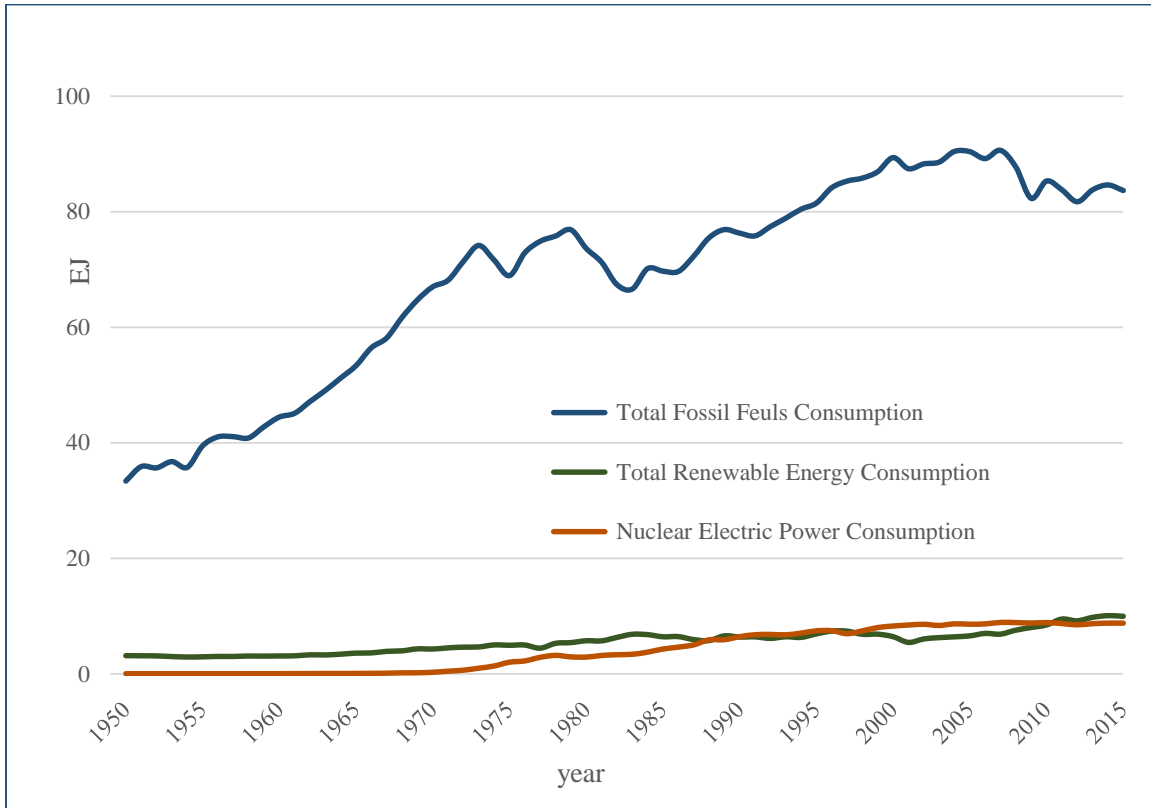


**Figure 2.1.** U.S. annual primary energy consumption by source from 1950 to 2015, data according to EIA [1].

During the last decade, the European Union energy strategy has been based on the utilization of the renewable energy sources. Based on Eurostat (European Commission portal for statistics) [5], the share of renewable energy in gross final energy consumption, in 28 countries of European Union, has increased more than 77% from 2004 to 2014.

Figure 2.2 shows Europe's final energy consumption by sector in 2015 [5]. It can be seen that after transport sector, residential consumption and industry were highest final energy consumer sectors in European Union in 2015. The figure shows that the residential sector and the service sector, both based on building operation, reach together about 40% of the total energy consumption. Hence, one important step towards the reduction of the use of fossil-based energy in Europe is to employ renewable energy sources for building operation, according to the Directive of the European Parliament [6].

Geothermal energy refers to the thermal energy projecting from the earth's crust (thermal energy in rock and fluid), which flows to the surface by conductive heat transfer mechanism and also by convection in regions where geological condition allows. It is believed that the earth would have cooled and become solid from a completely molten state thousands years ago and

observations have been shown that the ultimate source of geothermal energy is radioactive decay within the earth [7].

Geothermal energy is not only considered as a renewable energy, but it is also considered as a sustainable source of energy. Since any projected heat extraction from the ground is negligible compared to the internal earth's heat source, geothermal energy can be considered as a renewable energy. Thanks to the power of the earth's ecosystem, employing current sources of geothermal energy will not endanger the future generations' resources. Therefore, geothermal energy can be classified as a sustainable energy. Furthermore, geothermal energy is fully potential to mitigate the global warming problem because of its insignificant emissions.

Geothermal plants account for more than one-fourth of the electricity produced in Iceland. Figure 2.3 illustrates Iceland's Nesjavellir geothermal power station [8].

Since geothermal energy is categorized as a renewable energy source, by a Directive of the European Parliament [6], employing Ground-Source Heat Pumps (GSHPs) would be an appropriate solution to meet the European Union energy strategy. GSHPs can be used in buildings in order to supply heating, cooling (air conditioning), and Domestic Hot Water (DHW).

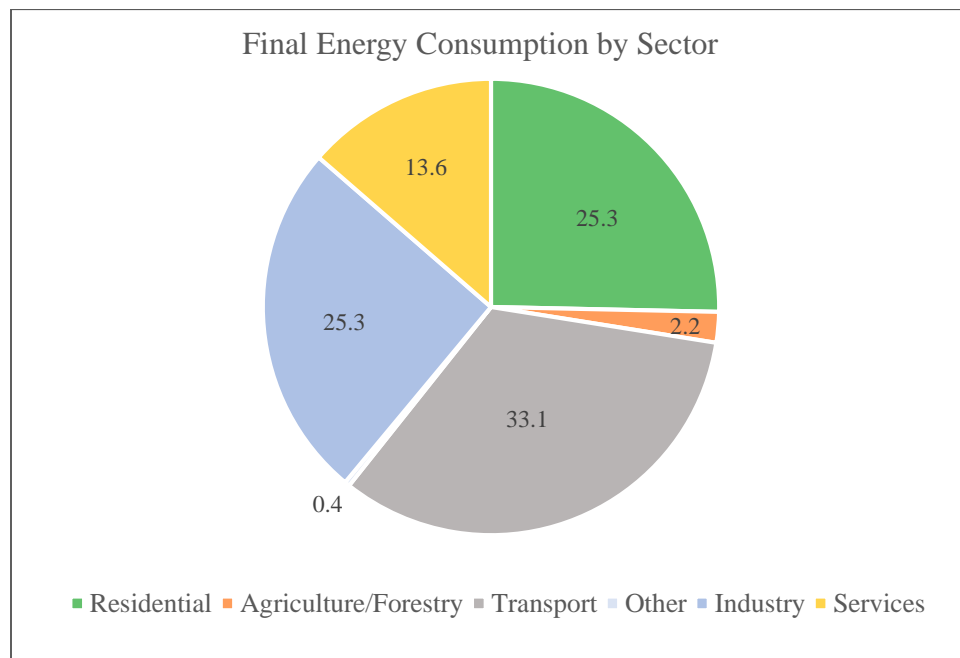


Figure 2.2. Europe final energy consumption percentage by sector in 2015, data according to Eurostat [5].

## 2.1 Ground-Source Heat Pumps (GSHPs) and their categories

In general, systems employing geothermal energy can be classified in three main types: Direct use and district heating systems, Electricity generation power plants and Geothermal heat pumps. GSHPs, referred to as geothermal heat pumps, were originally developed in the residential arena

and now are widely applied in the commercial sector [9]. While the temperatures above the ground surface change depending on time of day and season, temperatures more than 3m below the earth's surface are consistently between 10 °C and 15.6 °C. Thus, it can be said that the ground temperatures, for most areas, are usually warmer than the air in winter and cooler than the air in summer. Geothermal heat pumps use the ground's near-constant temperatures along seasons for both heating and cooling in buildings. Namely, the heat from the ground is transferred into the building during the winter, and the process is reversed in the summer [10]. Employing the earth instead of ambient air provides a lower-temperature sink for cooling and a higher-temperature source for heating with smaller temperature fluctuations, thereby yielding higher efficiency for the heat pump [11]. Figure 2.4 illustrates the schematic of a GSHP system in heating/cooling mode [12].



**Figure 2.3.** Iceland's Nesjavellir geothermal power station. Geothermal plants account for more than 25 percent of the electricity produced in Iceland. Photo: Gretar Ívarsson [8].

Thanks to their features, GSHPs have been recognized as being cost effective, energy efficient and environmentally friendly systems. GSHPs have the lowest CO<sub>2</sub> emissions and the lowest overall environmental costs among of all technologies analyzed, based on the US Environmental Protection Agency data [13]. In addition, these energy efficient systems incur low maintenance costs to heat and cool buildings [14]. As a consequence, the installation rate of GSHPs for heating and cooling in buildings is increasing in several countries.

According to Lund and Boyd [15], the worldwide installed capacity of GSHPs has increased from 1.854 GW to 50.258 GW, from 1995 to 2015 (figure 2.5). Moreover, GSHPs are the systems with the largest share of geothermal energy use and installed capacity worldwide in 2015, accounting for 55.15% of the annual energy use and 70.90% of the installed capacity.

The term GSHP is applied to a variety of systems exploiting the ground, groundwater or surface water as a heat sink and/or source. According to AHRAE [16], by considering the system features and sources, different subsets of GSHP can be defined as: Ground-Coupled Heat Pump (GCHP), Groundwater Heat Pump (GWHP) and Source Water Heat Pump (SWHP). Moreover,

other parallel terms would be used to meet a variety of marketing or institutional needs [17]. In the following, GCHP systems and their design methods will be discussed, since this technology is relevant to the present thesis.

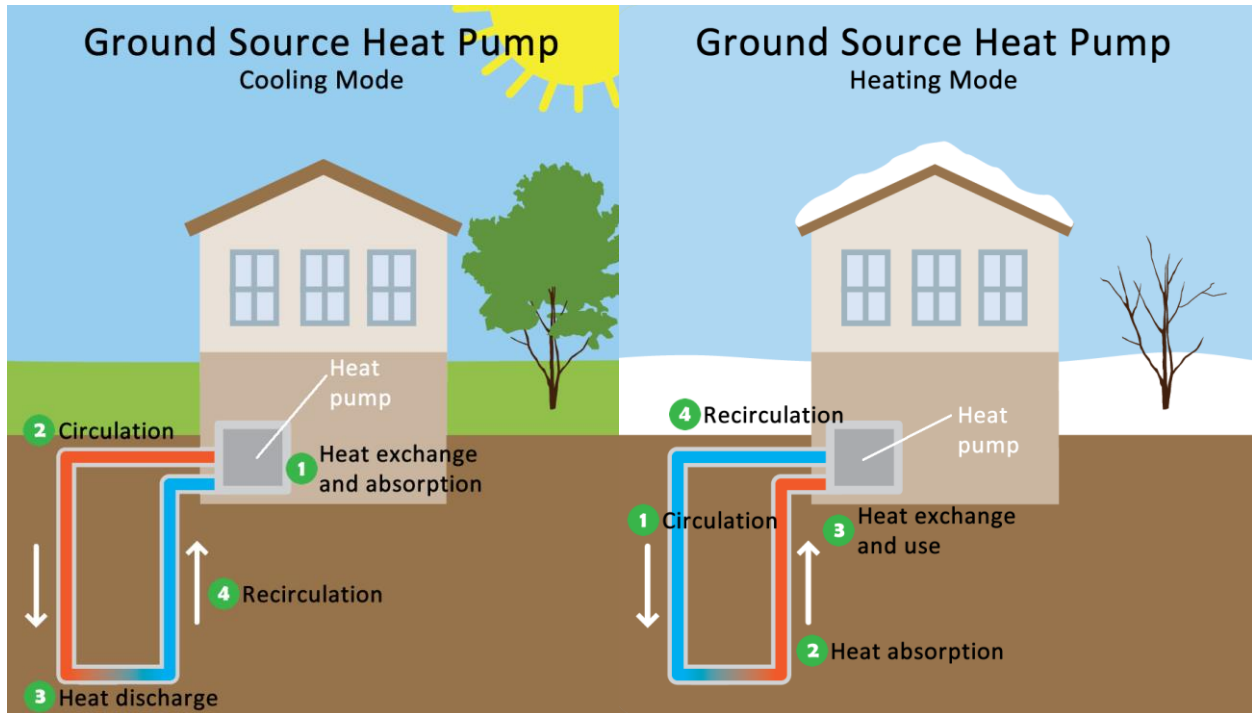


**Figure 2.4.** Schematic of a GSHP system in heating/cooling mode, reported by EPA [12].

## 2.2 Ground-Coupled Heat Pumps (GCHPs)

The GCHPs, which are called often a closed-loop heat pumps, are a subset of GSHPs. GCHPs appear as the most promising kind of GSHPs, due to their energy efficiency, environmental friendly features and applicability even where regional laws do not permit to extract the groundwater. The term GCHP refers to a system that consists of a reversible vapor compression cycle that is linked to a closed ground heat exchanger buried in soil [16].

According to Kavanaugh and Rafferty [9], in general three types of units are used in GCHPs. The most widely used unit is a water-to-air heat pump, which circulates a water or water/antifreeze solution through a liquid-to-refrigerant heat exchanger and a buried thermoplastic piping network. Another type is water-to-water heat pumps, which replaces the forced air system with a hydronic loop. Finally, the third type of GCHPs is the direct-expansion (DX) one, which uses a buried copper piping network through which refrigerant is circulated. Systems using water-to-air and water-to-water heat pumps are referred to as GCHPs with secondary solution loops in order to distinguish them from DX GCHPs.

According to the design of the ground heat exchanger, GCHPs are usually subdivided into two types: horizontal and vertical. In horizontal GCHPs, high-density synthetic plastic ground heat exchangers, connected in series or parallel, are horizontally buried in shallow trenches (1-3 m) in order to circulate the fluid in the ground. Horizontal GCHPs can be divided into several subgroups such as single pipe, multiple pipe, spiral, and horizontally bored. Although horizontal GCHPs are typically less expensive than vertical GCHPs, due to their low-cost installation, they require larger ground area for installation and have lower performance [16].

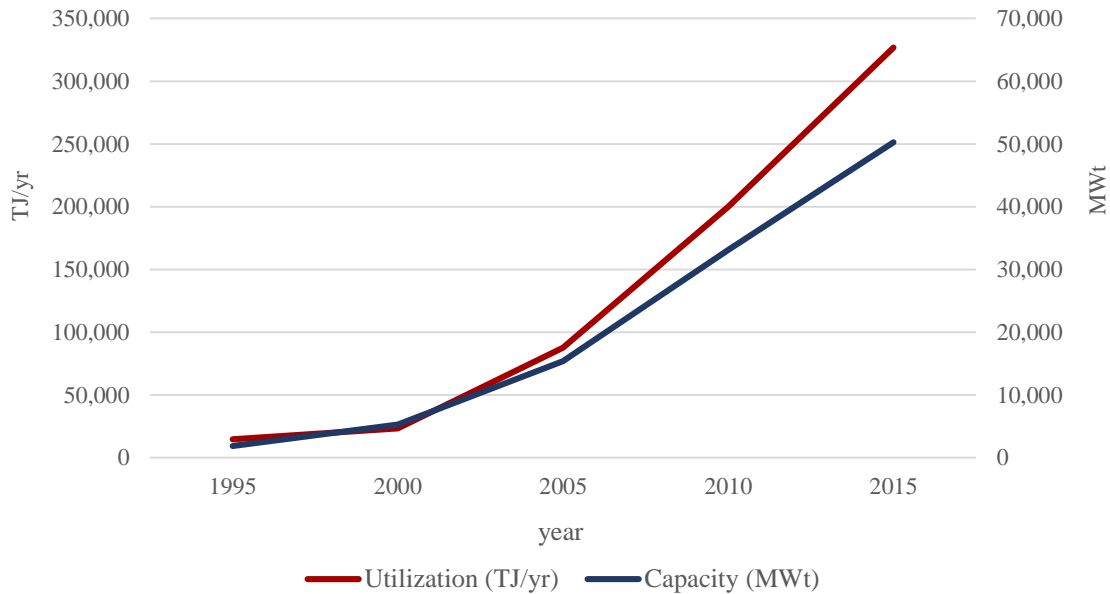


**Figure 2.5.** The installed capacity and annual utilization of geothermal heat pumps from 1995 to 2015 [15].

The most diffuse GCHP systems employ vertical ground heat exchangers often referred to as Borehole Heat Exchangers (BHEs); this technology is the case under study in this thesis. A BHE is composed of high-density polyethylene tube(s), inserted in a drilled hole which is then filled with a proper sealing grout. The pipe configuration within a BHE may be a single U-tube, a double U-tube or two coaxial tubes. The length of a BHE is usually between 50 and 150 m, and the most common diameter is about 15 cm. In addition, a typical external diameter of each tube is 40 mm for single U-tube and 32 mm for double U-tube BHEs. Figure 2.6 shows a schematic vertical GCHP system [18]. Sets of BHEs inserted in the ground along each other to form a closed loop system are considered as a BHE field.

According to ASHRAE [16], the most important advantages of the vertical GCHPs are that they require relatively small plots of ground and smallest amount of pipe and pumping energy, are in contact with soil which has little variation in temperature and thermal properties, and finally, can yield the most efficient GCHP system performance. However, higher cost of expensive equipment for drilling the borehole and limited number of available contractors to perform such projects are considered as disadvantages for the vertical GCHP system.

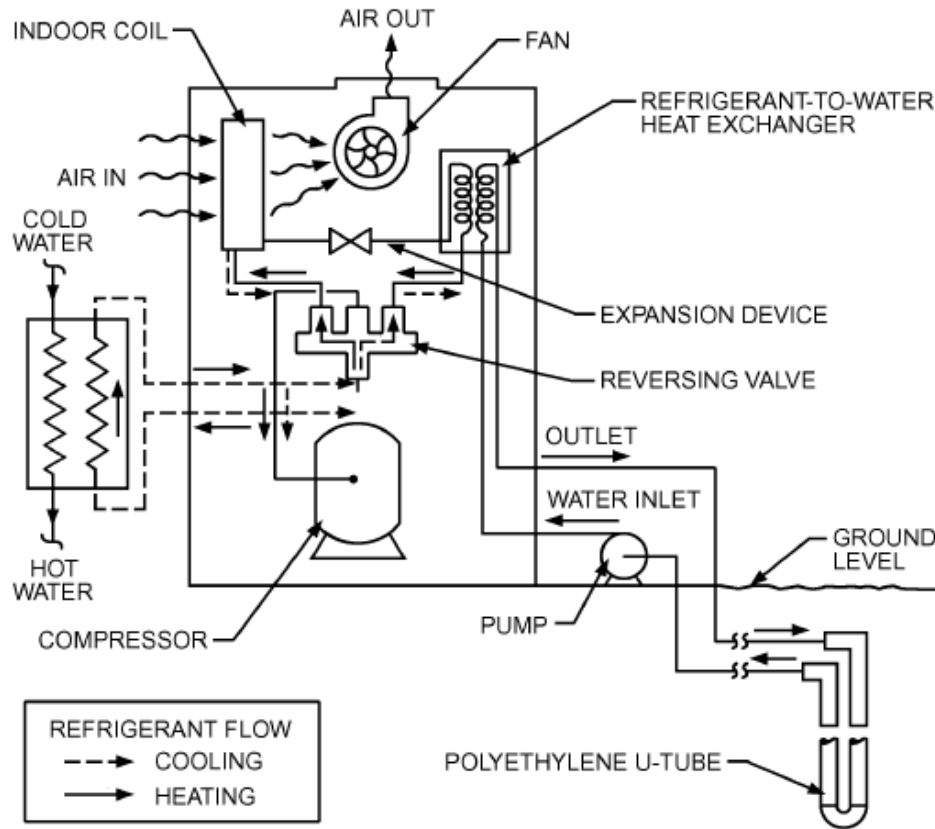


Figure 2.6. A vertical closed-loop GCHP system [18].

Since the heating/cooling load in GCHPs is extracted from/rejected into the ground via BHEs, the proper design of a BHE and its field is of great importance for GCHP systems. In the following, available design methods of the BHE fields in the literature are discussed.

### 2.3 BHE field design methods

The design of GCHP systems is often divided into two parts [19]:

- The choice of the heat pump and the evaluation of its seasonal performance
- The design of BHE field

In the design of a BHE field, the majority of design methods in the literature are based on the evaluation of the temperature distribution in the BHE field as a function of time. In this case, the ground is considered as an infinite solid medium with constant thermophysical properties.

Although groundwater movements might have an influence on the heat transfer process in some cases, it is usually neglected in the design of BHE field. Under such assumptions, the problem to be studied is a 3D transient conductive heat transfer in the ground. The problem can be solved either by using available analytical solutions or by employing numerical codes, including commercial software packages dedicated to the design of BHE field.

### 2.3.1 Analytical models

In general, analytical solutions are classified as follows, with reference to the scheme adopted to model the BHE:

- Infinite Line-Source model (ILS)
- Infinite Cylindrical Source model (ICS)
- Finite Line-Source model (FLS)

Solutions of the temperature distribution in the BHE field (produced by a BHE) are often obtained in a dimensionless form. The dimensionless forms of the radial coordinate  $r$ , vertical coordinate  $z$ , length  $L$ , time  $t$ , and temperature  $T$  employed in the following, denoted with asterisks, are listed below:

$$r^* = \frac{r}{D} \quad (2.1)$$

$$z^* = \frac{z}{D} \quad (2.2)$$

$$L^* = \frac{L}{D} \quad (2.3)$$

$$t^* = \frac{\alpha_g t}{D^2} \quad (2.4)$$

$$T^* = k_g \frac{T - T_{g_0}}{q_0} \quad (2.5)$$

where  $D$  is the BHE diameter,  $\alpha_g$  is the ground thermal diffusivity,  $k_g$  is the ground thermal conductivity,  $T_{g_0}$  is the undisturbed ground temperature, and  $q_0$  is a reference heat flux per unit length.

The ILS model is one of the most widely used analytical procedures based on the assumption considering the BHE as an infinitely long line heat/sink source in a homogeneous, isotropic, and infinite medium, which extract or inject a constant heat flux. Since the earliest application of this method was developed by Lord Kelvin, it is also known as *Kelvin's line-source theory*. Kelvin's theory of heat sources has a clear and simple physical meaning [11,20]: taking the solution of instantaneous point source (an abstract concept similar to the mass point in mechanics) as a

fundamental solution (Green's function for an infinite medium) enables the solution for a continuous point source to be obtained by the integration of the fundamental solution over time.

According to this model, the temperature field with reference to the introduced dimensionless quantities, for a BHE subjected to a constant heat flux per unit length, takes the following form [20]:

$$T^*(r^*, t^*) = \frac{q}{4\pi q_0} \int_{\frac{r^*}{4t^*}}^{\infty} \frac{e^{-u}}{u} du \quad (2.6)$$

This method has been applied to simulate the behavior of BHEs [21,22] and has been proposed by Mogensen [23] to be employed in the thermal response test (TRT) to evaluate the thermophysical properties of the ground.

In the ICS model, the finite diameter of the borehole is taken into account and the BHE is considered as an infinitely long cylindrical heat/sink source. The solution of the temperature field in ICS model was obtained by Carslaw and Jaeger [20] by employing the Laplace transformation and Bessel function, and can be written in dimensionless form as [24]:

$$T^*(r^*, t^*) = \frac{1}{\pi^2} \int_0^{+\infty} \left[ \frac{Y_0(2r^*u)J_1(u) - J_0(2r^*u)Y_1(u)}{J_1^2(u) + Y_1^2(u)} \frac{1 - e^{-4t^*u^2}}{u^2} \right] du \quad (2.7)$$

where  $J_n$  and  $Y_n$  are the Bessel functions of the first kind and second kind with order  $n$ , respectively.

ASHRAE [16] recommends a simple and widely employed method for BHE field design, developed by Kavanaugh and Rafferty [9]. This method is based on the ICS model, i.e. on the solution of the equation for the heat transfer from an infinitely long cylinder placed in a homogeneous solid medium, obtained and evaluated by Carslaw and Jaeger [20]. This model was suggested by Ingersoll et al. [25] as an appropriate method of sizing ground heat exchangers in cases where the ILS model yields inaccurate results.

The ASHRAE method considers the superposition of three heat pulses, each with a constant power, which account for seasonal heat imbalances, monthly average heat load during the design month, and peak heat pulse during the design day, respectively. Furthermore, the method takes into account the thermal interference between BHEs. However, it is limited to 10 years of operation and does not guarantee the long-term sustainability. The method is described below.

Employing the method of Ingersoll et al. [25] and by analogy with the steady-state case, one has:

$$q = L \frac{T_{g_0} - T_f}{R_{g, eff}} \quad (2.8)$$



In equation (2.8),  $q$  is the thermal load, positive if heat is extracted from the ground,  $L$  is required borehole length,  $T_f$  is the BHE fluid temperature, and  $R_{g, eff}$  is the effective thermal resistance of the ground, per unit BHE length. For solving the required bore length  $L$ , the equation can be rearranged as:

$$L = \frac{qR_{g, eff}}{T_{g_0} - T_f} \quad (2.9)$$

The thermal resistance of the ground per unit length depends on the duration of the considered thermal load and is calculated as a function of time corresponding to the time span over which a particular heat pulse occurs. In addition, a term should be considered to account for both the thermal resistance of the pipe wall and interfaces between the pipe and fluid and the pipe and the ground. Taking into account whether the design is based on the heating loads or on the cooling loads, two different equations are suggested to determine the required bore length:

$$L_h = \frac{q_{anl} R_{g, anl} + (q_{des, h} - W_h)(R_b + PLF_{mly} R_{g, mly} + R_{g, dly} F_{sc})}{T_{g_0} - T_{f, ave} - T_{pen}} \quad (2.10)$$

$$L_c = \frac{q_{anl} R_{g, anl} + (q_{des, c} - W_c)(R_b + PLF_{mly} R_{g, mly} + R_{g, dly} F_{sc})}{T_{g_0} - T_{f, ave} - T_{pen}} \quad (2.11)$$

where  $q_{anl}$  is the net annual average heat transfer to the ground,  $q_{des}$  is the building design load,  $W$  is the system power input at design load,  $PLF_{mly}$  is the part-load factor during design month,  $F_{sc}$  is the short-circuit heat loss factor and  $T_{pen}$  is the temperature penalty for interference of adjacent bores. It should be stated that heat transfer rate, building loads and temperature penalties are considered positive for heating and negative for cooling.

It can be noted from equations (2.10) and (2.11) that the higher difference between  $T_{g_0}$  and  $T_{f, ave}$  results in lower total BHE length. ASHRAE recommends to choose  $T_{f, ave}$  so that the absolute value of the difference  $T_{g_0} - T_{f, ave}$  is between 8 and 15 °C for equation (2.10), and between 15 and 20 °C for equation (2.11).

The required total length of the BHE field should be the larger of the two lengths  $L_h$  and  $L_c$ , obtained from the equations (2.10) and (2.11). If  $L_h$  is larger than  $L_c$ , the length  $L_h$  must be installed. If  $L_c$  is larger than  $L_h$ , using an oversized heat exchanger is beneficial during the heating season. It is also possible to install the smaller heating length and to couple a cooling tower, in order to obtain a balance of the seasonal loads.

As it was mentioned, these equations consider three different heat pulses to account for long-term heat imbalances  $q_{anl}$ , average monthly heat rates during the design month, and maximum heat rates for a short-term period during the design day [16]. The most critical parameters to evaluate are thermal resistances. To evaluate the effective thermal resistance of the ground, varying heat pulses are considered. The system can be modelled with three heat pulses, a 10 years (3650 days) pulse of  $q_{anl}$ , a 1 month (30 days) pulse of  $q_m$ , and a 6 hours (0.25 days) pulse of  $q_{dly}$ . Moreover, three corresponding time instant are defined as;

$$\begin{aligned} t_{dly} &= 6 \text{ hours} = 0.25 \text{ days}; \\ t_{mly} &= 1 \text{ month} + 6 \text{ hours} = 30.25 \text{ days}; \\ t_{anl} &= 10 \text{ years} + 1 \text{ month} + 6 \text{ hours} = 3680.25 \text{ days} \end{aligned} \quad (2.12)$$

By means of the dimensionless Fourier number  $Fo$ , time of operation, bore diameter, and thermal diffusivity of the ground can be related as:

$$Fo = \frac{4\alpha_g t}{D_b^2} \quad (2.13)$$

In correspondence of the three Fourier numbers representing the three time instants defined by equation (2.12), one evaluates the values of the  $G$ -factor, which is the dimensionless temperature at the interface of the BHE and the ground due to a constant heat load, namely:

$$G = \frac{k_g (T_{b-g} - T_{g0})}{q_l} \quad (2.14)$$

where  $T_{b-g}$  is the temperature at the BHE-ground interface and  $q_l$  is the constant heat load per unit length. Values of the  $G$ -factors can be determined by Fourier/ $G$ -factors graph, proposed by Kavanaugh and Rafferty [9], illustrated in figure 2.7.

After determination of values of the  $G$ -factors corresponding to the three Fourier numbers, the ground thermal resistances can be evaluated as follows:

$$\begin{aligned} R_{g, anl} &= \frac{G_{anl} - G_{mly}}{k_g}; \\ R_{g, mly} &= \frac{G_{mly} - G_{dly}}{k_g}; \\ R_{g, dly} &= \frac{G_{dly}}{k_g} \end{aligned} \quad (2.15)$$

More specific technical notes on the determination of the factors  $PLF_{mly}$ ,  $F_{sc}$  and  $T_{pen}$  can be found in detail in references [9] and [16].

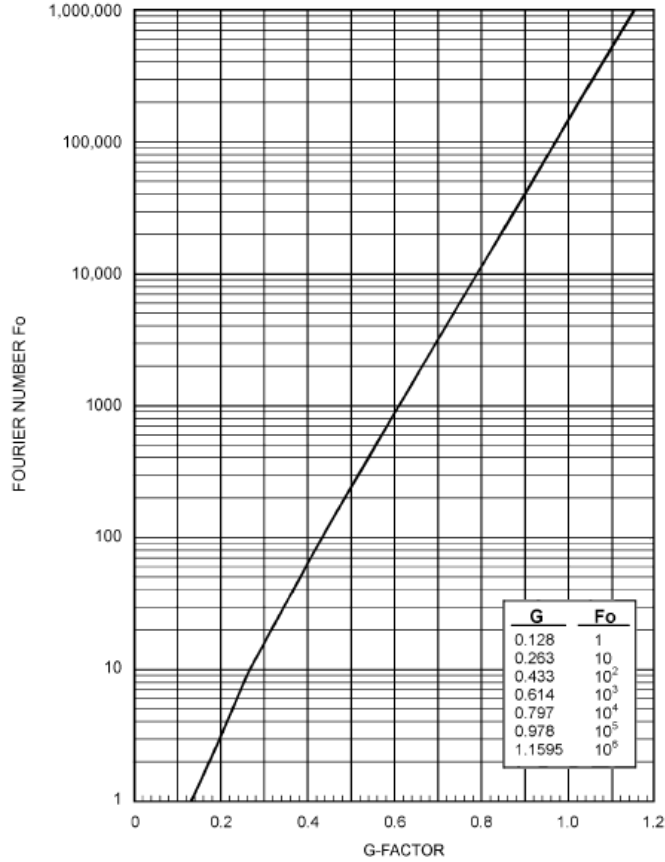


**Figure 2.7.** Fourier / G-factor graph for ground thermal resistance [9].

The FLS model considers a BHE as a line with finite length. The analytical solution of this model was determined by Eskilson and Claesson [26,27]. The dimensionless form corresponding to the definitions of dimensionless parameters is as follows [28]:

$$T^*(r^*, z^*, t^*) = \frac{1}{4\pi} \int_0^{L^*} \left[ \frac{\operatorname{erfc} \left[ 0.5 \sqrt{r^{*2} + (z^* - u)^2} / \sqrt{t^*} \right]}{\sqrt{r^{*2} + (z^* - u)^2}} - \frac{\operatorname{erfc} \left[ 0.5 \sqrt{r^{*2} + (z^* + u)^2} / \sqrt{t^*} \right]}{\sqrt{r^{*2} + (z^* + u)^2}} \right] du \quad (2.16)$$

where  $\operatorname{erfc}$  is the complementary error function.

Zeng et al. [29] mentioned that employing the semi-analytical expression of FLS model (equation (2.16)), evaluated at the middle of the BHE length, yields up to 5% overestimation of the mean temperature field at the BHE surface. They recommended to use the value given by that

expression when averaged along the BHE length, which has a double integral form and is called *g-function*. The *g-functions* are time-dependent expressions of the dimensionless temperature, averaged along the BHE length. The *g-function* expression based on the FLS model takes the following form:

$$g^*(r^*, t^*) = \frac{1}{4\pi L^*} \int_0^{L^*} \int_0^{L^*} \left[ \frac{\operatorname{erfc} \left[ 0.5\sqrt{r^{*2} + (z^* - u)^2} / \sqrt{t^*} \right]}{\sqrt{r^{*2} + (z^* - u)^2}} - \frac{\operatorname{erfc} \left[ 0.5\sqrt{r^{*2} + (z^* + u)^2} / \sqrt{t^*} \right]}{\sqrt{r^{*2} + (z^* + u)^2}} \right] du dz^* \quad (2.17)$$

Lamarche and Beauchamp [30], Bandos et al. [31] and Fossa [32,33] proposed other forms of this expression.

Classic models for *g-function* have been inspired by the seminal work of Ingressol et al. [25], who suggested the ILS model and the ICS model for heat transfer through the ground.

Although concrete expressions were not developed by them, ideas for dealing with additional complicated factors were proposed [11]. It is usually stated in the literature that Eskilson and Claesson [26,27] were those who introduced the concept of *g-function*, as a dimensionless thermal response due to a constant heat load, and proposed to employ a semi-analytical expression of the temperature field produced by a FLS subjected to a constant heat flux per unit length [34].

Accurate analytical expressions of the *g-function* were proposed by Zanchini and Lazzari [28], based on the Finite Cylindrical Source (FCS) model and for fields of BHEs with different values of the ratio between length and diameter. These *g-functions* were presented in the form of polynomial functions of the logarithm of dimensionless time by means of accurate interpolations. The ground was considered as a semi-infinite solid medium with constant thermophysical properties and the movement of groundwater was neglected. Each BHE was considered as a finite cylindrical heat source, subjected to a uniform heat load per unit length that is constant during each month but is variant during the year. Under such assumptions, their method can evaluate the long-term temperature distribution in a field of long BHEs subjected to a monthly averaged heat flux. This method yields faster computations, since it is based on *g-functions* expressed in polynomial form. However, it requires interpolations to obtain *g-functions* for dimensionless values of  $r^*$  and  $L^*$  not tabulated. Recently, new *g-functions* taking into account also the internal structure of the double U-tube BHE have been presented by same authors [34]. It should be noted that several expressions for *g-functions* were developed based on different types of models such as Infinite cylindrical-surface model, ILS model, FLS model, infinite moving line-source model, and infinite phase-change line-source model. A comparative study of various *g-functions* for BHEs can be found in reference [11].

Apart from the discussed analytical models, several models based on numerical techniques have been presented in the literature. For example, short time-step model for the simulation of transient heat transfer in vertical BHE, proposed by Yavuzturk and Spitler [35,36], and Shonder

and Beck's model [37], which is based on a parameter estimation technique. In the following, numerical models employed in the literature to simulate the BHE field are studied.

### 2.3.2 Numerical models

Numerical models can be employed to simulate the BHE fields and also TRTs. Simulations can be carried out by means of either commercial software packages or numerical methods. Earth Energy Designer (EED) is a commercial design software entirely dedicated to the simulation of BHEs, based on the line-source model. The algorithms were derived from modelling and parameter studies carried out by Hellström et al. [38,39]. EED performs simulations on a monthly basis and is based on expressions of the dimensionless temperatures produced by several configurations of BHE fields (*g-functions*), derived through 2D finite difference numerical simulations. Figure 2.8 shows the input data menu for a double U-tube BHE in the EED program [40].

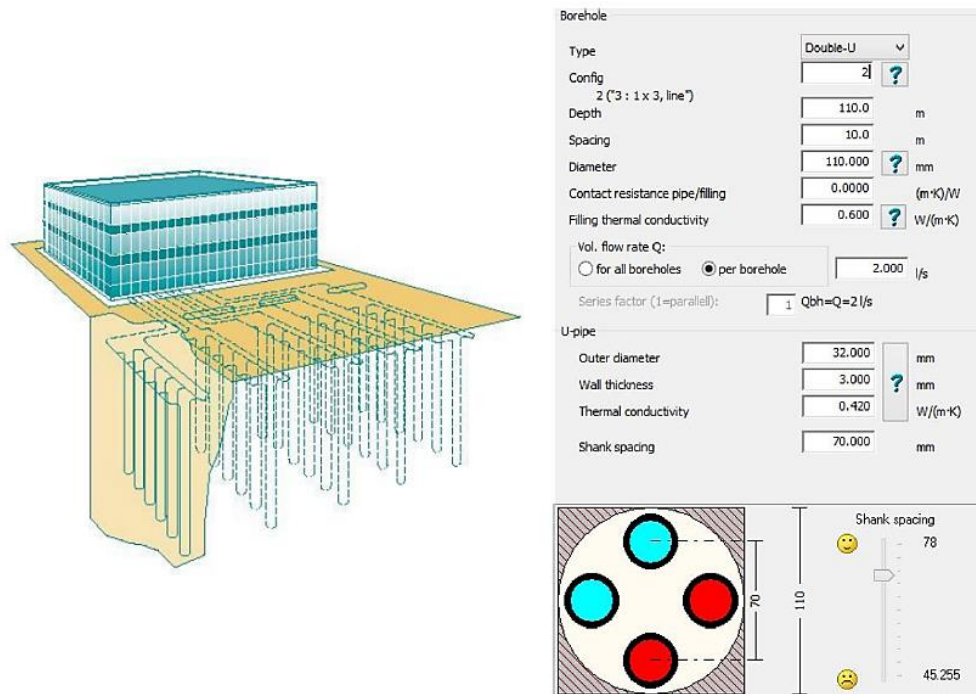


Figure 2.8. Earth Energy Designer - EED [40].

TRNSYS is a well-known simulation package based on finite difference method, employing the Duct Storage (DST) model, developed by Hellström [41,42]. DST model employs spatial superposition of three basic solutions of the conduction equation: the global temperature difference between the heat store volume and the undisturbed ground temperature, calculated numerically; the local temperature response inside the heat store volume, calculated numerically; the additional temperature difference which accounts for the local steady heat flux, calculated analytically [19,43]. As reported by Yang et al. [44], TRNSYS is a modular system package where users are

able to describe the components of the system and the manner in which these components are interconnected. Since the program is modular, the DST model for the vertical BHE can be easily added to the existing components libraries. Although the DST model is computationally efficient, it may not provide precise results for in line BHEs and unbalanced heat loads [43].

Another popular program is EnergyPlus which is based upon the line-source model. EnergyPlus employs the *g-function* model developed by Eskilson [26] to model BHE fields, by means of an enhanced algorithm (a short time step response model) proposed by Yavuzturk and Spitler [45].

GLHEPRO is a design tool for commercial building ground loop heat exchangers, developed by Spitler [46] and is on the basis of the line-source model. The design method of the program is based on the prediction of the temperature response of the ground loop heat exchangers to monthly heating and cooling loads, and monthly peak heating and cooling demands over a number of years. Moreover, the temperature of the fluid inside the BHE is calculated by employing a 1D steady-state BHE thermal resistance [44].

A majority of other commercial programs using different approaches are also available; GchpCalc is based on the cylindrical-source model and its detailed fundamental concepts can be found in reference [9]. The design tools eQUEST [47] and HVACSIM+ [48] are based upon the line-source model and employ *g-functions* algorithms. *GeoStar* [49,50] is based on the line-source model and employs two heat transfer schemes: heat conduction for the BHE-ground field and heat transfer inside the BHE. The second scheme utilizes a quasi-3D model which takes into account the fluid temperature variation along the BHE wall.

Numerical simulation of the BHE field can also be performed by means of typical numerical methods, such as codes on the basis of finite difference, finite element and finite volume methods. By employing a finite element method, Muraya, et al. [51] developed a transient model to investigate the heat transfer around a vertical U-tube heat exchanger. The effect of the backfills, separation distance, leg temperature, and different ambient soil temperature were studied.

Li and Zheng [52] utilized a 3D unstructured finite volume method for simulation of the vertical ground heat exchanger. In their model, it was considered that surrounding ground to be divided into various layers in vertical direction in order to take into account the effect of variant fluid temperature with depth. Validation of the model against the experimental data confirmed the accuracy of the model.

Finite difference method is also employed in the literature in order to simulate the BHE and its field for geothermal heat pump systems; Lee and Lam [53] conducted the simulation of borehole ground heat exchangers used in geothermal heat pump system, by employing a 3D implicit finite difference code with a rectangular coordinate system. In order to avoid using fine grids inside the BHE, they approximated each borehole by a square column. By calibrating the simulated data with the cylindrical-source model, the grid spacing was adjusted. A finite difference code based on quasi-steady-state condition was used to compute heat transfer inside the borehole. The results showed that neither the temperature nor the loading along the borehole was constant. A comparison between the model under study and the FLS model demonstrated that the deviation of the

calculated BHE temperature increased with the scale of the bore field. A modified 3D finite difference model of this study was developed out by Lee [54], who investigated the impacts of multiple ground layers on the analysis of TRT and on the performance of GCHP system. He found that the overall system performance predicted by considering multiple ground layer was nearly the same as that predicted by ignoring the ground layers.

The simulation of BHE field by employing numerical methods, such as finite volume or finite element methods, can be implemented in CFD packages. For instance, programs like COMSOL Multiphysics, ANSYS/ANSYS FLUENT, FRACTure, and FEFLOW could be suited to simulate coupled hydraulic-thermal problems under transient conditions.

### **2.3.3 Analytical models vs. numerical models**

In general, analytical models are often based on a number of simplifying assumptions to solve the complicated mathematical equations; hence, due to simplifications, such as considering the centerline of the BHE as a line source, the accuracy of the results in analytical models would be reduced to some extent. However, analytical models usually require much less computation time, compared with numerical models. Moreover, the straightforward algorithms deduced from analytical models can be readily integrated into a simulation program [44].

On the other hand, numerical models can offer a higher level of accuracy and also flexibility in modeling the physical characteristics of the problem. They are elaborate enough to represent the geometrical and thermal properties of a BHE field in more details. However, in many cases numerical approaches can be computationally inefficient, due to employing a large number of complex grids. In order to obtain computational efficiency, a sever reduction in the number of grid elements should be done, with the consequence of poor accuracy in results [55]. Furthermore, it is difficult to incorporate commercial codes into pre- and post-processing stages to carry out a system simulation for a particular application [11].

## **2.4 Fluid-to-ground thermal resistance**

A better design of a single BHE can improve the performance of a BHE field, which, on turn, improves the performance of a GCHP system. The BHEs are also responsible for a major part of the initial cost of a GCHP system, so that an oversized BHE field could yield a too high initial cost. Therefore, a correct design of the BHE field is essential to ensure both energy efficiency and economic feasibility.

The reduction and the correct knowledge of the BHE thermal resistance are both important, for the optimization of BHEs and for the correct design of a BHE field.

In fact, heat transfer from the fluid to the ground or vice versa, is a process where the concept of BHE thermal resistance between the fluid and the BHE surface appears. As illustrated by figure 2.9, heat transfer in a BHE depends on several factors such as the configuration of the pipes,

thermal properties of the circulating fluid, of grouting materials and of the surrounding ground, and the mass flow rate. The local heat transfer process within the BHE includes three components: convection between the inner wall of the U-tube pipes and the circulating fluid, conduction through the wall of U-tube pipes, and conduction through the grouting material. The thermal resistance corresponding to the first two thermal processes is considered as the thermal resistance of the U-tube pipe. The thermal resistive network for a single U-tube BHE is demonstrated in figure 2.10.

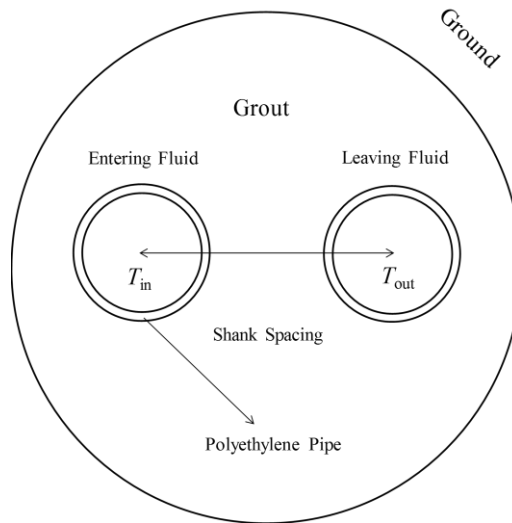


**Figure 2.9.** A BHE cross section.

The thermal resistance of the BHE can be expressed as follows:

$$R_b = R_p + R_{gt} \quad (2.18)$$

where  $R_{gt}$  is the thermal resistance of the grout and  $R_p$  refers to the thermal resistance of the U-tube pipe and is computed as:

$$R_p = R_{cond} + R_{conv} \quad (2.19)$$

where  $R_{cond}$  and  $R_{conv}$  stand for the conduction and convection heat transfer inside the pipe, respectively.



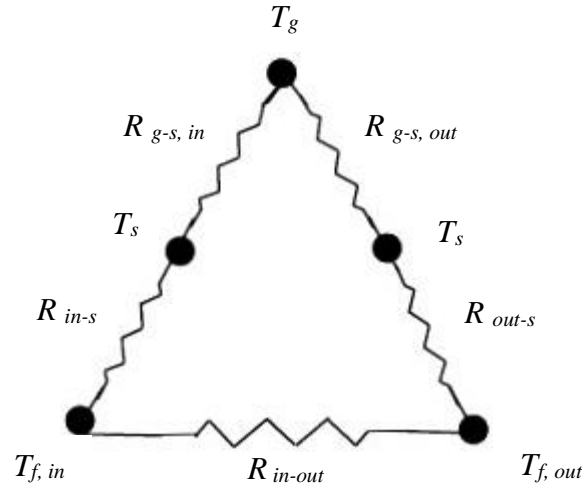


**Figure 2.10.** Thermal resistive network for a single U-tube BHE.

If one denotes by  $T_f$  the fluid bulk temperature, by  $T_s$  the external BHE wall surface temperature and by  $q_l$  the heat flux per unit length of the BHE (thermal power exchanged between the BHE and the ground), the thermal resistance of the BHE is defined as:

$$R_b = \frac{T_f - T_s}{q_l} \quad (2.20)$$

Since  $T_f$  and  $T_s$  are not uniform, and the real mean value of  $T_f$  is often not known, different definition of the BHE thermal resistance, i.e., different ways of application of equation (2.20), have been proposed. These definitions differ on the method to calculate  $T_f$  and on selecting either a 2D or a 3D domain to apply equation (2.20).

Lamarche et al. [56] have investigated the available methods to evaluate the BHE thermal resistance by a review paper. Recently, Zanchini and Jahanbin [57] have analyzed, by means of finite element simulations, the differences between the various definition of thermal resistance, for double U-tube BHEs. In addition, they have investigated the effects of the temperature distribution on the thermal resistance of double U-tube BHEs. The heat transfer process and the thermal resistance of a double U-tube BHE are analyzed in detail in chapters 3 and 7 of the present thesis.

## 2.5 Hybrid GCHP systems

Most building-plant systems have unbalanced seasonal heating and cooling loads. This circumstance can yield a decrease of the system performance of a GCHP system after some years. For instance, when a GCHP system is employed in a cooling-dominated building in a warm climate, more heat will be rejected to the ground than that extracted, on annual basis. This will

cause an increase of the ground temperature, which may deteriorate the performance of the GCHP system in a long term. Furthermore, a cooling-dominated building needs a BHE with larger size with respect to a situation with balanced loads. In a similar way, in a heating-dominated building, in a cold climate, a larger BHE field is needed to satisfy the higher heating demand; moreover, the ground will tend to cool down during the years, with a decrease of the system performance.

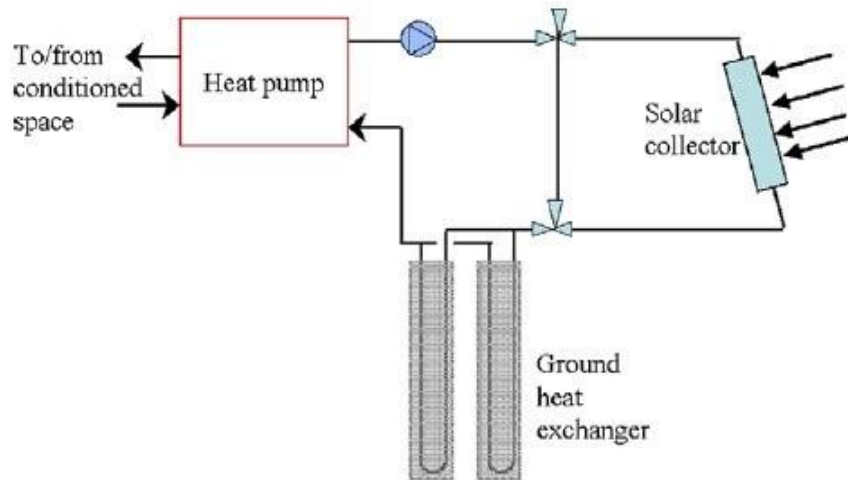


**Figure 2.11.** Schematic diagram of a HGCHP system with solar collector, presented in reference [44].

Hybrid Ground-Coupled Heat Pump (HGCHP) systems are an alternative way to increase the system performance and decrease the initial cost of the GCHP system, simultaneously. The HGCHP systems employ a supplemental heat rejecter/absorber which can reduce a significant amount of the heat rejected/extracted into/from the ground, in order to balance the ground thermal loads, leading to a better energy performance of the GCHP systems.

In recent years, remarkable studies have been done on the development of the various HGCHP systems. According to the Yang et al. [44], the main types of the HGCHP systems are:

- HGCHP systems with supplemental heat rejecters
- HGCHP systems with hot water supply
- HGCHP systems with solar collectors

Figure 2.11 shows a schematic diagram of a HGCHP system with solar collector [44].

A comprehensive study on different types of the HGCHP systems, design methods, and simulations for the HGCHP systems can be found in details in references [44, 58-61].



## *Chapter 3*

---

### *Heat transfer analysis of U-tube BHEs*



---

## *Heat transfer analysis of U-tube BHEs*

---

Heat transfer modeling in vertical ground heat exchangers is a rather complicated process. Considering the long time scale and the complexity of the problem, the heat transfer process is usually analyzed in two separated regions; one is the ground outside the BHE, and the other is region inside the BHE, including the U-tubes, the grout, and the fluid circulating inside the tubes. The heat transfer models of these two separated parts are interlinked on the wall of the BHE.

In fact, if we consider the ground as a homogeneous infinite medium, the heat transfer outside the BHE can be presumed as transient heat conduction which is bounded internally to the BHE wall. In reality, a major number of the geological-natural processes may affect the heat transfer process, such as groundwater movement, freezing, moisture transfer and so on. However, these phenomena are often neglected in modeling the heat transfer outside the BHE. Fourier's law states that the heat flow  $\vec{q}$  at a given point in a solid is proportional to the gradient of temperature:

$$\vec{q} = -k_g \nabla T \quad (3.1)$$

Then a transient heat balance for an element of the volume can be written as:

$$\nabla \cdot \vec{q} = -\rho_g c_g \frac{\partial T}{\partial t} \quad (3.2)$$

Inserting the equation (3.1) in equation (3.2), one obtains the 3D formulation of the time-dependent heat equation in cylindrical coordinates:

$$\frac{\partial^2 T}{\partial r^2} + \frac{1}{r} \frac{\partial T}{\partial r} + \frac{\partial^2 T}{\partial z^2} = \frac{1}{\alpha_g} \frac{\partial T}{\partial t} \quad (3.3)$$

Equation (3.3) is the general heat transfer equation for the ground, which is considered as a homogeneous infinite medium with constant properties.

As it was discussed, the heat transfer process outside the BHE is analyzed by either analytical methodologies or numerical models. The solution of the problem is usually given by means of *g-functions*, which represent the time-dependent dimensionless temperature averaged along the BHE length. Different design methods of BHE fields that take into account the heat transfer outside the BHE can be found in chapter 2. In the following, we concentrate on the heat transfer inside the BHE.

The heat transfer process inside the BHE is associated with the thermal properties of the grout and of the surrounding ground, the configurations of the tubes, and the mass flow rate. The local thermal process includes three components:

- Convective heat transfer inside the U-tube pipes
- Conductive heat transfer inside the wall of U-tube pipes
- Conductive heat transfer in grouting materials

As an example, figure 3.1 shows the isothermal temperature distribution in a double U-tube BHE and in the surrounding ground, taken from one of the simulations carried out in the present study, for cooling mode (summer) with inlet temperature  $T_{in}=32$  °C.

The thermal process in BHE is sometimes analyzed as being quasi-steady-state / steady-state and sometimes is considered as being time-dependent. As reported by Li and Lai [11], the thermal process in BHE can approach a steady-flux state (not a steady-state), in a strict sense, if  $t$  is greater than or equal to time scale  $5t_b$  ( $t_b \sim r_b^2 / \alpha_b$ ). The steady flux is a condition in which the temperature difference between the fluid and the BHE wall is constant. Under this condition, the three processes can be characterized by three constant thermal resistances. The sum of these resistances yields the fluid-to-ground BHE thermal resistance, according to Hellström [62].

In general, heat transfer process inside the BHE is interpreted and modelled by the BHE thermal resistance  $R_b$ . As briefly mentioned in chapter 2, the thermal resistance of the BHE is calculated by:

$$R_b = R_p + R_{gt} \quad (3.4)$$

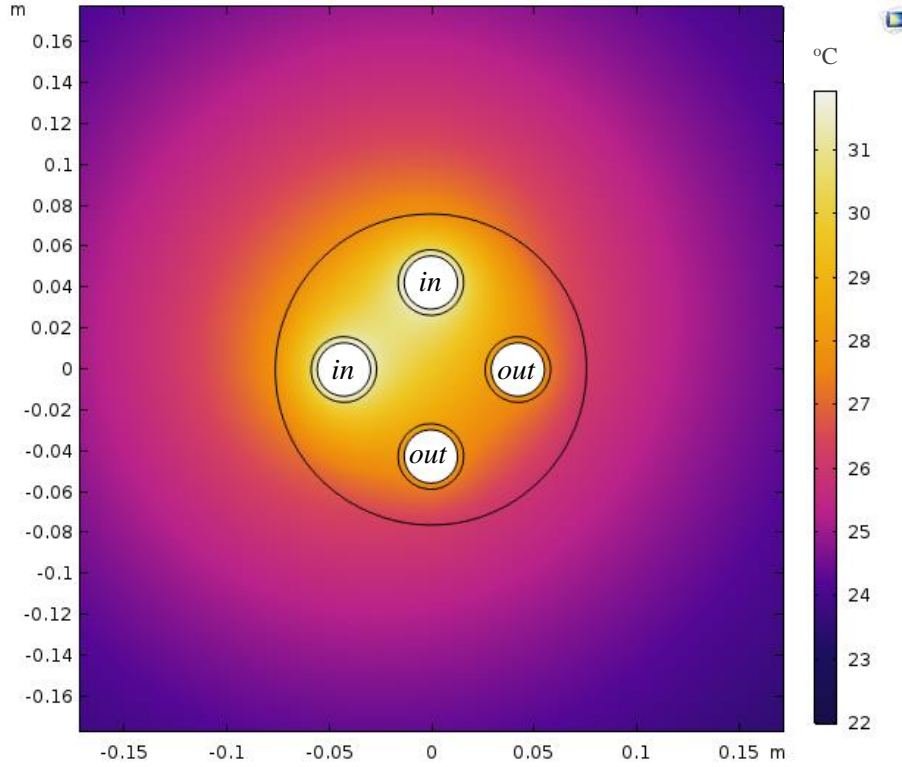


**Figure 3.1.** Temperature distribution in a double U-tube BHE and the surrounding ground.

where  $R_{gt}$  is the thermal resistance of the grout and  $R_p$  refers to the thermal resistance of the U-tube pipe and is computed as:

$$R_p = R_{cond} + R_{conv} \quad (3.5)$$

where  $R_{cond}$  and  $R_{conv}$  stand for the conductive and convective thermal resistances in the pipe, respectively, and are given by:

$$R_{cond} = \frac{1}{2\pi k_p} \ln \frac{D_e}{D_i} \quad (3.6)$$

$$R_{conv} = \frac{1}{\pi D_i h} \quad (3.7)$$

where  $D_e$  and  $D_i$  are the external and internal diameters of the pipe, illustrated in figure 3.2, and  $h$  is the heat transfer coefficient. In section 3.3, more details can be found about the heat transfer coefficient  $h$  and the convection process inside the tubes.



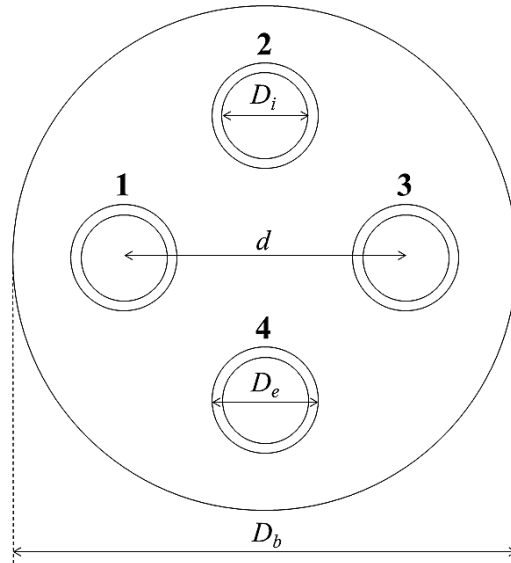


Figure 3.2. Cross section of a double U-tube BHE.

### 3.1 Heat transfer models for the BHE thermal resistance

In the design of GCHP systems, the heat transfer process from the fluid to the ground is influenced by the BHE thermal resistance, i.e. the thermal resistance between the fluid and the BHE surface, and also by the thermal interference resistance between the tubes (thermal short-circuiting effect). Heat transfer models to determine the thermal resistance of BHE can be divided into two groups:

- Empirical models
- Theoretical models



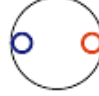
Empirical models, recommended for a simplified design of vertical ground heat exchangers, are often presented as a 1D model, which considers the U-tube pipe as a single “equivalent” pipe [63, 64]. In this case, a complicated multi-dimensional problem reduces to a 1D problem by simplifying assumption of equivalent pipe instead of a two-geometric region. In this model, not only the axial heat flow in the pipe walls and in the grout is negligible, but also the thermal capacitance of the BHE is inconsiderable, since the BHE dimensional scale is much smaller than the infinite surrounding ground [44]. Hence, the heat transfer process is considered as a steady-state 1D one.

In fact, empirical models may have several empirical constants, which may be determined by fitting experimental or computational data. A well-known 1D model for the single U-tube BHE thermal resistance, based on the use of shape-factor concept in heat conduction, is [65]:

$$R_b = \frac{1}{\beta_0 k_{gt} (r_b / r_e)^{\beta_1}} \quad (3.8)$$

where  $\beta_0$  and  $\beta_1$  are geometrical parameters depending on the U-tube configuration,  $r_b$  and  $r_e$  are the BHE radius and the external radius of pipe, respectively. The shape factors are calculated for three patterns of the shank spacing (the distance between the centers of opposite tubes) and can be obtained by means of the table below [66]:

**Table 3.1.** Shape factors for three different patterns of the shank spacing [66].

Coefficient	Pattern		
			
$\beta_0$	14.4509	17.4427	21.9059
$\beta_1$	-0.8176	-0.6052	-0.3796

One another expression for the 1D thermal resistance of a single U-tube is [64]:

$$R_b = \frac{1}{2\pi k_{gt}} \ln \frac{r_b}{\sqrt{nr_e}} \quad (3.9)$$

where  $n$  stands for the number of pipes in BHE.

Although the 1D empirical models are convenient and applicable for most engineering problems (except the short-term dynamic response analysis), they provide inadequate insight into the underlying heat transfer processes. Furthermore, these oversimplified models are incapable of evaluating the impact of thermal processes such as thermal short-circuiting between the U-tubes on the performance of the BHE [44].

The theoretical models are divided into 2D and 3D/quasi-3D models. Hellström [62] derived analytical 2D solutions of the thermal resistance of a single U-tube BHE, in the cross section perpendicular to the axis of BHE. Considering a 2D cross section of a BHE, the temperature of the fluid in tubes is expressed as a superposition of the two separate temperature responses caused by the corresponding heat fluxes, namely,

$$\begin{cases} T_{f1} - T_s = R_{11}q_1 + R_{12}q_2 \\ T_{f2} - T_s = R_{12}q_1 + R_{22}q_2 \end{cases} \quad (3.10)$$

where  $R_{11}$  and  $R_{22}$  are the thermal resistances between the fluid flowing in the corresponding tube and the BHE external surface, and  $R_{12}$  is the thermal resistance between two adjoining tubes. The steady-state conductive heat transfer problem was solved by means of the both line-source approximation and multipole method, latter proposed by Bennet et al. [67]. The line-source approximation yields:

$$R_b = \frac{1}{2}R_p + \frac{1}{4\pi k_{gt}} \ln \left[ \frac{r_b^2}{d r_e} \left( \frac{r_b^4}{r_b^4 - \frac{d^4}{16}} \right)^\sigma \right] \quad (3.11)$$

where  $d$  is the shank spacing and  $\sigma$  is a dimensionless parameter and is defined as:

$$\sigma = \frac{k_{gt} - k_g}{k_{gt} + k_g} \quad (3.12)$$

It is noticeable that via the dimensionless parameter  $\sigma$ , the thermal conductivity of the ground enters the 2D expression, so that it may affect the steady-flux heat transfer process within the BHE. This significant effect is neglected in empirical models, where a constant temperature boundary condition is imposed on the BHE wall. The 2D thermal resistance for single U-tube by means of the first-order multipole approximation gives:

$$R_b = \frac{1}{2}R_p + \frac{1}{4\pi k_{gt}} \ln \left[ \frac{r_b^2}{d r_e} \left( \frac{r_b^4}{r_b^4 - \frac{d^4}{16}} \right)^\sigma \right] - \frac{\left[ \frac{r_e}{d} \left( 1 - \frac{\frac{\sigma d^4}{4}}{r_b^4 - \frac{d^4}{16}} \right) \right]^2}{\frac{1 + 2\pi k_{gt} R_p}{1 - 2\pi k_{gt} R_p} + \frac{r_e^2}{d^2} \left[ 1 + \frac{\sigma d^4 r_b^4}{\left( r_b^4 - \frac{d^4}{16} \right)^2} \right]} \quad (3.13)$$

It can be seen that the difference between the line-source approximation and the multipole method lies in the term after minus in equation (3.13). As reported by Hellström [62], the sensitivity study between these models revealed that the error of the line-source approximation is on the order of 10%, while the first-order multipole approximation yields roughly 1% deviation from the exact

value. Recently, Claesson and Hellström [68] have reformulated the multipole method to calculate the BHE thermal resistance.

Another 2D analytical solution of the BHE thermal resistance by Hellström [62] is for the double U-tube BHE, and is based on assumption of identical temperature and heat fluxes for all pipes. The expression for the symmetrically disposed double U-tube BHE is given by:

$$R_b = \frac{1}{2\pi k_{gt}} \left[ \ln\left(\frac{D_b}{D_e}\right) - \frac{3}{4} + \left(\frac{d}{D_b}\right)^2 - \frac{1}{4} \ln\left(1 - \frac{d^8}{D_b^8}\right) - \frac{1}{2} \ln\left(\frac{\sqrt{2}d}{D_e}\right) - \frac{1}{4} \ln\left(\frac{2d}{D_e}\right) \right] + \frac{R_p}{4} \quad (3.14)$$

where  $D_b$  refers to the diameter of BHE.

Sharqawy et al. [69] proposed a new expression to estimate the BHE thermal resistance in the cross section perpendicular to the borehole, by means of best-fit correlation on the basis of 2D finite element results instead of experimental data:

$$R_b = \frac{1}{2\pi k_{gt}} \left[ \frac{-1.49}{\lambda_2} + 0.656 \ln(\lambda_1) + 0.436 \right] \quad (3.15)$$

where  $\lambda_1$  and  $\lambda_2$  are non-dimensional geometrical parameters.

It should be pointed out since mentioned models do not take into account heat transfer on the axial flow of fluid, it is impossible to distinguish the downward and upward pipes. Moreover, with assumption of identical (invariant) temperature for all pipes, the impact of thermal interference between the U-tube legs (thermal short-circuiting) remains hidden. To address the variation of the temperature in downward and upward pipes, Hellström [62] proposed two quasi-3D models, one employs a uniform flux boundary condition at BHE wall and another employs a uniform temperature boundary condition.

On the basis of the model proposed by Hellström [62], Zeng et al. [70] developed an analytical quasi-3D model for the effective thermal resistance of both single and double U-tube BHEs, for different configurations of the tubes, which takes into account the fluid temperature variation along the BHE, namely, thermal short-circuiting effect. They considered steady-state heat transfer within the BHE and assumed that the temperature of the external surface of the BHE is uniform. They neglected the heat conduction in the vertical direction, but considered the energy balance in the vertical direction for the fluid flow. By this scheme, they determined analytical expressions of the distribution of the difference between the bulk fluid temperature along the channels and temperature of the BHE external surface. Finally, they introduced expressions of the effective thermal resistance  $R_{b,eff}$ , based on the determined distributions of the bulk fluid temperature.

They presented rather complex expressions of the fluid outlet temperature, and of the dimensionless bulk temperatures of the downward and upward flows, by considering various

configurations of the tubes. They reported the following analytical expressions of thermal resistances between tubes and BHE surface and of those between pairs of tubes, obtained by means of the line-source approximation:

$$R_{11} = \frac{1}{2\pi k_{gt}} \left[ \ln \left( \frac{D_b}{D_e} \right) - \frac{k_{gt} - k_g}{k_{gt} + k_g} \ln \left( \frac{D_b^2 - d^2}{D_b^2} \right) \right] + R_p \quad (3.16)$$

$$R_{12} = \frac{1}{2\pi k_{gt}} \left[ \ln \left( \frac{D_b}{\sqrt{2}d} \right) - \frac{k_{gt} - k_g}{2(k_{gt} + k_g)} \ln \left( \frac{D_b^4 - d^4}{D_b^4} \right) \right] \quad (3.17)$$

$$R_{13} = \frac{1}{2\pi k_{gt}} \left[ \ln \left( \frac{D_b}{2d} \right) - \frac{k_{gt} - k_g}{k_{gt} + k_g} \ln \left( \frac{D_b^2 - d^2}{D_b^2} \right) \right] \quad (3.18)$$

where,  $R_{11}$  is the thermal resistance between the fluid flowing in any tube and the BHE external surface,  $R_{12}$  is the thermal resistance between two adjoining tubes, and  $R_{13}$  is the thermal resistance between two opposite tubes.

By means of Laplace transformation, a set of four linear differential equations for the energy equilibrium was solved and temperature profiles in four individual tubes along the BHE depth were obtained. The following expression of the effective BHE thermal resistance was proposed:

$$R_{b,eff} = \frac{L}{4\dot{m}c_{p,f}} \frac{1 + \Theta_{out}}{1 - \Theta_{out}} \quad (3.19)$$

where  $\dot{m}$ ,  $c_{p,f}$ , and  $\Theta_{out}$  refer to the mass flow rate in each tube, the specific heat capacity at constant pressure of the fluid, and the dimensionless outlet temperature.

In this thesis, in order to validate the results of 3D simulations, estimations of the fluid temperature distribution obtained by applying the analytical method of Zeng et al. [70] were compared to the simulation results. Since the problem under study here is the analysis of double U-tube BHE, we focused on the case denoted by Zeng et al. [70] as 1-3, 2-4 configuration.

The system of differential equations of Zeng et al. [70] was solved independently by means of the mathematical software WOLFRAM MATHEMATICA. The solution determined is:

$$\Theta_d(Z) = \frac{(2\Sigma_1 + \Sigma_{12}) \cosh \left[ \frac{\sqrt{2\Sigma_1 + \Sigma_{12}}(Z-1)}{\Sigma_1 \sqrt{\Sigma_{12}}} \right] - \sqrt{\Sigma_{12}} \sqrt{2\Sigma_1 + \Sigma_{12}} \sinh \left[ \frac{\sqrt{2\Sigma_1 + \Sigma_{12}}(Z-1)}{\Sigma_1 \sqrt{\Sigma_{12}}} \right]}{(2\Sigma_1 + \Sigma_{12}) \cosh \left[ \frac{\sqrt{2\Sigma_1 + \Sigma_{12}}}{\Sigma_1 \sqrt{\Sigma_{12}}} \right] + \sqrt{\Sigma_{12}} \sqrt{2\Sigma_1 + \Sigma_{12}} \sinh \left[ \frac{\sqrt{2\Sigma_1 + \Sigma_{12}}}{\Sigma_1 \sqrt{\Sigma_{12}}} \right]} \quad (3.20)$$

$$\Theta_u(Z) = \frac{(2\Sigma_1 + \Sigma_{12}) \cosh \left[ \frac{\sqrt{2\Sigma_1 + \Sigma_{12}}(Z-1)}{\Sigma_1 \sqrt{\Sigma_{12}}} \right] + \sqrt{\Sigma_{12}} \sqrt{2\Sigma_1 + \Sigma_{12}} \sinh \left[ \frac{\sqrt{2\Sigma_1 + \Sigma_{12}}(Z-1)}{\Sigma_1 \sqrt{\Sigma_{12}}} \right]}{(2\Sigma_1 + \Sigma_{12}) \cosh \left[ \frac{\sqrt{2\Sigma_1 + \Sigma_{12}}}{\Sigma_1 \sqrt{\Sigma_{12}}} \right] + \sqrt{\Sigma_{12}} \sqrt{2\Sigma_1 + \Sigma_{12}} \sinh \left[ \frac{\sqrt{2\Sigma_1 + \Sigma_{12}}}{\Sigma_1 \sqrt{\Sigma_{12}}} \right]} \quad (3.21)$$

where  $Z = z/L$  is the dimensionless vertical coordinate,  $\Theta_d$  and  $\Theta_u$  are the dimensionless bulk temperatures of the fluid going down (descending flow) and of the fluid going up (ascending flow),  $\Sigma_1$  and  $\Sigma_{12}$  are the dimensionless parameters defined in equation (17) of Zeng et al. [70], namely:

$$\begin{cases} \Sigma_1 = \frac{\dot{m} c_{p,f}}{L} (R_{11} + R_{13} + 2R_{12}) \\ \Sigma_{12} = \frac{\dot{m} c_{p,f}}{L} \frac{(R_{11} - R_{13})(R_{11} + R_{13} + 2R_{12})}{R_{12} + R_{13}} \end{cases} \quad (3.22)$$

where  $R_{11}$ ,  $R_{12}$  and  $R_{13}$  are determined through equations (3.16-3.18). The dimensionless temperatures  $\Theta_d$  and  $\Theta_u$  are defined as:

$$\begin{cases} \Theta_d(Z) = \frac{T_{f,d}(Z) - T_s}{T_{f,in} - T_s} \\ \Theta_u(Z) = \frac{T_{f,u}(Z) - T_s}{T_{f,in} - T_s} \end{cases} \quad (3.23)$$

where  $T_{f,d}$  and  $T_{f,u}$  are the bulk temperatures of the fluid going down and of that coming up,  $T_{f,in}$  is the inlet fluid temperature, and  $T_s$  is the temperature of the BHE surface, considered as uniform and constant by Zeng et al. [70]. In using of equations (3.20-3.23), it was assumed that, at each instant of time,  $T_s$  is equal to the mean temperature of the BHE surface determined by our finite element simulations.

Recently, Conti et al. [71] proposed both 2D and quasi-3D models for the thermal resistance of double U-tube BHEs, which consider different configurations of the tubes. The quasi-3D model employs an approach similar to that of Zeng et al. [70], and takes into account the axial variation of the fluid temperature along the BHE depth. Moreover, they proposed a useful final expression for the 2D BHE thermal resistance of a double U-tube BHE, which is given by:

$$R_b = \frac{1}{8\pi k_{gt}} \left[ \ln \left( \frac{D_b}{D_e} \right) + 2 \ln \left( \frac{D_b}{\sqrt{2}d} \right) + \ln \left( \frac{D_b}{2d} \right) - \sigma \left( \frac{D_b^8 - d^8}{D_b^8} \right) \right] + \frac{R_p}{4} \quad (3.24)$$

The authors stated that their 2D correlation is different from that reported by Hellström [62], also cited by Zeng et al. [70], and in some cases the relative deviation between two expressions may be significant, depending on the geometrical and thermophysical variables.

Other recent models to determine the thermal resistance of a BHE, called TRCMs (Thermal Resistance and Capacity Models), add the thermal capacity of the BHE components to the resistance model. TRCMs may reduce the time scale  $t_b$  to some extent, since they do not assume the steady-state condition. Numerical simulations to determine the thermal resistance of BHE usually employ the fully discretized models to be solved by computers. Therefore, calculation of a fully discretized 3D transient heat transfer process in BHE requires extensive computational time, even with aid of the powerful computers. TRCMs reduce significantly the number of the elements representing the BHE, without the drawback of obtaining poor results. However, TRCMs are not yet widely used to analyze heat transfer processes in BHEs.

Bauer et al. [55, 72] utilized both 2D and 3D TRCMs in the analysis of heat transfer in a BHE. In case of the 3D model, they validated their model against a fully discretized finite element model. The comparison showed that their model is well-suited for incorporation into a transient energy simulation program. Finally, the model was used to evaluate TRT data by the parameter estimation technique.

### 3.2 Estimation of the BHE thermal resistance

All the design methods, mentioned in chapter 2, require the knowledge of the undisturbed ground temperature, of the thermal conductivity and of the thermal diffusivity of the ground, as well as of the BHE thermal resistance per unit length. The thermal resistance of the BHE can be estimated by knowledge of the following parameters: bulk fluid temperature, BHE external surface temperature, and thermal power per unit length exchanged between BHE and ground.

Two definitions of the BHE thermal resistance per unit length are usually considered in the literature. The first, that we denote by  $R_{b,2D}$ , refers to a BHE cross section and is defined as:

$$R_{b,2D} = \frac{T_f - T_s}{q_l} \quad (3.25)$$

where  $T_f$  is the bulk fluid temperature in a BHE cross section (averaged between tubes),  $T_s$  is the mean temperature of the BHE surface in the same section, and  $q_l$  is the thermal power per unit length exchanged between BHE and ground in the neighborhood of that section, positive if supplied to the ground. If the thermal conductivity of the grout is known,  $R_{b,2D}$  can be easily calculated by performing a 2D numerical simulation of the BHE cross section, or by employing approximate expressions cited in the previous section (3.1).

The second definition, called *effective* thermal resistance, is given by:

$$R_{b,eff} = \frac{T_{f,ave} - T_{s,m}}{q_{l,m}} \quad (3.26)$$

where  $T_{f,ave}$  is the arithmetic mean of inlet and outlet fluid temperatures, and is defined as:

$$T_{f,ave} = \frac{T_{f,in} + T_{f,out}}{2} \quad (3.27)$$

$T_{s,m}$  is the mean temperature of the external surface of the BHE and  $q_{l,m}$  is the mean thermal power per unit length exchanged between BHE and ground, positive if supplied to the ground. It is clear that both cases are approximations of real conditions. As pointed out by Lamarche et al. [56], another possible definition is:

$$R_{b,3D} = \frac{T_{f,m} - T_{s,m}}{q_{l,m}} \quad (3.28)$$

where  $T_{f,m}$  is the real mean value of the bulk fluid temperature, namely:

$$T_{f,m} = \frac{1}{2L} \left( \int_0^L T_{f,d}(z) dz + \int_0^L T_{f,u}(z) dz \right) \quad (3.29)$$

where  $L$  is the BHE length,  $z$  is the vertical coordinate directed downwards,  $T_{f,d}$  is the local bulk temperature of the descending fluid (going down), and  $T_{f,u}$  is the local bulk temperature of the ascending fluid (coming up). Although equation (3.28) would be the natural 3D extension of equation (3.25), it is usually replaced by equation (3.27), because  $T_{f,ave}$  can be easily measured.

We will show in Chapter 7 that, while  $R_{b,3D}$  is practically coincident with the 2D thermal resistance of a BHE cross section, at low flow rates  $R_{b,eff}$  is strongly dependent on the distribution of the fluid bulk temperature along the tubes. Indeed, on account of the thermal short-circuiting between the descending and ascending flows, the bulk temperature distribution is nonlinear and considerable differences between  $R_{b,3D}$  and  $R_{b,eff}$  may occur.

The thermal resistance of a BHE is usually determined through a TRT performed as recommended by ASHRAE [16]. In a TRT, first one measures  $T_g$ , as suggested by ASHRAE [16] and Gehlin [73]. Then, hot water produced by electric resistances is circulated through the tested BHE, so that heat is injected into the ground. The basic monitored quantities are the heating power per unit BHE length,  $q_{l,m}$ , averaged along the BHE length, the inlet bulk fluid temperature,  $T_{f,in}$ , the outlet bulk fluid temperature,  $T_{f,out}$ , and the volume flow rate,  $\dot{V}$ . The evaluation of a TRT is usually performed by the infinite line-source model, which employs as input data  $q_{l,m}$  and a plot of  $T_{f,ave} - T_g$  versus the natural logarithm of time  $t$  [73-75]. The slope of the plot is equal to



$q_{l,m}/(4\pi k_g)$ , and yields the ground thermal conductivity; the value of  $T_{f,ave} - T_g$  for  $\ln t = 0$  yields a relation between  $q_{l,m}$ ,  $k_g$ ,  $\alpha_g$  and  $R_{b,eff}$ . In general,  $\alpha_g$  is estimated and the relation is employed to determine  $R_{b,eff}$ . The value obtained is then usually interpreted as a value of  $R_{b,2D}$ .

As reported by Marcotte and Pasquier [66], the thermal short-circuiting between the fluid going down and that coming up can cause a relevant difference between  $T_{f,m}$  and  $T_{f,ave}$ , so that confusing  $R_{b,eff}$  with  $R_{b,2D}$  can yield a significant overestimation of the latter. They pointed out that the difference between  $T_{f,m}$  and  $T_{f,ave}$  yields an overestimation of the BHE thermal resistance estimated through TRTs. Moreover, they performed 3D finite element evaluations of the mean fluid temperature of single U-tube BHEs in different working conditions and proposed the following expression, called  $p$ -linear average, to evaluate  $T_{f,m} - T_g$  as a function of  $T_{f,in} - T_g$  and  $T_{f,out} - T_g$  for this kind of BHEs:

$$T_{f,m} - T_g = \lim_{p \rightarrow -1} \frac{p \left( |T_{f,in} - T_g|^{p+1} - |T_{f,out} - T_g|^{p+1} \right)}{(1+p) \left( |T_{f,in} - T_g|^p - |T_{f,out} - T_g|^p \right)} \quad (3.30)$$

The improvements of the  $p$ -linear average model in order to determine the time dependence of  $p$  were proposed by Zhang et al. [76, 77].

Some other studies on the real distribution of  $T_f$  along  $z$  and on the errors in the evaluation of  $R_{b,2D}$  due to the approximation of  $T_{f,m}$  with  $T_{f,ave}$  were carried out in recent years.

Beier [78] developed an analytical model to determine the distribution of the bulk fluid temperature in the late-time period of TRTs performed on single U-tube BHEs, and presented a plot illustrating the percent error due to the assumption  $T_{f,m} = T_{f,ave}$  in the evaluation of  $R_{b,2D}$  through TRTs. Later, Beier and Spitler [79] extended the applicability of this model to the early part of TRTs and to other working conditions.

In chapter 7 of this study, the effects of the temperature distribution on the thermal resistance of a BHE and the relations between  $R_{b,eff}$ ,  $R_{b,3D}$  and  $R_{b,2D}$  are investigated by means of 2D and 3D finite element simulations.

### 3.3 Convective heat transfer inside tubes

Convective heat transfer between the circulating fluid and the inner surface of U-tubes is one of the three local heat transfer phenomena in the BHE. The heat transfer process between the circulating fluid and the wall of the pipe is a rather complicated process. It strongly depends on the fluid flow conditions, namely, the velocity and temperature distribution. Vice versa, the fluid flow conditions would be affected by the heat transfer magnitude and its variation on the pipe wall.

The circulating fluid is often water. However, in low-temperature applications, where the temperature of the circulating fluid would be lower than 0 °C, amounts of ethylen/propylen-glycol is added to the water as anti-freeze agent. Indeed, the mixture of water and ethylen/propylen-glycol

has a lower heat transfer coefficient, for a given flow rate. The relevant thermophysical properties of the circulating fluid are functions of pressure and temperature. For the fluid circulating in a BHE, the pressure variation is not of the order that affects the thermophysical properties significantly. The thermal conductivity  $k_f$ , the density  $\rho_f$ , the heat capacity at constant pressure  $c_{p,f}$  and the dynamic viscosity  $\mu_f$  of the fluid are the thermophysical properties which affect the thermal process.

The boundary conditions along the flow channel have a considerable impact on the convective heat transfer. Generally, the two extreme cases for the boundary conditions in analytical and experimental studies are constant wall temperature and constant heat flux along the length of the channel. The heat transfer coefficient obtained at constant heat flux is always greater than that for constant wall temperature. This difference is significant in laminar flow, but becomes quite negligible in turbulent regime [80]. In the case of constant wall temperature, the fluid temperature  $T_f$  satisfies:

$$\dot{V} \rho_f c_{p,f} \frac{dT_f}{dz} = -\frac{1}{R} (T_f - T_p) \quad (3.31)$$

where  $\rho_f c_{p,f}$  stands for the volumetric heat capacity,  $\dot{V}$  is the volume flow rate,  $R$  is the thermal resistance between the bulk fluid and the pipe wall, and  $T_p$  is the temperature of the pipe wall.

With assumption of constant inlet temperature  $T_{in}$ , the fluid temperature along the flow channel in  $z$  direction can be obtained as:

$$T_f(z) = T_p + (T_{in} - T_p) e^{-z/(R\dot{V}\rho_f c_{p,f})} \quad (3.32)$$

In the case of constant heat flux, it gives:

$$\dot{V} \rho_f c_{p,f} \frac{dT_f}{dz} = q \quad (3.33)$$

$$T_f(z) = T_{in} - \frac{qz}{\dot{V} \rho_f c_{p,f}} \quad (3.34)$$

The development of the temperature profile, i.e. the thermal boundary layer, in fluid flow is similar to the development of the hydrodynamic boundary layer. The hydrodynamic boundary layer develops as the fluid flows along the duct, and it increases in thickness until a fully developed velocity profile has been established. In a similar way, for the thermal boundary layer, at the entrance of the pipe, the temperature profile is uniform. As the fluid flows along the channel, the thermal layer increases in thickness until heat is transferred to/from the fluid in the center of the

pipe [62, 81]. The thermal entry length  $L_{th}$  for laminar flow with fully developed velocity profile at the entrance of the channel can be given as [82]:

$$\begin{cases} L_{th} = 0.0335RePrD & \text{for constant wall temperature} \\ L_{th} = 0.0431RePrD & \text{for constant heat flux} \end{cases} \quad (3.35)$$

where  $Re$  and  $Pr$  are Reynolds and Prandtl numbers, respectively.

For turbulent flow, the thermal and hydrodynamic entry lengths are characteristically much shorter than for laminar flow. The turbulent flow becomes fully developed after just 10-15 pipe diameters. Therefore, the entrance effects are frequently neglected in heat transfer design [62, 80].

The heat transfer between the circulating fluid and pipe wall is usually determined by the dimensionless Nusselt number  $Nu$ , which is defined as:

$$Nu = \frac{hD_i}{k_f} \quad (3.36)$$

Depending on the type of convective heat transfer, the Nusselt number is a function of two dimensionless parameters: the Rayleigh number  $Ra$  and the Prandtl number  $Pr$  for free/natural convection; the Reynolds number  $Re$  and the Prandtl number  $Pr$  for forced convection. These dimensionless numbers are defined as:

$$Ra = Gr Pr = \frac{\bar{g} L^3}{\alpha_f \nu_f} \beta \Delta T \quad (3.37)$$

$$Pr = \frac{\nu_f}{\alpha_f} \quad (3.38)$$

$$Re = \frac{\rho_f u_f D_i}{\mu_f} \quad (3.39)$$

where  $\bar{g}$  is the gravitational acceleration constant,  $\nu_f$  is the kinematic viscosity,  $u_f$  is the fluid velocity and  $Gr$  refers to the Grashof number which is defined as:

$$Gr = \frac{\bar{g} L^3}{\nu_f^2} \beta \Delta T \quad (3.40)$$

The Nusselt number depends on the flow conditions inside the channel. In other words, the flow regime (laminar, transition zone or turbulent) can significantly affect the heat transfer coefficient and, consequently, the Nusselt number. In fact, the regime of the flow is determined by

means of the Reynolds number:  $Re < 2300$  for laminar flow,  $Re > 10\,000$  for fully developed turbulent flow and the range between them is considered as a transition zone. In laminar flow, streamlines and particles path are in parallel layers and there is not disruption between the flow layers. In this case, the heat transfer coefficient is rather small, hence, the laminar flow gives rise to a relevant thermal resistance between the circulating fluid and the wall of the channel. The laminar flow regime is unsuitable for industrial heat exchangers. However, as it pointed out by Hellström [62], the relative influence of the heat transfer coefficient is smaller for a ground heat exchanger, because of the large thermal resistance between the duct wall and the ground.

In contrast to the laminar regime, when the flow is turbulent, chaotic changes in flow velocity and pressure can be observed. Due to eddy motions, the fluid is constantly mixed and the temperature becomes rather uniform around the channel. A higher velocity of the fluid results in a thinner boundary layer, which enhances the convective heat transfer process. Therefore, for high values of the Reynolds number, the thermal resistance between the circulating fluid and the pipe wall is negligible. Indeed, when the fluid flow is in transition zone or fully turbulent regime, the thermal resistance of the pipe wall is dominant. Therefore, the overall resistance varies a little if the fluid has a high Reynolds number value ( $Re > 10\,000$ ), compared to that which occurs with moderate values of the Reynolds number ( $Re = 3000$ ) [9].

As mentioned by Kreith [81], commercial heat-exchange equipment employs flow velocities corresponding to a Reynolds number of about 50 000. However, in ground heat exchangers, where the heat transfer coefficient in the tube is less important, the optimum flow velocity for the heat exchange is lower, when economical aspects are taken into account [62].

In the application of the ground heat exchangers, fluid flow is usually turbulent, particularly for standard volume flow rates. To clarify the flow conditions considered in the present study, the thermophysical properties and the fluid flow characteristics of a sample case analyzed in our simulations, are reported in table 3.2. The highest and lowest volume flow rates are presented, in summer working condition, in order to illustrate limit values of the flow condition inside the tubes.

The estimation of the Nusselt number and the heat transfer coefficient in turbulent regime can be performed by means of different formulas in the literature. One of the most common formulas proposed for turbulent flow inside a circular tube is Dittus-Boelter's formula [83]:

$$Nu = 0.023Re^{4/5}Pr^n \quad (3.41)$$

When the fluid is being heated  $n=0.4$  and when is being cooled  $n=0.3$ . As it was claimed by Rohsenow et al. [80], this correlation is a good approximation to the available experimental data when the ratio of length to diameter is greater than 60 and  $0.7 \leq Pr \leq 120$ ,  $10\,000 \leq Re \leq 120\,000$ .

**Table 3.2.** Thermophysical properties and fluid flow characteristics in a simulation performed in the present study.

$T_{in}$	$\dot{V}$	$\rho_f$	$\mu_f$	$c_{p,f}$	$k_f$	$Pr$	$Re$	$Nu$	$h$
(°C)	(dm <sup>3</sup> min <sup>-1</sup> )	(kg m <sup>-3</sup> )	(mPa s)	(J kg <sup>-1</sup> K <sup>-1</sup> )	(W m <sup>-1</sup> K <sup>-1</sup> )	-	-	-	-
32	12	995.03	0.76456	4179.5	0.6187	5.165	6373.3	53.65	1276.58
32	24	995.03	0.76456	4179.5	0.6187	5.165	12746.5	92.33	2197.11

Another well-known formula to determine the Nusselt number in turbulent regime was proposed by Gnielinski [80], which also takes into account the transition zone:

$$Nu = \frac{(fr/2)(Re - 1000)Pr}{1 + 12.7(fr/2)^{1/2}(Pr^{2/3} - 1)} \quad (3.42)$$

where  $fr$  is the friction factor and is determined as:

$$fr = [1.58 \ln(Re) - 3.28]^{-2} \quad (3.43)$$

In the present study, the Nusselt number was calculated by the correlation for the fully developed forced convection flow, proposed by Churchill [84]. The overall equation for the fully developed condition is presented as:

$$(Nu)^{10} = (Nu_l)^{10} + \left[ \frac{e^{(2200-Re)/365}}{(Nu_{lc})^2} + \left( \frac{1}{Nu_0^0 + \frac{0.079 Re \sqrt{fr} Pr}{(1 + Pr^{4/5})^{5/6}}} \right)^2 \right]^{-5} \quad (3.44)$$

where  $Nu_l$ ,  $Nu_{lc}$  and  $Nu_0^0$  stand for the laminar Nusselt number, the laminar Nusselt number at  $Re = 2100$ , the asymptotic Nusselt number where  $Re \rightarrow 2100$  and  $Pr \rightarrow 0$ . The friction factor  $fr$  is defined as:

$$\frac{1}{fr} = \left( \frac{1}{\left[ \left( \frac{8}{Re} \right)^{10} + \left( \frac{Re}{36500} \right)^{20} \right]^{0.5} + \left( 2.21 \ln \left[ \frac{Re}{7} \right] \right)^{10}} \right)^{1/5} \quad (3.45)$$

In addition, following expressions were proposed for Nusselt number in turbulent and transient regimes:

$$Nu_t = Nu_0^0 + \frac{0.079 Re \sqrt{fr} Pr}{(1 + Pr^{4/5})^{5/6}} \quad (3.46)$$

$$Nu_{tr} = Nu_{lc} e^{(Re-2200)/730} \quad (3.47)$$

It should be pointed out that in the laminar regime,  $Re < 2100$ , for fully developed conditions  $Nu_t = 3.657$  for uniform wall temperature boundary condition, and  $Nu_t = 4.364$  for uniform heat flux boundary condition, and  $Nu_t = Nu_{lc}$ .

The boundary condition of uniform wall heat flux was considered for the present study.

Employing empirical correlations often yields a rough estimation of heat transfer coefficient, due to the inherent complexity of convective heat transfer. However, except in the laminar flow, the impact of such a rough estimate on the calculation of the thermal resistance is negligible, since the convective thermal resistance accounts for only 2-3% of  $R_b$  in most situations [85].



# *Chapter 4*

---

## *Numerical method*





## *Numerical method*

---

In the present chapter, the numerical method employed in this study is presented. It provides a review on finite element analysis method and on the software utilized. It contains explanations regarding the mathematical modeling, model validation, and boundary and working conditions. Moreover, it renders some explanatory notes on the program solver, convergence results, meshes employed and grid independence.

### **4.1 Finite element analysis**

The finite element approach is a numerical method to solve various problems in engineering applications, physics and etc. The finite element method formulates the problem in a set of algebraic equations. In fact, the method yields approximate values of the unknowns at a discrete number of points over the domain under study. The problem can be solved by subdividing a large domain into smaller elements, which are called finite elements. By subdividing the problem into smaller and simpler parts, the large and complex geometry can be represented in a more accurate and simpler way, where mathematical equations help to predict the behavior of each element. These simple equations are then assembled into a system of equations for the whole geometry. Apart from the quality of approximations, one of the most remarkable features of the finite element

method is the ability of handling complex geometries. As reported by Reddy [86], the finite element subdivision of the entire geometry into simpler parts has several advantages such as easy representation of the total solution, accurate representation of complex geometries and capture of the local effects.

In general, the finite element method is characterized by the following items:

- Variational formulation, such as Galerkin method or discontinuous Galerkin method
- Discretization strategy, such as p-version or x-FEM
- Solution algorithm(s), such as direct or iterative solver
- Procedures of post-processing, such as convergence and error estimation

From a historical point of view, finite element analysis is traditionally a branch of solid mechanics. The early development of the finite element method can be traced back to the early 1940s. It was originated from the solving of the elasticity and structural analysis problem in civil and aeronautical engineering. However, nowadays, it is used for solving multiphysics problems and can be applied to the wide range of engineering problems such as thermal analysis, electrical analysis, solid mechanics, structural analysis, vibration and etc.

Due to the 3D nature of the thermal field perturbed by an operating BHE system, a 3D finite element code is suitable to simulate coupled multiphysics processes such as hydraulic, thermal, and even elastic processes, under transient conditions. In addition, the finite element approach permits a flexible mesh generation for the complex geometry of the BHE. By employing the finite element method, the thermal and hydraulic properties of each element in the computational domain can be modified, Dirichlet and Neumann boundary conditions can be applied, and the transient behavior of selected parameters or boundary conditions can be simulated employing time-dependent functions [75]. Hence, finite element based simulations are frequently adopted to analyze the thermal and hydraulic behavior of the BHE [34, 56, 66, 87, 88].

Numerical simulations in the present study are performed by means of the finite element method implemented in COMSOL Multiphysics environment. COMSOL Multiphysics is a comprehensive simulation package employing finite element analysis to solve various multiphysics problems in engineering, physics and chemistry.

The main advantage of COMSOL Multiphysics over other finite element analysis programs is its ability to solve the coupled phenomena. Indeed, in many engineering applications there are multiphysics problems and the solution of each individual physical problem cannot be obtained independently. For example, COMSOL Multiphysics is able to simulate heat transfer-mechanical engineering problems with a high level of accuracy.

The general procedure of modeling in COMSOL Multiphysics starts by defining the geometry under study. After assigning the values of the material properties in all subdomains, the corresponding physics for each subdomain is defined. The entire geometry is then meshed and the study setting is determined. Solving the problem, post-processing and obtaining the results are next

steps. However, many other processes in between can be added to the mentioned steps. Figure 4.1 illustrates the COMSOL Multiphysics environment in desktop.

## 4.2 Numerical model

In order to describe correctly all aspects of the problem, such as the real BHE geometry, the vertical heat transport in and outside the BHE, the vertical gradient of undisturbed ground temperature, the transient fluid transport inside the tubes, the thermal short-circuiting effect between the upward and downward flow, and the boundary conditions at the upper and lower boundaries, only 3D numerical models are able to simulate the transient heat and mass transfer processes in BHE with satisfactory accuracy. However, the main disadvantage of fully discretized 3D models is their extensive computational time and effort, even with powerful computers [55].

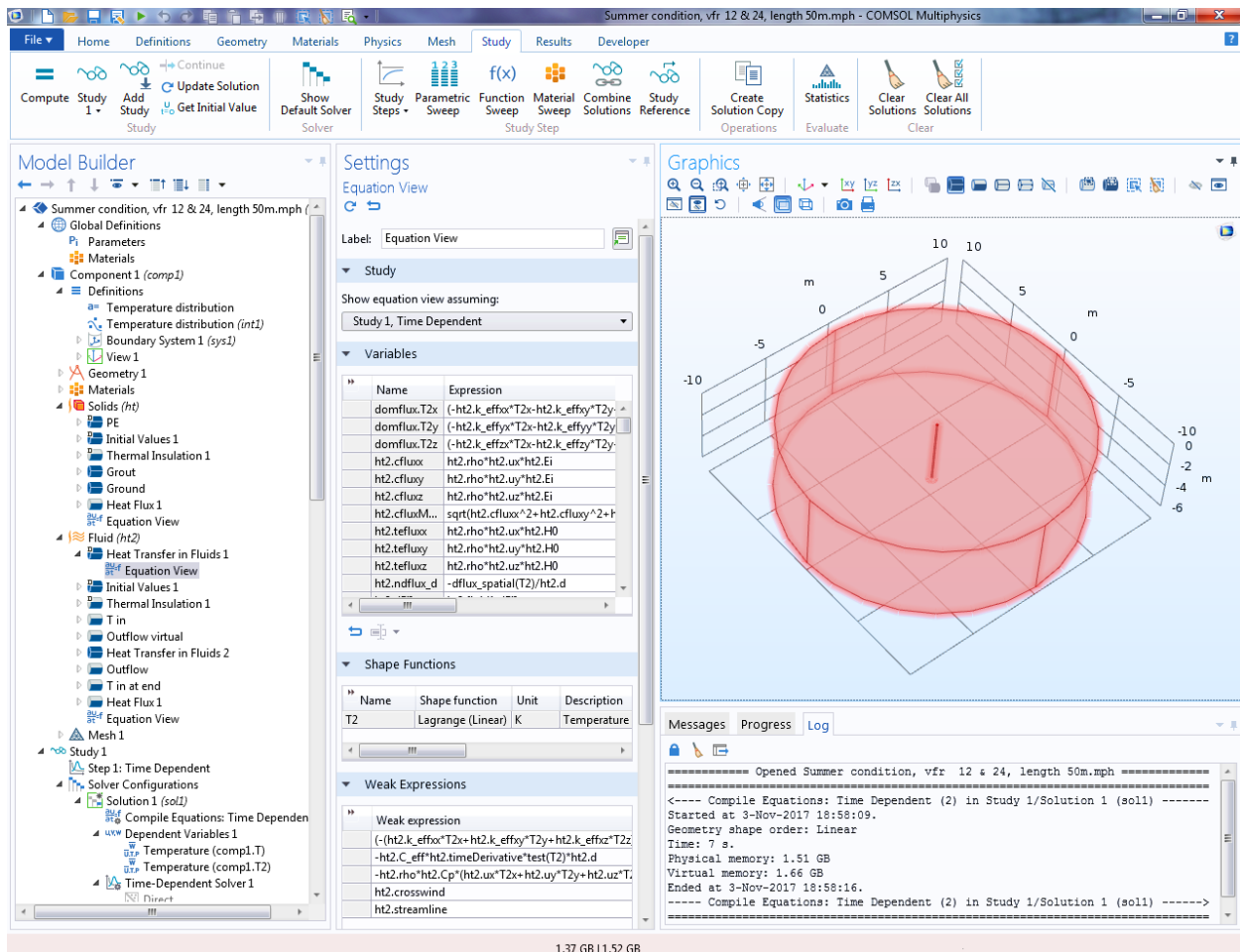


Figure 4.1. COMSOL Multiphysics desktop environment.

In the present study, many transient 3D finite element simulations were performed, by means of COMSOL Multiphysics 5.3, in order to investigate the heat transfer process in BHEs. Moreover, where it was relevant, 2D cases were investigated too.

The ground around the BHE was modeled as a cylinder with a diameter of 20 m and a length of 110 m, coaxial with the BHE and containing it. The transient heat transfer problem for the ground around the BHE and for the grouting materials inside the BHE was solved by means of the “Heat Transfer in Solids” model in COMSOL Multiphysics. The Heat Transfer in Solids model solves the following heat balance equations [89]:

$$\rho c_p \frac{\partial T}{\partial t} - \nabla \cdot (k \nabla T) = Q \quad (4.1)$$

where  $Q$  stands for the heat source/sink.

Two main codes to simulate the heat transfer process inside the tubes were employed: “Pipe Flow Module” and “Heat Transfer in Fluids”.

For the analysis of the fluid temperature distribution in double U-tube BHE, described in chapter 5, the Pipe Flow Module was used. Since for the estimation of the BHE thermal resistance and to propose the correlations to determine the mean fluid temperature (chapters 6 & 7) a very precise model was required to simulate the fluid flow inside the tubes, the previous code was modified by using the Heat Transfer in Fluids model. The first simulation code, containing the Pipe Flow Module and employed in chapter 5, will be referred to as “Code I”; the modified code, containing Heat Transfer in Fluid model and employed in chapters 6 & 7, will be referred to as “Code II”.

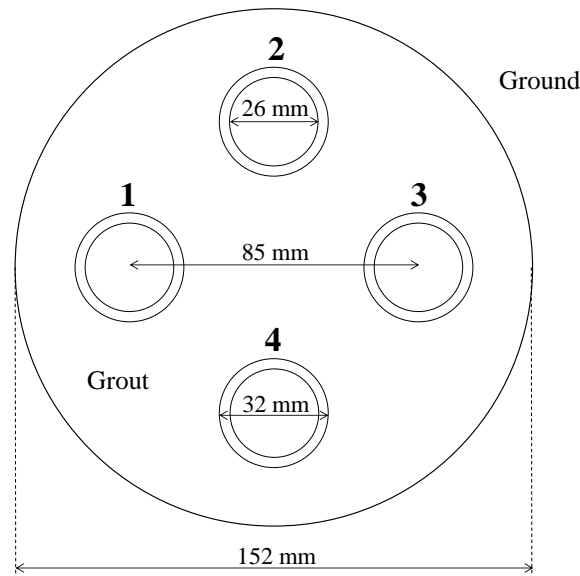


**Figure 4.2.** Sketch of the BHE cross section considered.

For both cases, a double U-tube BHE commonly employed in Northern Italy was considered, with tubes in high density polyethylene PE 100 and the following geometrical parameters: diameter 0.152 m, length 100 m, tubes with external diameter 0.032 m and internal diameter 0.026 m, and distance between the axes of opposite tubes (shank spacing) 0.085 m. Sketch of the BHE cross section considered is shown in figure 4.2. The mathematical modeling, working and boundary conditions, values of the thermophysical properties, and adopted meshes for the codes are described in the following.

### Code I

The Pipe Flow Module employed in Code I, is used to model the fluid flow in conjugate conduction-convection heat transfer problems in pipes and channel networks. The Pipe Flow Module is suitable for modeling incompressible flow in pipes and channels whose lengths are sufficient to allow considering the flow as fully developed. With this assumption, it uses edge elements, solving for the tangential cross section averaged velocity along the edges, to avoid meshing the cross section of the pipe with a full 3D mesh. This means that the modeled variables are averaged in the pipe's cross sections and vary only along the length of the pipe [90]. Under the category of the Pipe Flow Module, the Non-Isothermal Pipe Flow (nipfl) interface was adopted, which approximates the pipe flow profile by 1D assumptions in curve segments, or lines. These lines can be drawn in 2D or 3D and represent simplifications of hollow tubes. The physics interface is available in 3D on edges and 2D on boundaries. The heat balance equation for an incompressible fluid is defined as [89]:

$$\rho_f c_{p,f} A \frac{\partial T_f}{\partial t} + \rho_f c_{p,f} A \mathbf{u}_f \cdot \nabla T_f = \nabla \cdot (A k_f \nabla T_f) + f r_{Darcy} \frac{\rho A}{2 D_{hyd}} |\mathbf{u}_f|^3 + Q + Q_w + Q_p \quad (4.2)$$

where  $A$  is the area of the pipe cross section,  $\mathbf{u}_f$  is defined as the fluid velocity field,  $f r_{Darcy}$  is the Darcy friction factor and  $D_{hyd}$  is the hydraulic diameter of the pipe.  $Q_w$  represents the external heat exchange through the pipe wall, namely, convective heat transfer and  $Q_p$  represents the pressure work and is taken into account if the pressure drop is expected to be considerable and the fluid is compressible.

In this code, the inlet fluid temperature was assumed as constant, and an operation time of 100 hours was considered. The analysis was performed for two design choices. In the first choice, the BHE field was designed so that the lowest temperature of the working fluid is 4 °C and the working fluid is water. For this choice, the inlet water temperature was set equal to 4 °C. In the second choice, the BHE field was designed so that the fluid temperature can be lower than 0 °C and the working fluid is a 20% water-glycol mixture. For this choice, the inlet water temperature was set equal to -2 °C. Three volume flow rates were considered for each choice, namely 12, 16 and 24 liters per minute (L/min). The thermophysical properties of the BHE materials

(polyethylene and grout), of the ground and of the working fluids are reported in table 4.1, taken from reference [91].

As it was mentioned, the ground around the BHE was modeled as a cylinder, coaxial with the BHE, and the corresponding heat transfer problem was solved by means of the Heat Transfer in Solids model.

**Table 4.1.** The thermophysical properties adopted in Code I, taken from reference [91].

Thermophysical properties	Water	Water/Glycol 20% mixture	PE 100 tube	Grout	Ground
Thermal conductivity [W/(m K)]	0.569	0.501	0.4	1.6	1.8
Heat capacity per unit volume [MJ/(m <sup>3</sup> K)]	4.207	4.009	1.824	1.600	2.500
Dynamic viscosity [mPa s]	1.567	3.430	-	-	-

As boundary conditions, the lateral and bottom surfaces of the ground were considered as adiabatic, and the top surface, at ground level, was assumed as isothermal at 4 °C. The convection coefficient between fluid and pipes is calculated automatically by the Pipe Flow Module. As initial condition, the whole domain was set at the undisturbed ground temperature, which was assumed as varying with the depth  $z$  according to the equation:

$$\begin{cases} T_{g_0} = 4 + z & 0 \leq z \leq 10 \text{ m} \\ T_{g_0} = 14 + 0.03z & z > 10 \text{ m} \end{cases} \quad (4.3)$$

Equation (4.3) takes into account a geothermal gradient of 0.03 °C/m starting from  $z = 10$  m and has the mean value 14.715 °C from the ground surface to the bottom.

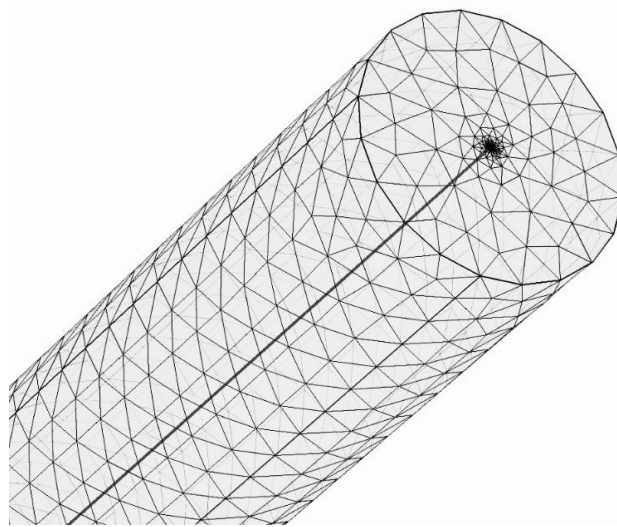


**Figure 4.3.** 3D mesh of the BHE and the surrounding ground.

An unstructured mesh containing 346 309 tetrahedral elements was employed for the computational finite element domain. Figure 4.3 shows 3D mesh of the BHE and the surrounding ground.

To solve the transient problem in Code I, the Fully Coupled time-dependent solver was employed with time steps varying from 0.1 s to 3600 s. The relative tolerance 0.01 and absolute tolerance 0.001 were considered.

## ✚ Code II

For the modified code, the 3D fluid flow was included in the computational domain. Two heat transfer models, namely “Heat Transfer in solids” and “Heat transfer in fluids”, were selected for solid and fluid domains, respectively. For the fluid domain, the water velocity was assumed to be uniform, in the vertical direction, and only the energy balance equation was solved. The energy balance equation for the fluid domain is given by [89]:

$$\rho_f c_{p,f} \frac{\partial T_f}{\partial t} + \rho_f c_{p,f} \mathbf{u}_f \cdot \nabla T_f = \nabla \cdot (k_f \nabla T_f) + Q \quad (4.4)$$

Water was considered to be the circulating fluid. With reference to figure 4.2, one U-tube was assumed to have inlet in tube 1 and outlet in tube 3, the other was assumed to have inlet in tube 2 and outlet in tube 4. For each simulation run, the water properties were assumed to be constant. For the working conditions with constant inlet temperature, the water properties were evaluated at the reference temperature  $T_{ref} = T_{in}$  (32 °C for summer operation, 4 °C for winter operation). For TRTs, the water properties were evaluated at  $T_{ref} = 20$  °C. Values of the reference water temperature, of the volume flow rate, of the water properties, of the Reynolds number, of the Nusselt number and of the heat transfer coefficient employed in Code II, are reported in table 4.2.

**Table 4.2.** Values of water thermophysical properties and flow characteristics [91].

$T_{ref}$ (°C)	$\dot{V}$ (dm <sup>3</sup> min <sup>-1</sup> )	$\rho_f$ (kg m <sup>-3</sup> )	$\mu_f$ (mPa s)	$c_{p,f}$ (J kg <sup>-1</sup> K <sup>-1</sup> )	$k_f$ (W m <sup>-1</sup> K <sup>-1</sup> )	$Re$ -	$Nu$ -	$h$ -
4	12	999.97	1.5672	4207.5	0.5687	3124.6	14.557	318.39
4	24	999.97	1.5672	4207.5	0.5687	6249.3	72.827	1592.87
20	12	998.21	1.0016	4184.1	0.5985	4880.5	47.795	1100.14
20	24	998.21	1.0016	41.84.1	0.5985	9761.0	84.917	1954.59
32	12	995.03	0.76456	4179.5	0.6187	6373.3	53.65	1276.58
32	24	995.03	0.76456	4179.5	0.6187	12746.5	92.33	2197.11



For water, a thermal conductivity equal to 100 kW/(mK) in the horizontal directions was considered, to obtain a nearly uniform temperature profile in each cross section. Furthermore, it was assumed that the thermal conductivity of high-density polyethylene,  $k_p$ , as well as the heat capacity per unit volume of polyethylene,  $(\rho c)_p$ , that of grout,  $(\rho c)_{gt}$ , and that of the ground,  $(\rho c)_g$ , have the following values:  $k_p = 0.4$  W/(mK),  $(\rho c)_p = 1.824$  MJ/(m<sup>3</sup>K),  $(\rho c)_{gt} = 1.600$  MJ/(m<sup>3</sup>K),  $(\rho c)_g = 2.500$  MJ/(m<sup>3</sup>K).

As boundary conditions, at the external boundary of the computational domain, the surface at  $z = 0$  of the BHE (circle with radius 0.076 m) was considered as adiabatic, while that of ground was considered as isothermal, with temperature 4 °C for winter operation, 14 °C for TRTs, and 24 °C for summer operation. The lateral and bottom surfaces of the ground were considered as adiabatic. Material continuity was assumed between the BHE and the surrounding ground. Moreover, continuity of temperature and heat flux was assumed between the pipes and the grout, and between the BHE and the surrounding ground.

In addition, the following boundary condition was imposed at the surface between the fluid domain and the solid domain, both for the fluid and for the solid:

$$q_a = \pm hA(T_f - T_{pf}) \quad (4.5)$$

where  $q_a$  is the heat flux per unit area flowing in the outward normal direction of the considered domain (directed towards the solid, or towards the fluid),  $h$  is the heat transfer coefficient,  $T_f$  is the bulk temperature of the fluid,  $T_{pf}$  is the local temperature of the surface between pipe and fluid, the sign + holds for the fluid domain and the sign - holds for the solid domain. Equality of boundary temperatures and heat fluxes was imposed as a coupling condition. As noted in chapter 3, the value of  $h$  was calculated by the Churchill correlation at constant heat flux [84], and imposed as a third-kind boundary condition at the internal surface of the tubes.

As initial condition, the temperature was set equal to the undisturbed ground temperature, both in the ground and in the BHE. The undisturbed ground temperature was supposed to be 14 °C at a depth  $z = 10$  m and increasing with a geothermal gradient of 0.03 °C per meter for  $z > 10$  m. For  $z < 10$  m, an exponential change of the ground temperature with  $z$  was considered, namely:

$$T(z) = T(10) + [T(0) - T(10)] \times e^{-z} \quad (4.6)$$

with  $T(0) = 24$  °C for summer operation,  $T(0) = 4$  °C for winter operation,  $T(0) = 14$  °C (i.e., uniform temperature for  $0 \leq z \leq 10$  m) for TRTs. The mean value of the undisturbed ground temperature between 0 and 100 m turns out to be 15.315 °C for summer operation, 15.115 °C for winter operation, and 15.215 °C for TRTs.

Apart from the above-mentioned configuration for Code II, other values of the shank spacing, BHE diameter, and thermal conductivity of the grout and of the ground were considered in order to evaluate their effects on the BHE thermal resistance and on the difference  $T_{ave} - T_m$ , presented in relevant chapters.

Considering the fact that the ratio of the BHE diameter to the total length in the 3D domain is extremely small, having a computational domain with satisfactory accuracy is a hard task, even with powerful computers. This task is even more difficult when a fluid flow, which requires very small mesh elements, is included in the 3D computational domain. Hence, obtaining a more compact shape of the geometry could be a useful method to improve the computational domain and, consequently, the adopted mesh, without extensive computational costs.

According to reference [92], the vertical coordinate  $z$  was replaced by a reduced one,  $\tilde{z} = z/10$ , in order to have a more compact shape of the computational domain. As a consequence, for each material the real thermal conductivities  $k_x$  and  $k_y$  were considered in the horizontal directions, and a reduced thermal conductivity  $\tilde{k}_z = k_z/100$  was assumed in the vertical direction; moreover, a reduced water velocity  $\tilde{u} = u/10$  (along  $z$ ) was considered. If one denotes the properties of the  $i$ -th solid with subscript  $i$  and those of fluid with subscript  $f$ , one can write the energy balance equations as:

$$(\rho c)_i \frac{\partial T}{\partial t} = k_{i,x} \frac{\partial^2 T}{\partial x^2} + k_{i,y} \frac{\partial^2 T}{\partial y^2} + k_{i,z} \frac{\partial^2 T}{\partial z^2} \quad (4.7)$$

$$\rho_f c_{p,f} \left( \frac{\partial T}{\partial t} + u \frac{\partial T}{\partial z} \right) = k_{f,x} \frac{\partial^2 T}{\partial x^2} + k_{f,y} \frac{\partial^2 T}{\partial y^2} + k_{f,z} \frac{\partial^2 T}{\partial z^2} \quad (4.8)$$

By introducing the transformation explained above, equations (4.7) and (4.8) become:

$$(\rho c)_i \frac{\partial T}{\partial t} = k_{i,x} \frac{\partial^2 T}{\partial x^2} + k_{i,y} \frac{\partial^2 T}{\partial y^2} + \tilde{k}_{i,z} \frac{\partial^2 T}{\partial \tilde{z}^2} \quad (4.9)$$

$$\rho_f c_{p,f} \left( \frac{\partial T}{\partial t} + \tilde{u} \frac{\partial T}{\partial \tilde{z}} \right) = k_{f,x} \frac{\partial^2 T}{\partial x^2} + k_{f,y} \frac{\partial^2 T}{\partial y^2} + \tilde{k}_{f,z} \frac{\partial^2 T}{\partial \tilde{z}^2} \quad (4.10)$$

It can be verified that, for each pair of corresponding values of  $z$  and  $\tilde{z}$ , the terms containing  $z$  in equations (4.7) and (4.8) have exactly the same values as those containing  $\tilde{z}$  in equations (4.9) and (4.10). Therefore, the solution of equations (4.9) and (4.10) in the rescaled domain  $0 \leq \tilde{z} \leq 11$  m, with the boundary conditions described above, coincides with that of equations (4.7) and (4.8) in the original domain  $0 \leq z \leq 110$  m, for every pair of corresponding values of  $z$  and  $\tilde{z}$ .

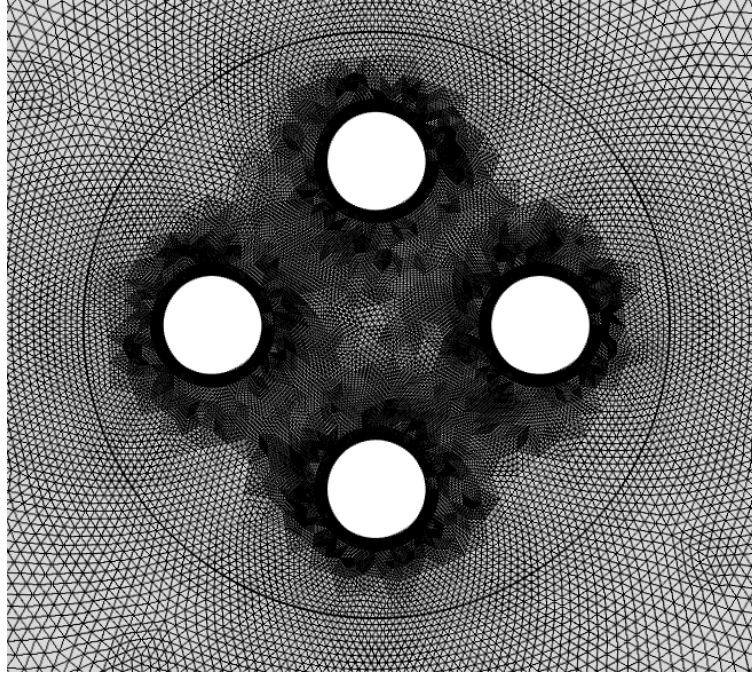


**Figure 4.4.** Mesh of the BHE for a 2D simulation case.

Depending on the configurations, various meshes were adopted for the computational domain. The mesh adopted in the main case study has 1881913 tetrahedral elements. The main meshes adopted in the present study for 2D and 3D simulations are illustrated in figures 4.4 and 4.5, respectively.

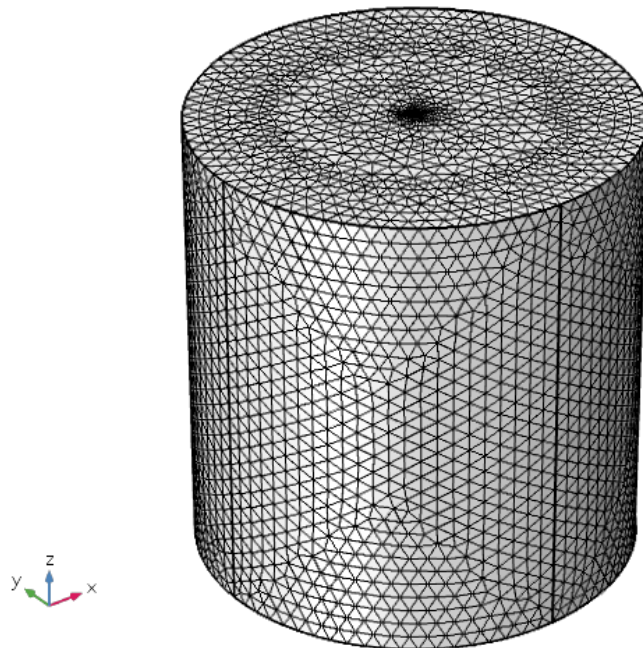


**Figure 4.5.** 3D mesh of the BHE and the surrounding ground.

The direct (PARDISO) time dependent solver was employed to solve the problem, with relative tolerance 0.001 and absolute tolerance 0.0001. Time steps ranging from less than 0.1 s to 3600 s were employed to run the 100 hours of time-dependent simulation.

For both codes employed in the present study, post-processing procedures such as convergence criteria and error estimation were carried out for the adopted solver. Figure 4.6 shows a convergence plot for a time-dependent simulation, namely, the plot of reciprocal of step size versus time step.

### 4.3 Model validation & grid independence

To validate numerical models and simulation results, our numerical models were validated against the available analytical methods in the literature and also by comparison with experimental data. The validations are illustrated in the chapters where the results are reported. An example of the model validation, namely the plot of the fluid temperature distribution along the vertical coordinate, compared with that yielded by the method of Zeng et al. [70], is illustrated in figure 4.7.

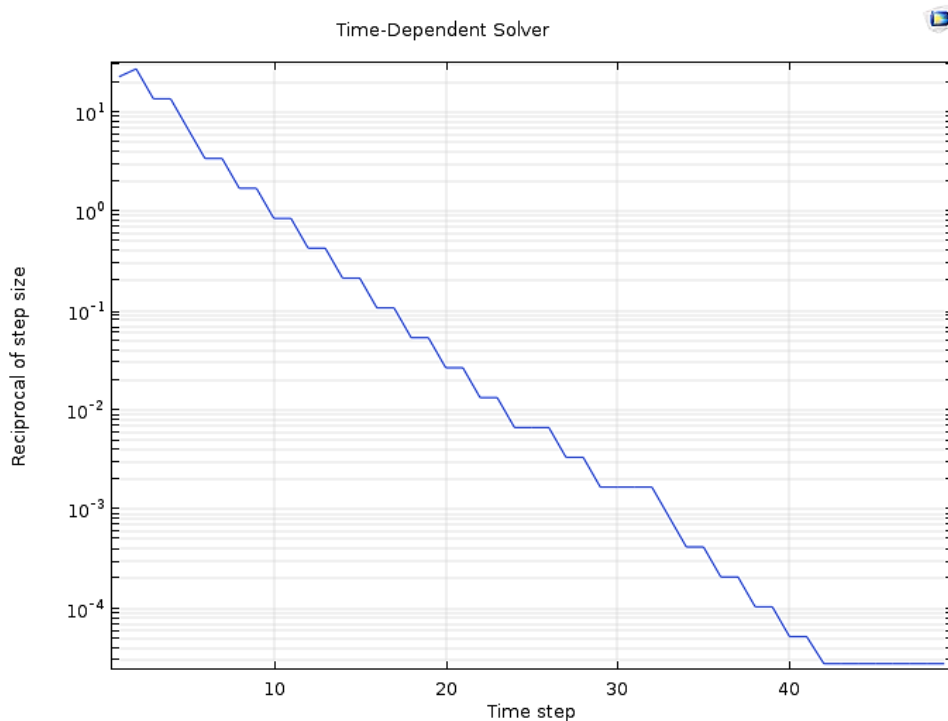


**Figure 4.6.** Convergence plot for a time-dependent solver.

In order to check the mesh independence of the results for the first code employed (Code I), computations were performed with three different unstructured meshes, denoted as Mesh 1, Mesh 2 and Mesh 3, with increasing numbers of tetrahedral elements. Values of the mean fluid temperature at three different times with these meshes were evaluated and compared, for water

with volume flow rate 16 L/min. The results, reported in table 4.3, shows that the highest deviation from Mesh 3, adopted for final computations, is 0.042 °C for Mesh 1 and 0.026 °C for Mesh 2.

**Table 4.3.** Mesh independence check for the first code employed (Code I).

Mesh	Elements	$T_m$ [°C]			Discrepancy from Mesh 3 [°C]		
		5 h	20 h	100 h	5 h	20 h	100 h
1	178 561	6.539	6.007	5.626	0.042	0.030	0.024
2	218 735	6.523	5.993	5.614	0.026	0.016	0.012
3	346 309	6.497	5.977	5.602	---	---	---

The mesh independence of the results obtained by the second code (Code II), was ensured by performing preliminary computations with three different unstructured meshes, having 1 256 561, 1 881 913 and 2 342 356 tetrahedral elements, respectively.

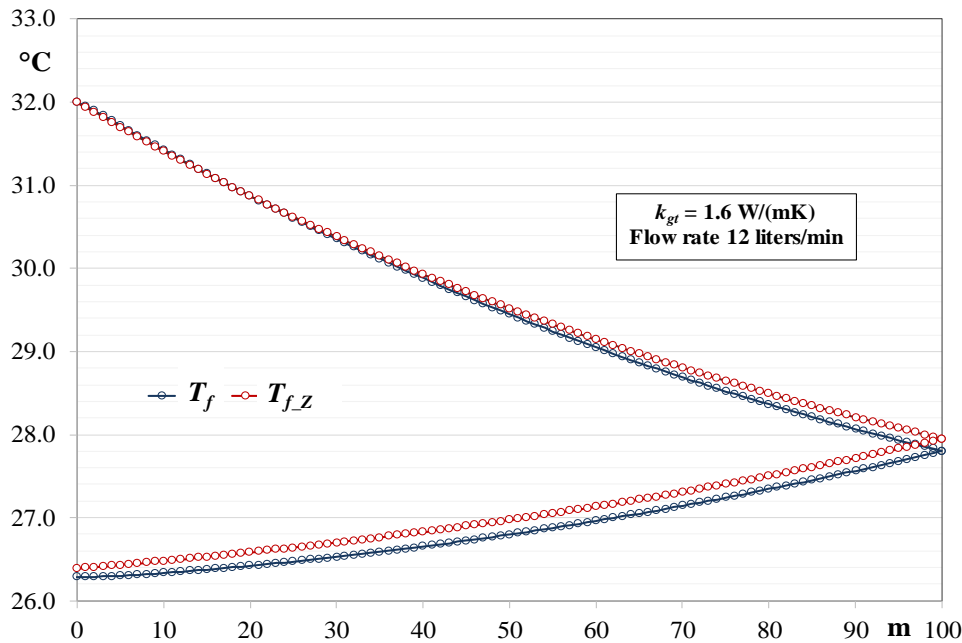


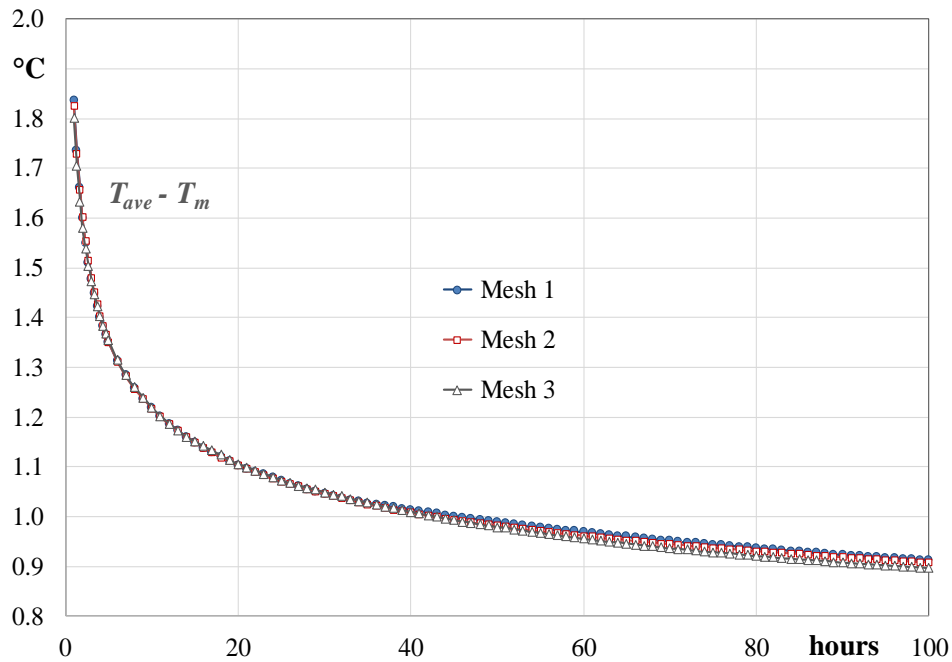
**Figure 4.7.** Plot of fluid temperature distribution along the vertical coordinate  $z$ , compared with that yielded by the method of Zeng et al. [70], for  $k_{gt} = 1.6$  W/(mK) and volume flow rate 12 L/min.

Mesh independence simulations were performed under the following conditions: constant inlet temperature  $T_{in} = 32$  °C, flow rate 12 L/min,  $k_{gt} = 1.6$  W/(mK) and  $k_g = 1.8$  W/(mK). Values of the 3D thermal resistance of the BHE,  $R_{b,3D}$ , obtained by three different meshes and of the corresponding percent deviations from the values obtained by Mesh 2 are reported in table 4.4.

**Table 4.4.** Mesh independence check for modified code (Code II).

Mesh	Elements	$R_{b,3D}$ [mK/W]			Percent deviation from Mesh 2		
		20 h	50 h	100 h	20 h	50 h	100 h
1	1 256 561	0.0702	0.0702	0.0702	- 0.36	- 0.32	- 0.35
2	1 881 913	0.0705	0.0704	0.0704	0.00	0.00	0.00
3	2 342 354	0.0713	0.0713	0.0712	1.19	1.18	1.17

The table shows that the absolute value of the percent deviation is lower than 1.2% in all cases. It shows also that  $R_{b,3D}$  nearly reaches its steady-state value after 20 hours.

**Figure 4.8.** Mesh independence check for modified code (Code II), plots of  $T_{ave} - T_m$  versus time.

In addition, plots of  $T_{ave} - T_m$  versus time obtained by these meshes are reported in figure 4.8. The figure illustrates both the excellent agreement between the results obtained by different meshes and the decreasing trend of  $T_{ave} - T_m$ . Mesh 2 has been employed for final computations.



## *Chapter 5*

---

*Analysis of the fluid temperature distribution*





## *Analysis of the fluid temperature distribution*<sup>1</sup>

---

The design of a BHE field requires the knowledge of the undisturbed ground temperature  $T_{g_0}$  and of the thermal properties of the ground. Except for very small BHE fields,  $T_{g_0}$ , the thermal conductivity  $k_g$  and the thermal diffusivity  $\alpha_g$  of the ground, as well as the BHE thermal resistance per unit length  $R_b$ , are determined through a TRT performed as recommended by ASHRAE [16].

In this method, one assumes that the mean fluid temperature is given by the arithmetic mean of the inlet  $T_{in}$  and outlet  $T_{out}$  temperatures, that we denote by  $T_{ave}$ . Several authors have pointed out that, on account of the internal thermal short-circuiting, a relevant difference between  $T_m$  and  $T_{ave}$  can occur [66, 76-79, 94] and can yield a significant overestimation of the BHE thermal resistance as well as an underestimation of the thermal conductivity of the ground. Therefore, a correct estimation of  $T_m$  from measured values of  $T_{in}$  and  $T_{out}$  could be useful in the evaluation of TRTs. Another technical problem in which the knowledge of the relation between  $T_{in}$ ,  $T_{out}$  and  $T_m$  would be useful is the hourly simulation of GCHP systems. In fact, accurate analytical expressions of dimensionless response functions of BHEs, *g-functions*, can be used to determine the time evolution of  $T_m$  by fast computation codes. Since the difference between  $T_{in}$  and  $T_{out}$  can be easily determined by an energy balance, the knowledge of the difference between  $T_m$  and  $T_{ave}$  could allow to determine an accurate value of  $T_{out}$ , the relevant parameter to determine the heat pump COP.

---

<sup>1</sup> This chapter is based on the following publication [93]:

- E. Zanchini, A. Jahanbin. Finite-element analysis of the fluid temperature distribution in double U-tube Borehole Heat Exchangers. Journal of Physics 745 (2016) 032003.

The scope of this chapter is to determine typical values of the difference between  $T_m$  and  $T_{ave}$  which occur in double U-tube BHEs working in heating mode. The results are compared with those determined by applying the  $p$ -linear average model proposed in reference [66].

The numerical code presented in previous chapter (Code I) is employed in simulations. The analysis was performed for two winter design choices: in first choice, water is the working fluid with inlet temperature equal to 4 °C; in second one, the working fluid is a water-glycol 20% mixture with inlet temperature equal to -2 °C. Three volume flow rates were considered for each choice, namely 12, 16 and 24 L/min. A 3D transient model was implemented in the finite element code COMSOL Multiphysics. The conjugate conduction-convection heat transfer problem inside the tubes was studied by means of the Pipe Flow Module. The time-dependent problem was solved with time steps varying from 0.1 s to 3600 s. Figure 5.1 illustrates a sketch of the BHE cross section.

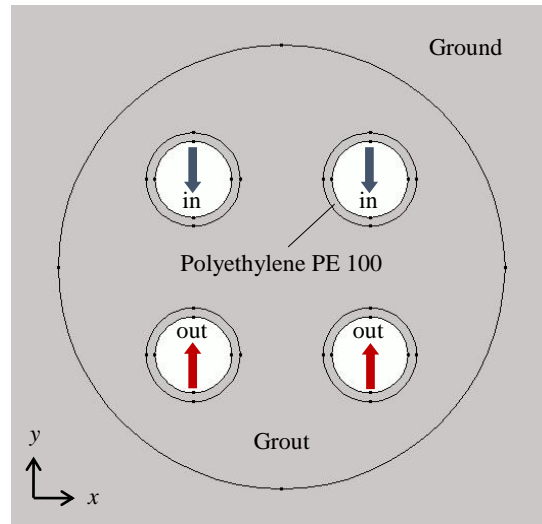


**Figure 5.1.** Illustration of the BHE cross section.

The main results of this study concern the analysis of the difference between the mean fluid temperature  $T_m$  and the arithmetic mean of inlet and outlet temperatures,  $T_{ave}$ , which is commonly used as an approximation of  $T_m$ .

In order to validate our simulation results, the values of  $T_m - T_{ave}$  determined through the finite element simulations have been compared with those obtainable by applying the  $p$ -linear average model [66], discussed in section 3.2, to determine the mean fluid temperature for single U-tube BHEs denoted by  $T_{m, MP}$ , namely:

$$T_{m, MP} - T_g = \lim_{p \rightarrow -1} \frac{p \left( |T_{f, in} - T_g|^{p+1} - |T_{f, out} - T_g|^{p+1} \right)}{(1+p) \left( |T_{f, in} - T_g|^p - |T_{f, out} - T_g|^p \right)} \quad (5.1)$$

The input values of  $T_{out}$  for equation (5.1) have been taken from the present simulations.

Plots of the power extracted from the ground per unit BHE length versus time for the case of water with inlet temperature 4 °C are reported in figure 5.2, where  $q_{12}$ ,  $q_{16}$  and  $q_{24}$  denote the power obtained with a volume flow rate of 12, 16 and 24 L/min, respectively. Power values higher than 60 W/m were not reported, to improve the readability of the plots. The figure shows that the power is a decreasing function of time and that a higher flow rate yields a higher power, mainly because the mean fluid temperature is lower. A flow rate increase from 12 to 16 L/min yields a power enhancement of about 6% (from 28.20 to 29.94 W/m) at  $t = 100$  hours; a similar power enhancement (from 29.94 to 31.74 W/m at  $t = 100$  hours) is obtained with a flow rate increase from 16 to 24 L/min; the latter, however, is a very high flow rate.

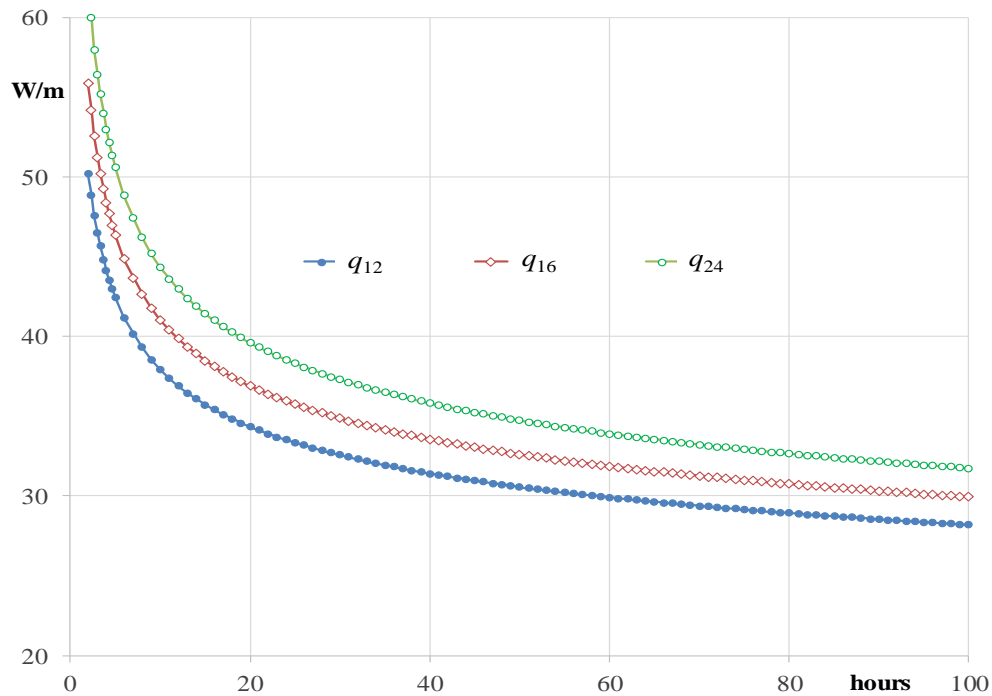


**Figure 5.2.** Power per unit length extracted from the ground: water with inlet temperature 4 °C.

Plots of the power extracted from the ground per unit BHE length versus time for the case of water-glycol with inlet temperature -2 °C are reported in figure 5.3. A comparison between figure 5.2 and figure 5.3 shows that the decrease in inlet temperature from 4 °C to -2 °C yields a relevant increase in power extracted from the ground (from 28.20, 29.94 and 31.74 W/m to 42.34, 45.58 and 49.03 W/m, for  $t = 100$  hours).

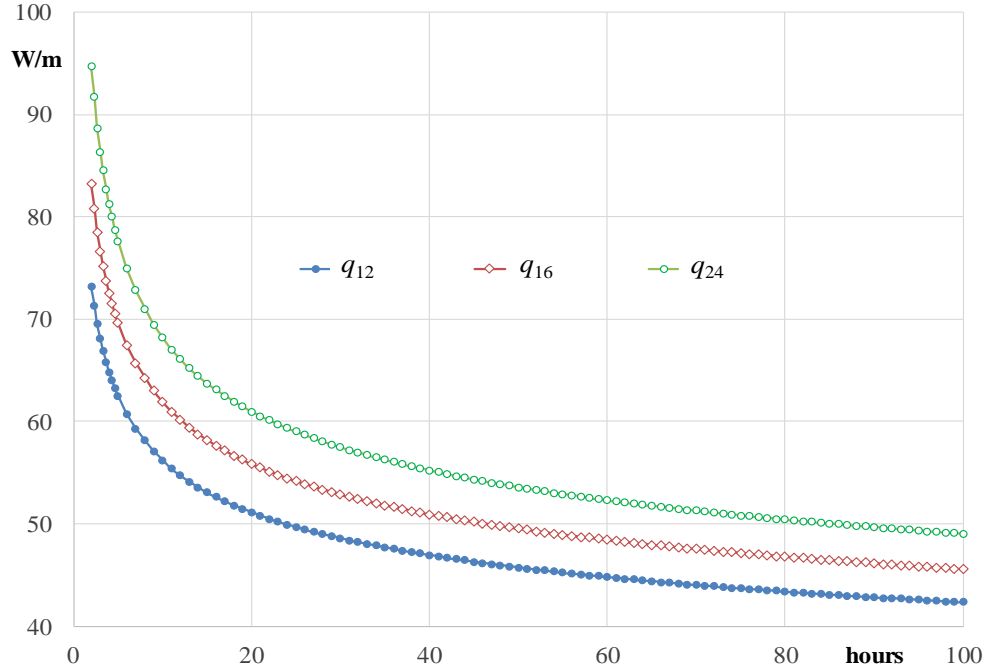


**Figure 5.3.** Power per unit length extracted from the ground: water-glycol with inlet temperature  $-2\text{ }^{\circ}\text{C}$ .

The values of  $T_{out}$ ,  $T_m$ ,  $T_{ave}$ ,  $T_m - T_{ave}$  and  $(T_m - T_{ave})_{MP}$  for all flow rates, at  $t = 5$  hours,  $t = 20$  hours and  $t = 100$  hours, are reported in table 5.1 for water and in table 5.2 for water-glycol 20% mixture. In all cases, especially for  $t = 20$  hours and  $t = 100$  hours, the values of  $T_m - T_{ave}$  obtained through the  $p$ -linear average model are lower than that those obtained by our simulations. Most probably, the relevant differences are due to the different BHE kind and to the higher distance between the centers of opposite tubes (shank spacing) considered in reference [66] (single U-tube BHE instead of double U-tube, 11 cm instead of 8.5 cm).

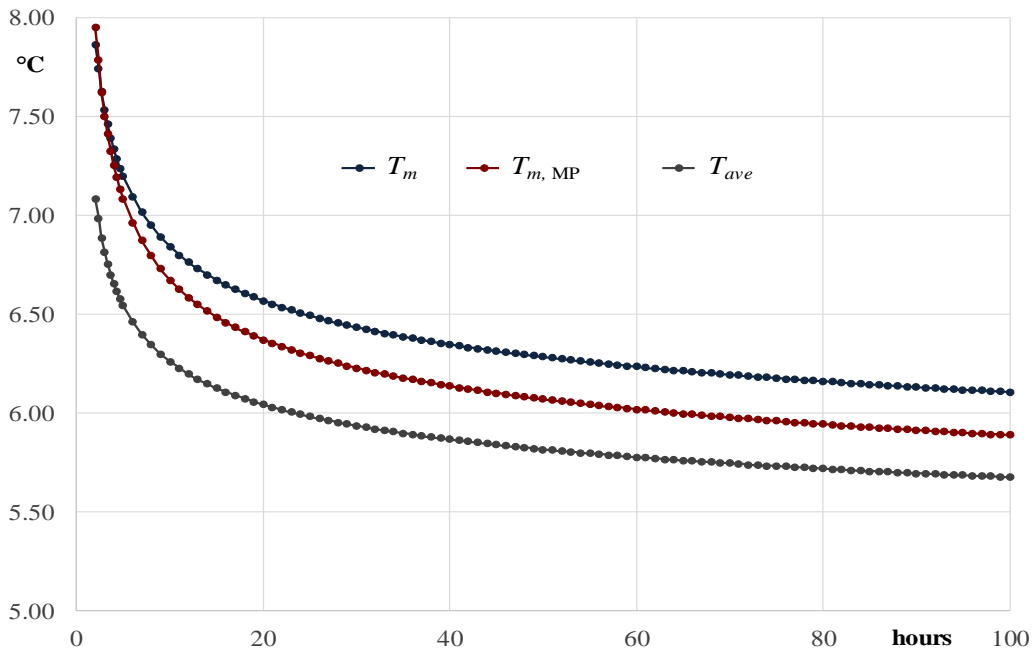
**Table 5.1.** Values of  $T_{out}$ ,  $T_m$ ,  $T_{ave}$ ,  $T_m - T_{ave}$  and  $(T_m - T_{ave})_{MP}$  for water, with  $T_{in} = 4\text{ }^{\circ}\text{C}$ .

$^{\circ}\text{C}$	12 L/min			16 L/min			24 L/min		
	5 h	20 h	100 h	5 h	20 h	100 h	5 h	20 h	100 h
$T_{out}$	9.089	8.088	7.354	8.174	7.304	6.679	7.026	6.360	5.891
$T_m$	7.199	6.570	6.108	6.497	5.977	5.602	5.713	5.337	5.071
$T_{ave}$	6.544	6.044	5.677	6.087	5.652	5.339	5.513	5.180	4.946
$T_m - T_{ave}$	0.655	0.526	0.431	0.410	0.325	0.263	0.200	0.156	0.125
$(T_m - T_{ave})_{MP}$	0.543	0.329	0.213	0.345	0.206	0.132	0.171	0.102	0.065

**Table 5.2.** Values of  $T_{out}$ ,  $T_m$ ,  $T_{ave}$ ,  $T_m - T_{ave}$  and  $(T_m - T_{ave})_{MP}$  for water-glycol, with  $T_{in} = -2$  °C.

°C	12 L/min			16 L/min			24 L/min		
	5 h	20 h	100 h	5 h	20 h	100 h	5 h	20 h	100 h
$T_{out}$	5.856	4.385	3.284	4.572	3.245	2.278	2.869	1.812	1.064
$T_m$	2.804	1.905	1.231	1.887	1.102	0.530	0.753	0.156	-0.267
$T_{ave}$	1.928	1.192	0.642	1.286	0.622	0.139	0.434	-0.094	-0.468
$T_m - T_{ave}$	0.876	0.712	0.589	0.600	0.480	0.391	0.318	0.250	0.201
$(T_m - T_{ave})_{MP}$	0.820	0.508	0.333	0.542	0.327	0.210	0.278	0.164	0.103

Plots of the  $T_m$ ,  $T_{ave}$  and  $T_{m,MP}$  versus time for the volume flow rate 12 L/min are reported in figure 5.4 for the case of water with  $T_{in} = 4$  °C, and in figure 5.5 for the case of water-glycol with  $T_{in} = -2$  °C.


**Figure 5.4.**  $T_m$ ,  $T_{ave}$  and  $T_{m,MP}$  versus time for the volume flow rate 12 L/min: water with inlet temperature 4 °C.

It can be observed that, in both cases, using the approximation of the arithmetic mean of inlet and outlet temperatures,  $T_{ave}$ , underestimates the real value of the mean fluid temperature. Plots of  $T_m$  and  $T_{m,MP}$  for both figures are practically coincident for first 5 hours of simulations, and start to diverge after 5 hours. When the quasi-stationary state is nearly reached (after 20 hours), the difference between the  $T_m$  and  $T_{m,MP}$  has almost a constant positive value: 0.22 °C for water and 0.26 °C for water-glycol mixture.

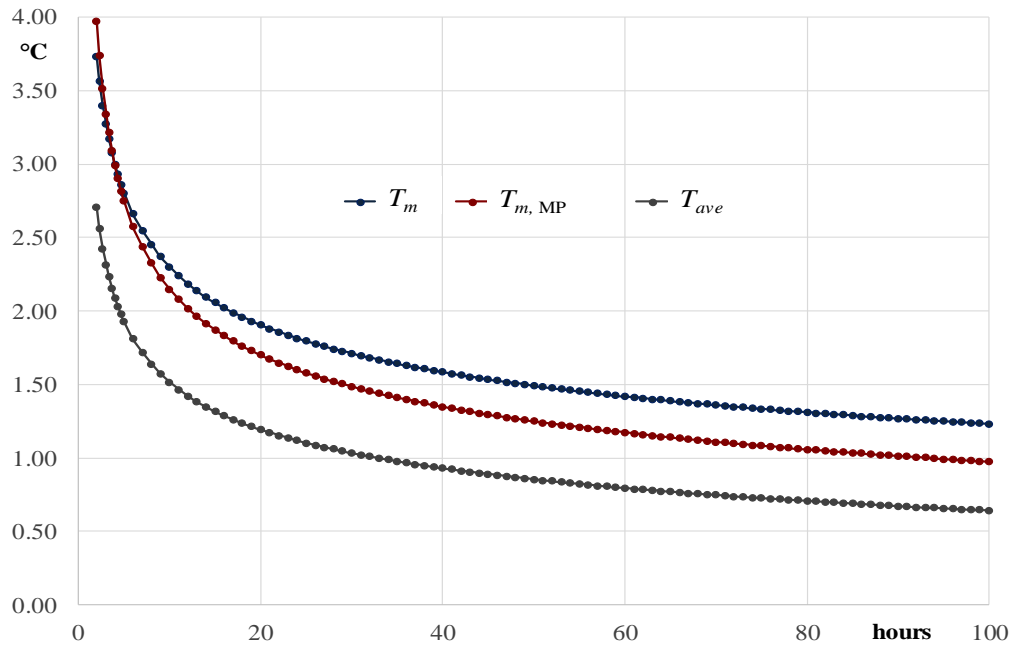


**Figure 5.5.**  $T_m$ ,  $T_{ave}$  and  $T_{m, MP}$  versus time for the volume flow rate 12 L/min: water-glycol with inlet temperature  $-2\text{ }^{\circ}\text{C}$ .

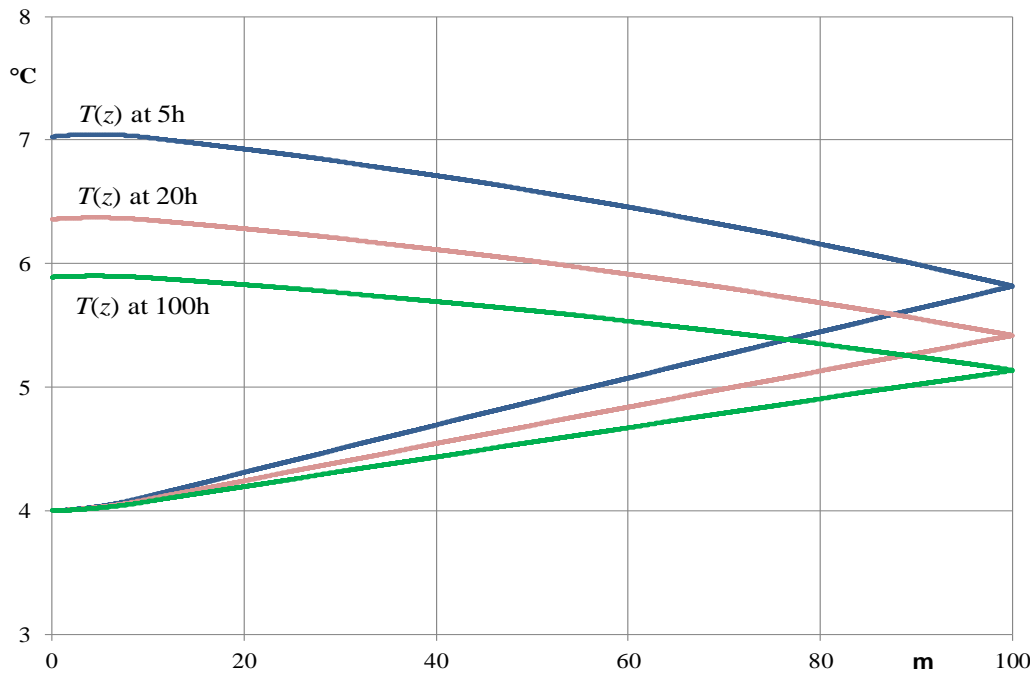


**Figure 5.6.** Fluid temperature distribution versus height  $z$  (m) for the volume flow rate 24 L/min: water with inlet temperature  $4\text{ }^{\circ}\text{C}$ .

The distribution of the bulk fluid temperature along the U-tubes,  $T(z)$ , is illustrated in figure 5.6, for water with  $4\text{ }^{\circ}\text{C}$  inlet temperature, at  $t = 5$  hours,  $t = 20$  hours and  $t = 100$  hours. The figure

shows that the temperature profile is far from being linear, due to the thermal short-circuiting between the descending flow (lower leg of each plot) and ascending flow (upper leg of each plot). As evident, the fluid temperature increase in the descending flow is much higher than that in the ascending flow, where the fluid is cooled by the descending one. The figure also shows that the difference between the outlet and inlet temperature is a decreasing function of time.

It is possible to conclude that the  $p$ -linear average expression, equation (5.1), yields values of  $T_m - T_{ave}$  lower than the real ones for a typical double U-tube BHE. Therefore, specific expressions for this kind of BHEs seem valuable. To determine these expressions is the scope of our study in the next chapter.





## *Chapter 6*

---

*Correlations to determine  
the mean fluid temperature*



## *Correlations to determine the mean fluid temperature*<sup>2</sup>

---

As discussed, the incorrect approximation of mean fluid temperature  $T_m$  with average of inlet and outlet temperatures  $T_{ave}$ , can introduce an error in the applications of ground heat exchangers. In TRTs, this approximation causes an overestimation of the thermal resistance and underestimation of the ground thermal conductivity, and in dynamic simulation of GCHPs, it causes an error in the evaluation of the outlet temperature from ground heat exchangers. Hence, expressions to estimate accurate values of  $T_m$  seem valuable.

The aim of the present chapter is to provide simple and accurate expressions that yield  $T_m$  as a function of  $T_{in}$ ,  $T_{out}$  and of the volume flow rate  $\dot{V}$ , for double U-tube BHEs with a typical geometry. These relations can be directly applied to determine the time evolution of  $T_m$  in TRTs and the time evolution of  $T_{out}$  in dynamic simulations of GCHP systems, without the need of special calculation algorithms. Thus, the precision in measuring  $R_b$  by TRTs and in predicting the heat pump coefficient of performance by dynamic simulations is improved by employing the usual measurement and simulation procedures.

The results are obtained by applying the 3D finite element simulation code (Code II) implemented in COMSOL Multiphysics, presented in chapter 4.

---

<sup>2</sup> This chapter is based on the following publication [95]:

- E. Zanchini, A. Jahanbin. Correlations to determine the mean fluid temperature of double U-tube borehole heat exchangers with a typical geometry. Applied Energy 206 (2017) 1406-1415.

The difference between  $T_{ave}$  and  $T_m$  is expressed through the positive dimensionless parameter:

$$\varphi = \frac{\dot{V} T_{ave} - T_m}{\dot{V}_0 T_{in} - T_{out}} \quad (6.1)$$

where  $\dot{V}_0$  is a reference volume flow rate, which has been selected equal to 12 L/min. It is shown that, for a given BHE geometry, after one or two hour(s) of operation with a constant inlet temperature or heat injection  $\varphi$  reaches a time independent asymptotic value  $\varphi_\infty$  that can be considered as a function of the grout thermal conductivity  $k_{gt}$  alone. In transient conditions,  $\varphi$  can be expressed as a function of  $k_{gt}$ ,  $\dot{V}/\dot{V}_0$  and the dimensionless time,  $t^* = t/t_0$ , where  $t$  is the time from the operation start and  $t_0$  is two hours. Values of  $\varphi_\infty$  for each value of  $k_{gt}$  and expressions  $\varphi$  for each value of  $k_{gt}$  and  $\dot{V}/\dot{V}_0$  are reported.

The results apply to 100 m long double U-tube BHEs with 85 mm distance between the axes of opposite tubes (shank spacing), any BHE diameter compatible with this distance, any heat input rate and volume flow rate, any kind of working condition, any grout thermal conductivity between 0.9 and 1.6 W/(mK), any ground thermal conductivity between 1.4 and 2.2 W/(mK).

The simulation results are validated by comparison with those obtainable by applying the analytical model proposed by Zeng et al. [70], presented in chapter 3.

The computation results have shown that, after two hours of operation,  $T_m - T_{ave}$  can be expressed as a homogeneous linear function of  $(T_{in} - T_{out})/\dot{V}$ , independent of time and of flow rate, and practically independent also of the thermal conductivity of ground, of the BHE diameter and of working conditions (summer operation, winter operation, TRT). In this regime, that we will call quasi-stationary, three expressions of  $T_m - T_{ave}$  as a function of  $(T_{in} - T_{out})/\dot{V}$  have been determined, by considering summer operation with constant inlet temperature  $T_{in} = 32$  °C, BHE diameter 152 mm, and ground thermal conductivity  $k_g = 1.8$  W/(mK). Each expression refers to a given value of the grout thermal conductivity, namely  $k_{gt} = 0.9, 1.2$  or  $1.6$  W/(mK), and was obtained by considering three different values of the volume flow rate,  $\dot{V} = 12, 18$  and  $24$  L/min.

The validity of the correlations for  $k_{gt} = 0.9$  and  $k_{gt} = 1.6$  W/(mK) for different values of  $k_g$  was checked by performing simulations for summer operation with  $T_{in} = 32$  °C and different values of the ground thermal conductivity, namely  $k_g = 1.4$  and  $2.2$  W/(mK), and by considering  $\dot{V} = 12$  and  $24$  L/min. The validity of the correlation for  $k_{gt} = 1.2$  W/(mK) for other BHE diameters was checked by considering summer operation with  $T_{in} = 32$  °C,  $k_g = 1.8$  W/(mK), flow rates 12 and 24 L/min, and diameters 127 and 177 mm.

The validity of the obtained correlations under winter working conditions was checked for  $k_{gt} = 1.6$  W/(mK), by considering winter operation at constant inlet temperature  $T_{in} = 4$  °C,  $k_g = 1.8$  W/(mK), volume flow rates  $\dot{V} = 12$  and  $24$  L/min.

The validity for TRTs was checked for  $k_{gt} = 1.6 \text{ W/(mK)}$  and  $k_g = 1.8 \text{ W/(mK)}$ , by considering a TRT with  $\dot{V} = 12 \text{ L/min}$  and supplied power per unit length  $q_l = 50 \text{ W/m}$ , and a TRT with  $\dot{V} = 24 \text{ L/min}$  and supplied power per unit length  $q_l = 80 \text{ W/m}$ . Thus, 25 simulation runs were carried out in total, each with reference to an operation period of 100 hours.

The correlations for the dimensionless parameter  $\varphi$  during the first two hours have been determined by considering the same conditions as those employed to determine the correlations for quasi-stationary regime.

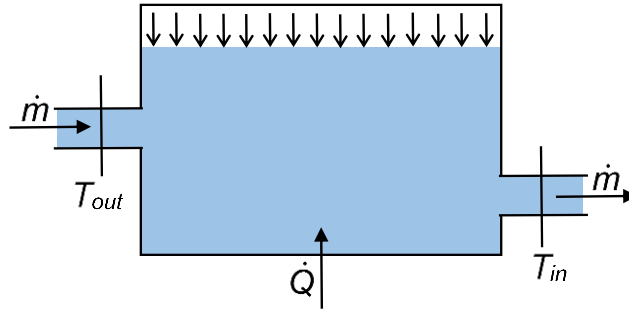


**Figure 6.1.** Enthalpy balance of the fluid heating tank.

For the simulation of TRTs, a method to determine the time evolution of the inlet fluid temperature was carried out. In a TRT, a constant thermal power  $q$  is supplied by electric resistances to a thermally insulated fluid tank, as illustrated in figure 6.1. The fluid enters the tank at temperature  $T_{out}$  (outlet temperature from the BHE), and is heated to temperature  $T_{in}$  (inlet temperature in the BHE). If one denotes by  $\dot{m}$  the fluid mass flow rate, the enthalpy balance can be written as:

$$C_f \frac{dT_m}{dt} = \dot{m} c_{p,f} (T_{out} - T_{in}) + q \quad (6.2)$$

where  $C_f = \rho_f V c_{p,f}$  is the heat capacity at constant pressure of the fluid contained in the tank, having volume  $V$  and mean fluid temperature  $T_m$ . After some hours, the left hand side becomes negligible with respect to  $q$ , so that one has:

$$T_{in} = T_{out} + \frac{q}{\dot{m} c_{p,f}} \quad (6.3)$$

On the other hand, in the early stage of the heating process the difference between  $T_{in}$  and  $T_{out}$  is smaller and must be determined by solving equation (6.2). The following simplifying assumptions can be employed. The fluid is mixed, so that  $dT_m/dt$  is well approximated by  $dT_{in}/dt$ . During the very first part of the heating period, the rate of change of  $T_{out}$  is negligible, so

that one can solve equation (6.2) by considering  $T_{out}$  as a constant. Under these assumptions, equation (6.2) becomes:

$$\frac{dT_{in}}{dt} + \frac{\dot{m}c_{p,f}}{C_f} T_{in} = \frac{\dot{m}c_{p,f}}{C_f} T_{out} + \frac{q}{C_f} \quad (6.4)$$

where the right hand side is a constant. The solution of equation (6.4) with the initial condition  $T_{in}(0) = T_{out}$  is given by:

$$T_{in}(t) = T_{out} + \frac{q}{\dot{m}c_{p,f}} \left( 1 - e^{-\frac{\dot{m}c_{p,f}}{C_f} t} \right) \quad (6.5)$$

It is immediately verified that equation (6.5) yields equation (6.3) in the limit of infinite time.

## 6.1 Model validation

To validate simulation results, the time evolutions of  $T_{ave} - T_m$  obtained through numerical simulations, for summer operation at constant inlet temperature  $T_{in} = 32$  °C, with  $k_{gt} = 0.9$  and  $k_{gt} = 1.6$  W/(mK), have been compared with those obtained by applying the analytical method proposed by Zeng et al. [70]. Since the analytical method assumes steady-state heat transfer in the BHE, the time interval from 2 to 100 hours has been considered. The flow configuration analyzed in this chapter is that denoted by Zeng et al. [70] as (1-3, 2-4). The system of differential equations of Zeng et al. [70] was solved independently.

The analytical method proposed by Zeng et al. [70], the expressions involved, and the solution determined by means of the mathematical software WOLFRAM MATHEMATICA, were presented in chapter 3. Some relevant expressions are repeated here for completeness. The solution determined is:

$$\Theta_d(Z) = \frac{(2\Sigma_1 + \Sigma_{12}) \cosh \left[ \frac{\sqrt{2\Sigma_1 + \Sigma_{12}}(Z-1)}{\Sigma_1 \sqrt{\Sigma_{12}}} \right] - \sqrt{\Sigma_{12}} \sqrt{2\Sigma_1 + \Sigma_{12}} \sinh \left[ \frac{\sqrt{2\Sigma_1 + \Sigma_{12}}(Z-1)}{\Sigma_1 \sqrt{\Sigma_{12}}} \right]}{(2\Sigma_1 + \Sigma_{12}) \cosh \left[ \frac{\sqrt{2\Sigma_1 + \Sigma_{12}}}{\Sigma_1 \sqrt{\Sigma_{12}}} \right] + \sqrt{\Sigma_{12}} \sqrt{2\Sigma_1 + \Sigma_{12}} \sinh \left[ \frac{\sqrt{2\Sigma_1 + \Sigma_{12}}}{\Sigma_1 \sqrt{\Sigma_{12}}} \right]} \quad (6.6)$$

$$\Theta_u(Z) = \frac{(2\Sigma_1 + \Sigma_{12}) \cosh \left[ \frac{\sqrt{2\Sigma_1 + \Sigma_{12}}(Z-1)}{\Sigma_1 \sqrt{\Sigma_{12}}} \right] + \sqrt{\Sigma_{12}} \sqrt{2\Sigma_1 + \Sigma_{12}} \sinh \left[ \frac{\sqrt{2\Sigma_1 + \Sigma_{12}}(Z-1)}{\Sigma_1 \sqrt{\Sigma_{12}}} \right]}{(2\Sigma_1 + \Sigma_{12}) \cosh \left[ \frac{\sqrt{2\Sigma_1 + \Sigma_{12}}}{\Sigma_1 \sqrt{\Sigma_{12}}} \right] + \sqrt{\Sigma_{12}} \sqrt{2\Sigma_1 + \Sigma_{12}} \sinh \left[ \frac{\sqrt{2\Sigma_1 + \Sigma_{12}}}{\Sigma_1 \sqrt{\Sigma_{12}}} \right]} \quad (6.7)$$

where  $Z = z/L$  is the dimensionless vertical coordinate,  $\Theta_d$  and  $\Theta_u$  are the dimensionless bulk temperatures of the fluid going down (descending flow) and of the fluid going up (ascending flow),  $\Sigma_1$  and  $\Sigma_{12}$  are the dimensionless parameters defined in equation (17) of Zeng et al. [70], namely:

$$\begin{cases} \Sigma_1 = \frac{\dot{m} c_{p,f}}{L} (R_{11} + R_{13} + 2R_{12}) \\ \Sigma_{12} = \frac{\dot{m} c_{p,f}}{L} \frac{(R_{11} - R_{13})(R_{11} + R_{13} + 2R_{12})}{R_{12} + R_{13}} \end{cases} \quad (6.8)$$

where  $R_{11}$ ,  $R_{12}$  and  $R_{13}$  are determined through equations (3.16 - 3.18). The dimensionless temperatures  $\Theta_d$  and  $\Theta_u$  are defined as:

$$\begin{cases} \Theta_d(Z) = \frac{T_{f,d}(Z) - T_s}{T_{f,in} - T_s} \\ \Theta_u(Z) = \frac{T_{f,u}(Z) - T_s}{T_{f,in} - T_s} \end{cases} \quad (6.9)$$

The results of the comparison for  $k_{gt} = 1.6$  W/(mK) and  $k_g = 1.8$  W/(mK) are illustrated in figure 6.2, for  $\dot{V} = 12$  L/min, and in figure 6.3, for  $\dot{V} = 24$  L/min. Both figures show a fair agreement and a slight underestimation of  $T_{ave} - T_m$  by the analytical method. The relative discrepancy is nearly constant, with final value 7.5% for  $\dot{V} = 12$  L/min and 7% for  $\dot{V} = 24$  L/min. The final value of absolute discrepancy is 0.07 °C for the lower flow rate and 0.02 °C for the higher one.

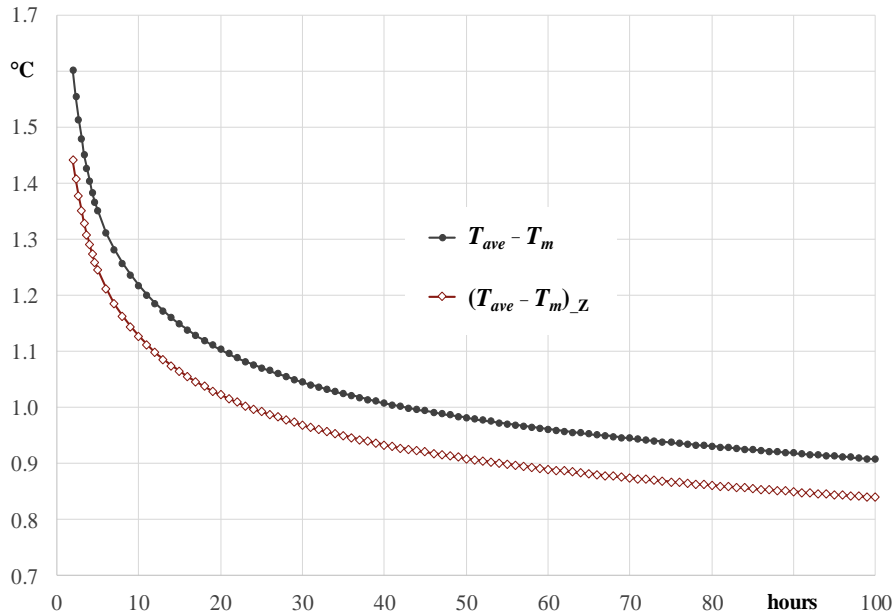


**Figure 6.2.** Time evolution of  $T_{ave} - T_m$  obtained numerically and through the analytical model by Zeng et al. [70], for  $k_{gt} = 1.6$  W/(mK),  $k_g = 1.8$  W/(mK), flow rate 12 L/min.



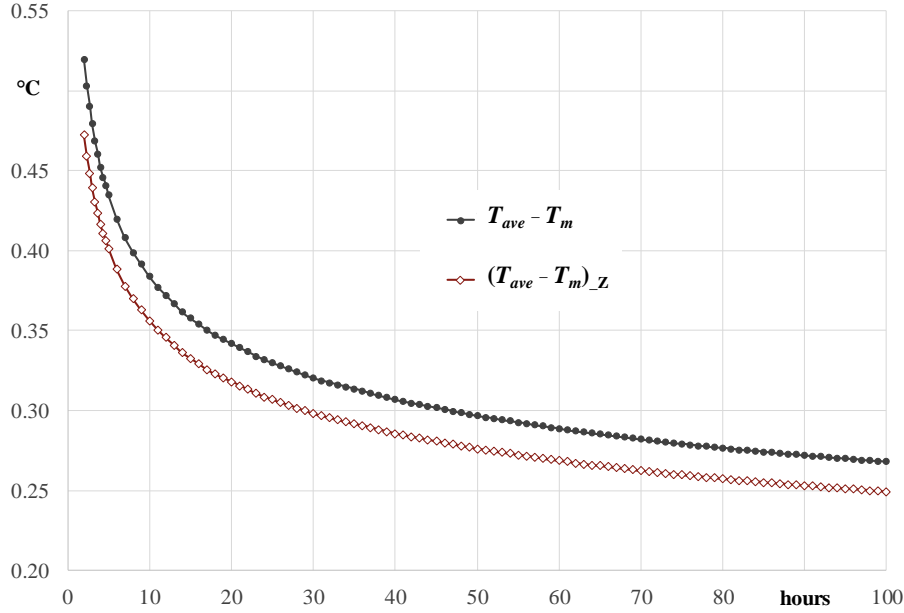


**Figure 6.3.** Time evolution of  $T_{ave} - T_m$  obtained numerically and through the analytical model by Zeng et al. [70], for  $k_{gr} = 1.6 \text{ W/(mK)}$ ,  $k_g = 1.8 \text{ W/(mK)}$ , flow rate 24 L/min.

To validate the model employed in TRT simulation, the accuracy of equation (6.5) was checked by comparing its output with the experimental trend of  $T_{in}$  recorded during a TRT performed on a 100 m long double U-tube BHE located at Fiesso d'Artico (Venice) [96]. The volume  $V$  of the fluid contained in the heating tank was  $V = 0.098 \text{ m}^3$ , and the mean temperature of the fluid during the first 15 minutes of the heating process was about  $16 \text{ }^\circ\text{C}$ . Thus, for that case one has  $\rho_f = 998.95 \text{ kg/m}^3$ ,  $c_{p,f} = 4187.4 \text{ J/(kg K)}$ ,  $C_f = 409.934 \text{ kJ/K}$ . The mean value of the electric power supplied during the first 15 minutes was 6490 W, with an estimated heat loss of 50 W, so that  $q = 6440 \text{ W}$ ; the volume flow rate was  $\dot{V} = 26.5 \text{ L/min}$ . Therefore, one has  $q/(\dot{m}c_{pw}) = 3.486 \text{ K}$ ,  $\dot{m}c_{pw}/C_w = 0.04507 \text{ s}^{-1}$ .

Plots of the experimental values of  $T_{out\_exp}$  and  $T_{in\_exp}$ , and of the value of  $T_{in}$  obtained through equation (6.5), denoted by  $T_{in\_num}$ , are reported in figure 6.4. Due to the previous fluid circulation with only the pump on, the initial value of  $T_{in\_exp}$  was  $0.13 \text{ }^\circ\text{C}$  higher than that of  $T_{out\_exp}$ . Therefore, the constant  $0.13 \text{ }^\circ\text{C}$  was added to the values of  $T_{in\_exp}$  given by equation (6.5) to obtain the plot of  $T_{in\_num}$  reported in figure 6.4. The figure shows a good agreement between  $T_{in\_exp}$  and  $T_{in\_num}$ ; the small discrepancies are probably due to oscillations of the electric power that occurred during the considered part of the heating period. Note that  $T_{out\_exp}$  remained nearly constant during the first 500 s and that, during the same period, the difference  $(T_{in} - T_{out})_{exp}$  nearly reached the constant value  $q/(\dot{m}c_{p,f})$ . This circumstance, usual in TRTs, is the reason why the approximations employed to obtain equation (6.5) are acceptable.

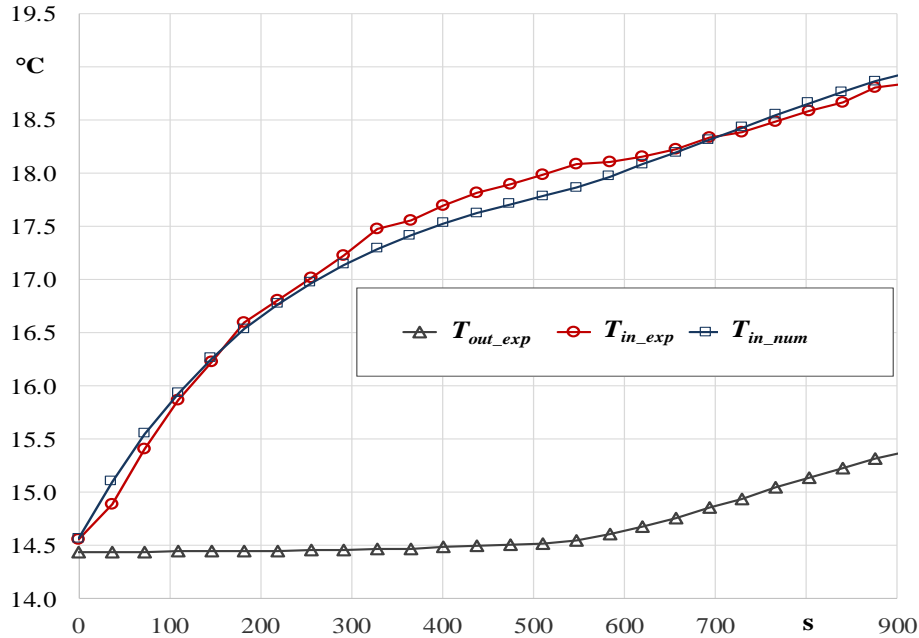


**Figure 6.4.** Comparison between the experimental time evolution of  $T_{in\_exp}$  and that obtained through equation (6.5), denoted by  $T_{in\_num}$ , for a TRT performed at Fiesso d'Artico (Venice) [96].

## 6.2 Results for quasi-stationary regime

The results of the time evolution of  $T_{ave} - T_m$  reported in figures 6.2 and 6.3 show that, at fixed inlet temperature and volume flow rate, the difference  $T_{ave} - T_m$  is a decreasing function of time. However, the ratio  $\Omega = (T_{ave} - T_m) / (T_{in} - T_{out})$  becomes time independent after about two hours from the operation start, as is shown in figure 6.5, which refers to the same working conditions ( $T_{in} = 32$  °C,  $k_{gt} = 1.6$  W/(mK),  $k_g = 1.8$  W/(mK), and flow rates 12 and 24 L/min) but includes also time values lower than 2 hours. Moreover, figure 6.5 shows that if  $\dot{V}$  doubles, the time-independent value of  $\Omega$  becomes one half, with an acceptable approximation: in fact, the mean values of  $\Omega$  from 2 hours to 100 hours are 0.159 and 0.082, for  $\dot{V} = 12$  and for  $\dot{V} = 24$  L/min, respectively.

Therefore, after about two hours of operation at constant inlet temperature and flow rate, the difference  $T_{ave} - T_m$  can be considered as a homogeneous linear function of  $(T_{in} - T_{out}) / \dot{V}$ , independent of the flow rate. Many other simulation results, which will be presented in the following part of this section, have shown that, after two hours of operation at constant flow rate, this homogeneous linear function depends only on the thermal conductivity of grout. Indeed, the linear function can be considered as independent not only of the volume flow rate, but also of the thermal conductivity of ground, of the BHE diameter (for fixed distances between tubes), and of operative conditions (summer operation, winter operation TRT).

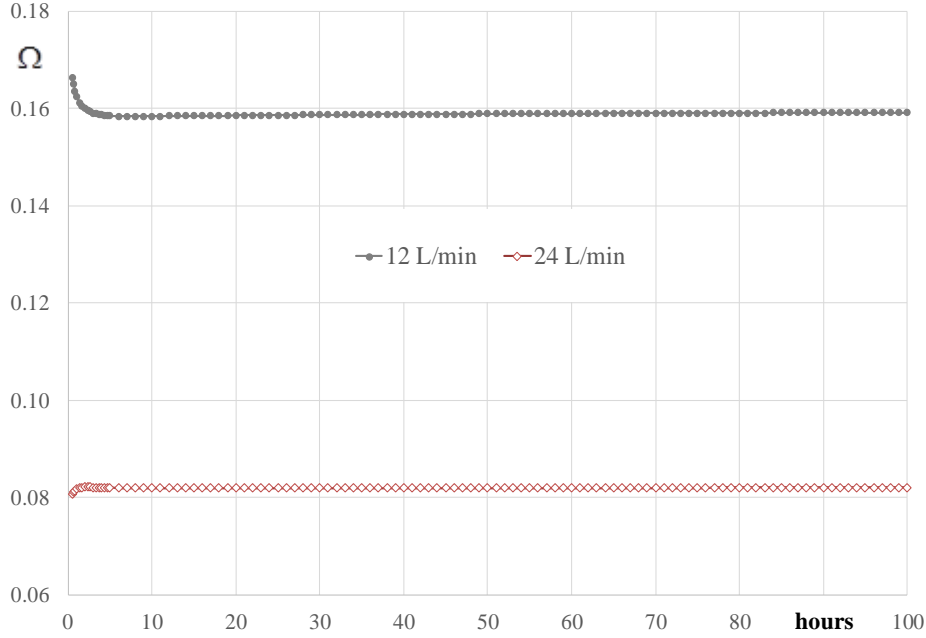


**Figure 6.5.** Time evolution of  $\Omega$  for  $k_{gt} = 1.6$  W/(mK),  $k_g = 1.8$  W/(mK), flow rates 12 and 24 L/min.

The determined expressions of  $T_{ave} - T_m$  as a function of  $(T_{in} - T_{out})/\dot{V}$ , with temperature in °C (or K) and volume flow rate in L/min, are:

$$T_{ave} - T_m = 1.420 \frac{T_{in} - T_{out}}{\dot{V}} \quad , \quad \text{for } k_{gt} = 0.9 \text{ W/(mK)} \quad (6.10)$$

$$T_{ave} - T_m = 1.662 \frac{T_{in} - T_{out}}{\dot{V}} \quad , \quad \text{for } k_{gt} = 1.2 \text{ W/(mK)} \quad (6.11)$$

$$T_{ave} - T_m = 1.918 \frac{T_{in} - T_{out}}{\dot{V}} \quad , \quad \text{for } k_{gt} = 1.6 \text{ W/(mK)} \quad (6.12)$$

Each correlation was achieved by a linear best fit of 315 simulation outcomes obtained by considering summer operation with  $T_{in} = 32$  °C in the time interval between 2 and 100 hours from start, with  $k_g = 1.8$  W/(mK) and volume flow rates 12, 18 and 24 liters per minute. The numerical results leading to equations (6.10 - 6.12) are illustrated in figure 6.6. The figure clearly evidences that the determined correlations hold for every flow rate between 12 and 24 L/min. The mean square deviation from the correlating equation is 0.004 °C for  $k_{gt} = 0.9$  W/(mK), 0.005 °C for  $k_{gt} = 1.2$  W/(mK), and 0.008 °C for  $k_{gt} = 1.6$  W/(mK).

The applicability of equations (6.10 - 6.12) to other values of  $k_g$  is illustrated in figure 6.7 for  $k_{gt} = 0.9$  W/(mK) and in figure 6.8 for and  $k_{gt} = 1.6$  W/(mK). In each case, the discrepancy of the numerical outcomes with respect to the correlation determined by assuming  $k_g = 1.8$  W/(mK) is evidenced, for  $k_g = 1.4$  and 2.2 W/(mK). The mean square deviation from the correlation obtained with  $k_g = 1.8$  W/(mK) is 0.015 °C in the first case, 0.021 °C in the second.

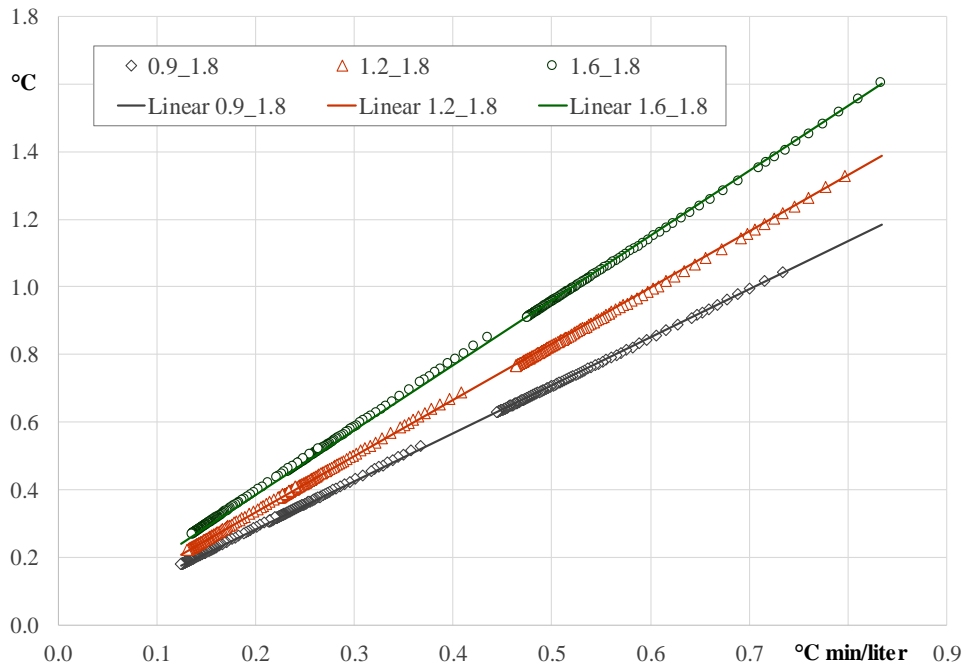


**Figure 6.6.** Linear interpolations of  $T_{ave} - T_m$  as a function of  $(T_{in} - T_{out})/\dot{V}$ , for  $k_{gt} = 0.9, 1.2, 1.6$  W/(mK).

The applicability of equations (6.10 - 6.12) to other values of the BHE diameter is illustrated in figure 6.9, where computation results corresponding to  $D_b = 127$  mm and  $D_b = 177$  mm are compared with the correlation obtained for  $D_b = 152$  mm. The figure refers to  $k_{gt} = 1.2$  W/(mK),  $k_g = 1.8$  W/(mK) and flow rates 12 L/min (higher values of  $T_{ave} - T_m$ ) and 24 L/min (lower values of  $T_{ave} - T_m$ ). Note that  $D_b = 127$  mm corresponds to the borderline case of tubes in contact with the ground. The mean square deviation from the correlation is 0.018 °C for the borderline case  $D_b = 127$  mm and 0.012 °C for the case  $D_b = 177$  mm.

Finally, the applicability of equations (6.10 - 6.12) to other working conditions is illustrated in figure 6.10, where computation outcomes for winter working conditions with  $T_{in} = 4$  °C (circles) and for TRTs (squares) are compared with the outputs of the correlation for summer working conditions. The figure refers to:  $k_{gt} = 1.6$  W/(mK) and  $k_{gt} = 1.8$  W/(mK); flow rates 12 and 24 L/min for winter operation; flow rate 12 L/min and supplied power 50 W/m for one TRT; flow rate 24 L/min and supplied power 80 W/m for the other TRT. The results for the lower flow rate are those with higher values of  $T_{ave} - T_m$ .

In a TRT, the differences  $T_{ave} - T_m$  and  $T_{in} - T_{out}$  remain nearly constant in the quasi-stationary regime, so that only one point has been reported in the plot of figure 6.10 for each TRT, obtained by considering the mean values of  $T_{ave} - T_m$  and  $T_{in} - T_{out}$  between 2 and 100 hours of operation. The overall mean square deviation from the correlation, for winter working conditions and TRTs, is 0.029 °C.

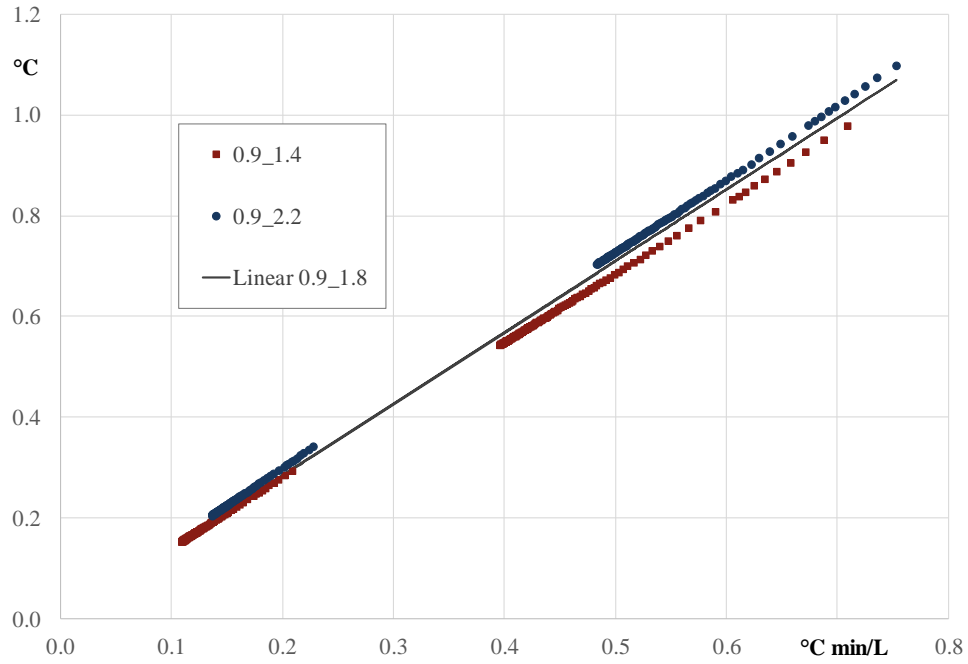


Figure 6.7. Effects of different values of  $k_g$ , namely 1.4 and 2.2 W/(mK), for  $k_{gt} = 0.9$  W/(mK).

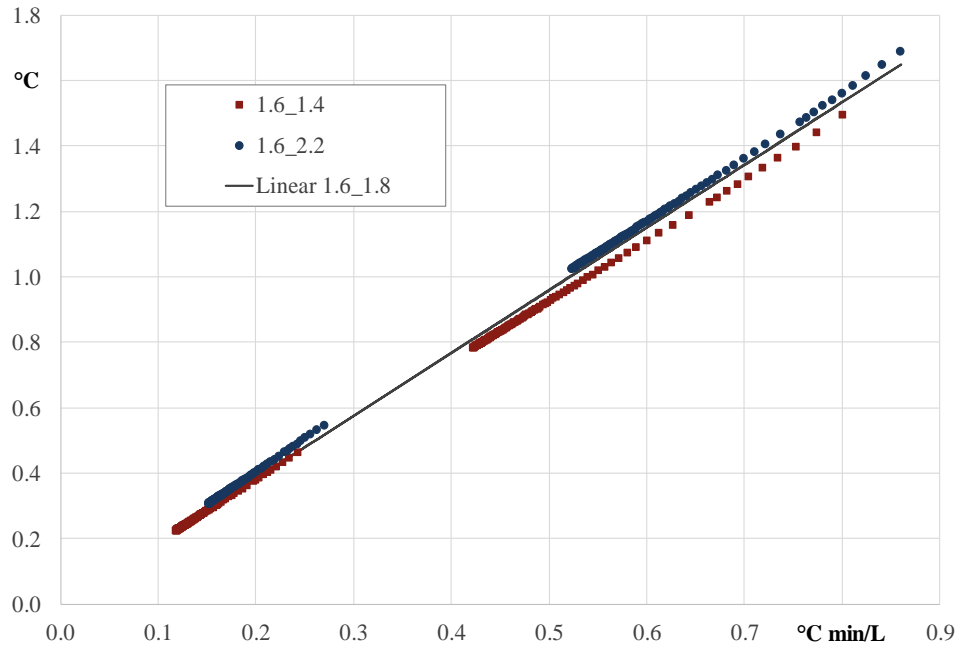
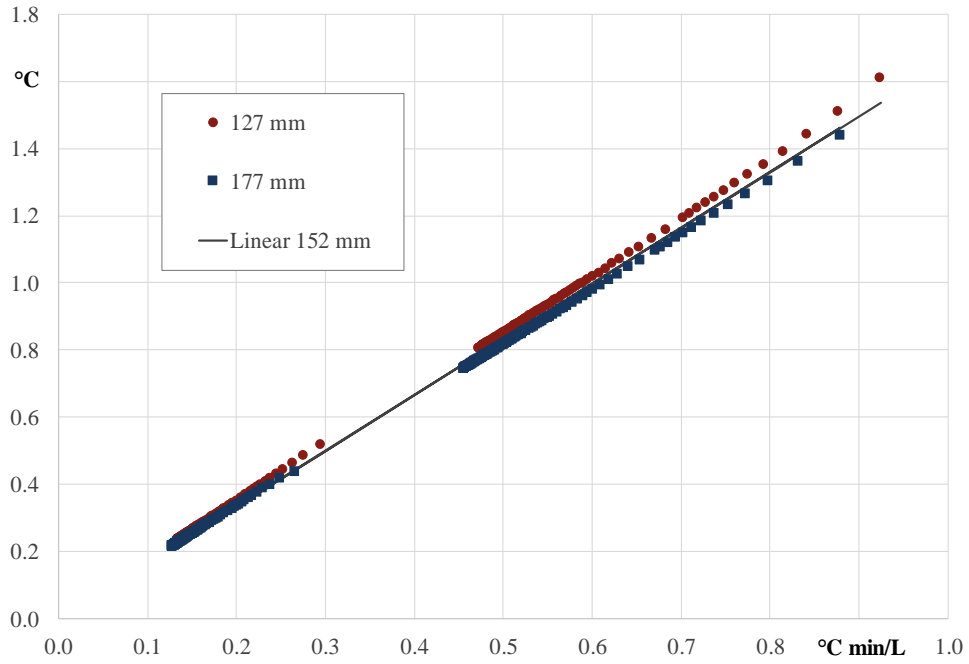
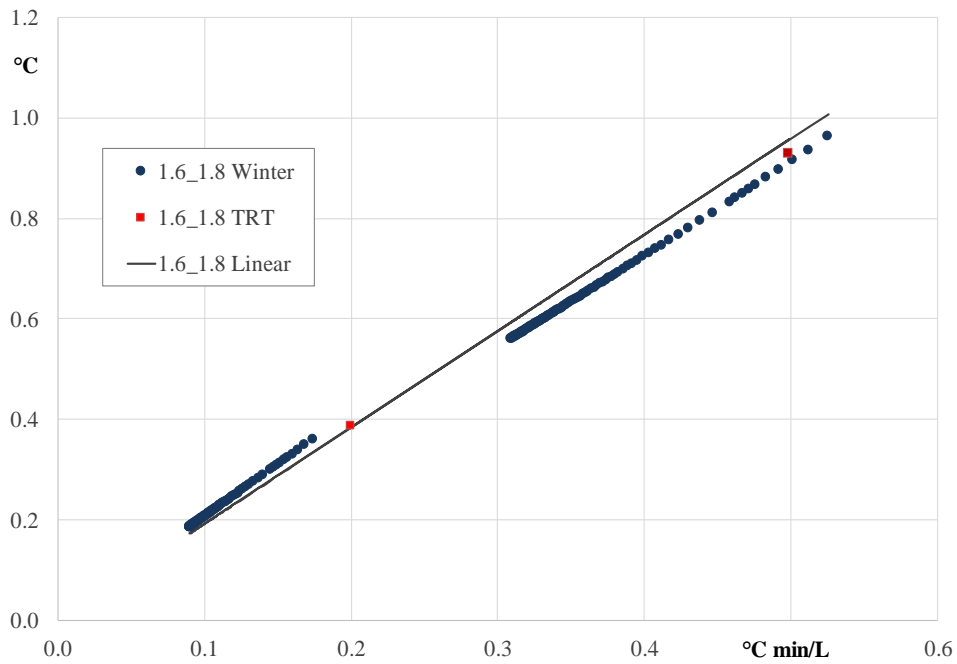


Figure 6.8. Effects of different values of  $k_g$ , namely 1.4 and 2.2 W/(mK), for  $k_{gt} = 1.6$  W/(mK).



**Figure 6.9.** Effects of different values of the BHE diameter, for  $k_{gt} = 1.2 \text{ W/(mK)}$  and  $k_g = 1.8 \text{ W/(mK)}$ .



**Figure 6.10.** Effects of different working condition, for  $k_{gt} = 1.6 \text{ W/(mK)}$  and  $k_g = 1.8 \text{ W/(mK)}$ .

The values of  $T_{ave} - T_m$  can be expressed through the dimensionless coefficient  $\varphi$  defined in equation (6.1), that we denote here with  $\varphi_\infty$  to evidence that we refer to the quasi-stationary regime. From equations (6.1) and (6.10 - 6.12) one obtains:

$$\varphi_\infty = 0.1183 \quad , \quad \text{for } k_{gt} = 0.9 \text{ W/(mK)} \quad (6.13)$$

$$\varphi_\infty = 0.1385 \quad , \quad \text{for } k_{gt} = 1.2 \text{ W/(mK)} \quad (6.14)$$

$$\varphi_\infty = 0.1598 \quad , \quad \text{for } k_{gt} = 1.6 \text{ W/(mK)} \quad (6.15)$$

### 6.3 Results for the first two hours

During the first hour of operation,  $\varphi$  is a decreasing function of time which depends not only on  $k_{gt}$ , but also on the volume flow rate. Through suitable interpolations of the results of the simulation runs employed to determine the correlations given in equations (6.10 - 6.12) and (6.13 - 6.15), dimensionless equations that describe the time evolution of  $\varphi$  during the first two hours were determined. The equations have the form:

$$\varphi = \varphi_\infty \left( 1 + a e^{-bt^*} \right) \quad (6.16)$$

where  $t^*$  is the dimensionless time, defined as the ratio between the time  $t$  from operation start and the total time interval of 2 hours,  $a$  and  $b$  are dimensionless coefficients that depend on  $k_{gt}$  and on the volume flow rate. The determined values of  $a$  and  $b$  are reported in table 6.1, where  $\dot{V}_0$  is the reference flow rate of 12 L/min. Also the values of  $\varphi_\infty$  are reported in table 6.1, for completeness.

**Table 6.1.** Values of  $\varphi_\infty$  and of the coefficients  $a$  and  $b$  of equation (6.16).

$k_{gt}$ W/(mK)	$\varphi_\infty$	$a$	$b$
0.9	0.1183	$3.1 + 3.5 (\dot{V}/\dot{V}_0 - 1)$	$13 + 11 (\dot{V}/\dot{V}_0 - 1)$
1.2	0.1385	$2.45 + 3.1 (\dot{V}/\dot{V}_0 - 1)$	$13 + 11 (\dot{V}/\dot{V}_0 - 1)$
1.6	0.1598	$1.96 + 2.7 (\dot{V}/\dot{V}_0 - 1)$	$13 + 11 (\dot{V}/\dot{V}_0 - 1)$

Diagrams that illustrate the time evolution of  $\varphi/\varphi_\infty$  in the time interval between 1 minute and 1.2 hours ( $1/120 \leq t^* \leq 0.6$ ) and the discrepancies between numerical results and the interpolating equations are reported in figure 6.11, for  $\dot{V} = 12$  L/min, and in figure 6.12, for  $\dot{V} =$

18 L/min. The figures show that the asymptotic value  $\varphi/\varphi_\infty = 1$  is practically reached at  $t^* = 0.4$  (48 minutes) in the first case and  $t^* = 0.3$  (36 minutes) in the second case.

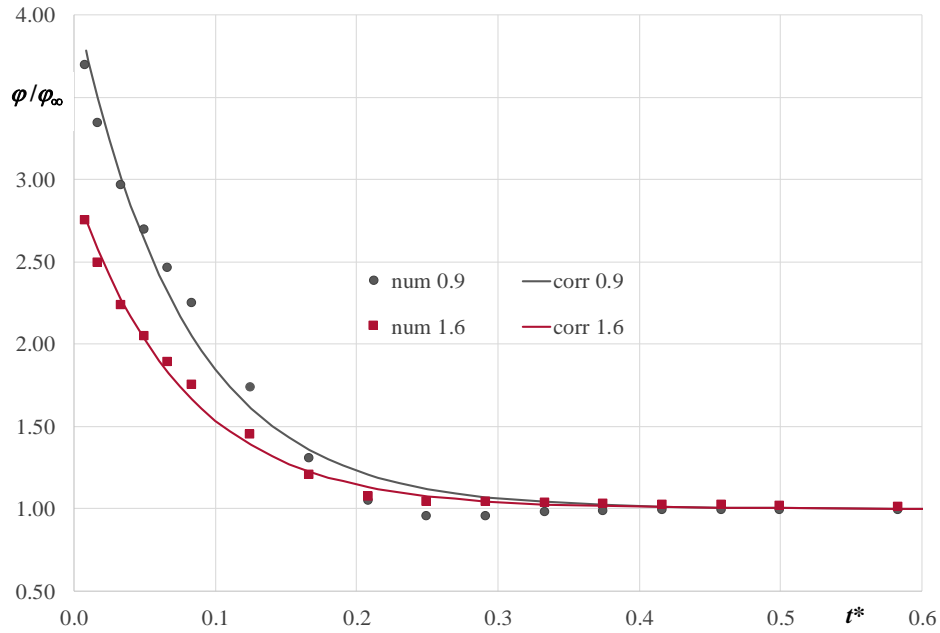


**Figure 6.11.** Plots of  $\varphi/\varphi_\infty$  versus  $t^*$ , for  $k_{gt} = 0.9$  and  $k_{gt} = 1.6$  W/(mK), with flow rate 12 L/min, in the range  $1/120 \leq t^* \leq 0.6$ .

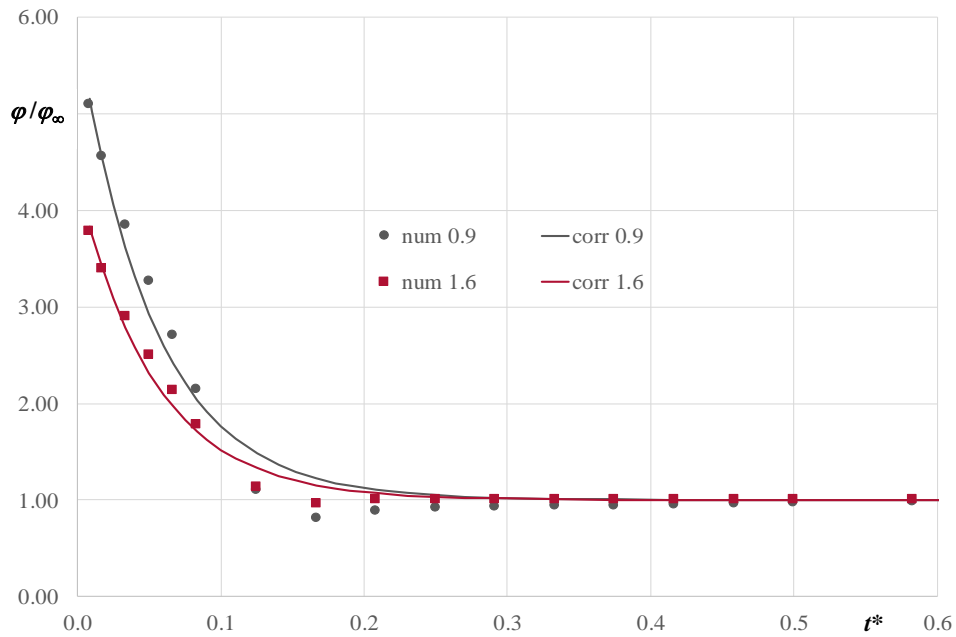


**Figure 6.12.** Plots of  $\varphi/\varphi_\infty$  versus  $t^*$ , for  $k_{gt} = 0.9$  and  $k_{gt} = 1.6$  W/(mK), with flow rate 18 L/min, in the range  $1/120 \leq t^* \leq 0.6$ .

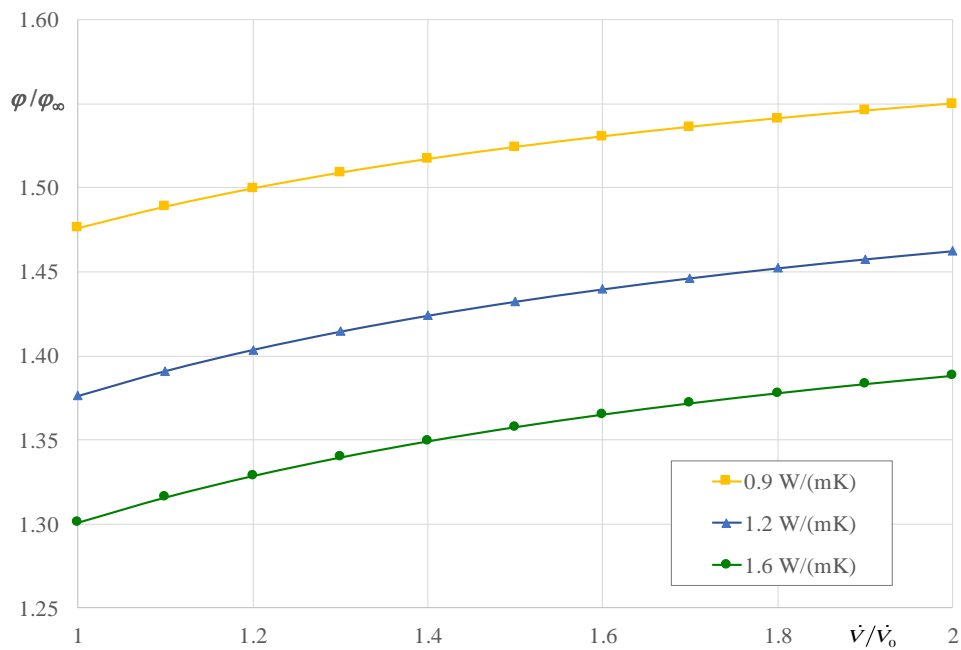


**Table 6.2.** Values of  $\varphi_{mean1}/\varphi_\infty$  as a function of  $k_{gt}$  and of  $\dot{V}/\dot{V}_0$ .

$\dot{V}/\dot{V}_0$	$k_{gt} = 0.9 \text{ W/(mK)}$	$k_{gt} = 1.2 \text{ W/(mK)}$	$k_{gt} = 1.6 \text{ W/(mK)}$
1.0	1.476	1.376	1.301
1.1	1.489	1.391	1.316
1.2	1.500	1.404	1.329
1.3	1.509	1.415	1.340
1.4	1.517	1.424	1.349
1.5	1.524	1.432	1.358
1.6	1.531	1.440	1.365
1.7	1.536	1.446	1.372
1.8	1.541	1.452	1.378
1.9	1.546	1.458	1.383
2.0	1.550	1.462	1.388

Indeed, the values of  $\varphi_\infty$  given by equations (6.13-6.15), although determined by considering simulation results between 2 hours and 100 hours after the operation start, can be employed also in the time interval between 1 hour and 2 hours.

Mean values of  $\varphi$  during the first hour of operation,  $\varphi_{mean1}$ , can be useful for the hourly simulation of GCHPs, to determine the mean value of  $T_{out}$  (inlet temperature in the heat pump) during that hour. Values of  $\varphi_{mean1}/\varphi_\infty$  obtained by analytical integration of equation (6.16) are reported in table 6.2.

**Figure 6.13.** Plots of  $\varphi_{mean1}/\varphi_\infty$  versus  $\dot{V}/\dot{V}_0$ , for  $k_{gt} = 0.9, 1.2$  and  $1.6 \text{ W/(mK)}$ .

A graphical illustration of table 6.2 is reported in figure 6.13. The figure shows that  $\varphi_{mean1}/\varphi_{\infty}$  is a decreasing function of  $k_{gt}$  and an increasing function of the flow rate, with values between 1.3 and 1.55.

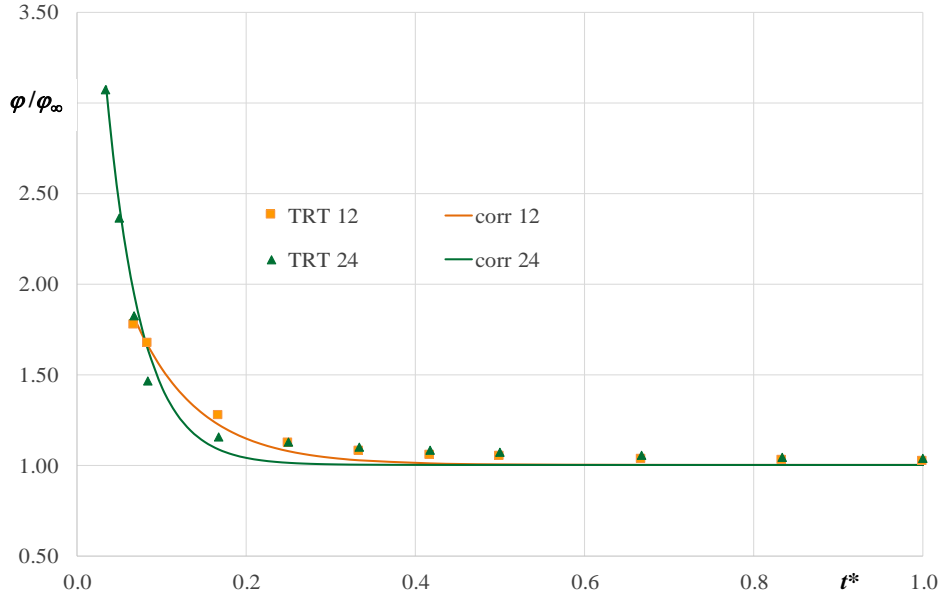


**Figure 6.14.** Plots of  $\varphi/\varphi_{\infty}$  versus  $t^*$  for TRTs with  $k_{gt} = 1.6$  and  $k_g = 1.8$  W/(mK): flow rate 12 L/min, power 50 W/m,  $8/120 \leq t^* \leq 1$ ; flow rate 24 L/min, power 80 W/m,  $4/120 \leq t^* \leq 1$ .

The correlations given by equation (6.16) and table 6.2 have been obtained by considering a constant inlet fluid temperature. The applicability of these correlations to TRTs has been checked for the TRT conditions, namely:  $k_{gt} = 1.6$  W/(mK) and  $k_{gt} = 1.8$  W/(mK); flow rate 12 L/min and supplied power 50 W/m for one TRT; flow rate 24 L/min and supplied power 80 W/m for the other TRT. In figure 6.14, the values of  $\varphi/\varphi_{\infty}$  obtained by numerical simulations, for the first two hours of operation, are compared with those obtained by the correlation for  $k_{gt} = 1.6$  W/(mK). The figure shows a good agreement, after 4 minutes from start for the higher flow rate and after 8 minutes from start for the lower flow rate. Thus, equation (6.16) is applicable also to TRTs, except for the very first minutes. Indeed, TRTs are usually performed with flow rates between 18 and 24 L/min.

## 6.4 Possible applications

The results presented in sections 6.2 and 6.3 can be employed in the evaluation of TRTs by the infinite line-source method and in hourly simulation codes for GCHP systems, with reference to double U-tube BHEs. Since we have proved that the obtained correlations for the evaluation of  $T_{ave} - T_m$  can be considered as independent of the ground conductivity, the BHE diameter, and the working conditions, the results need to be extended only to other values of the distance between

the axes of opposite tubes (shank spacing) and other values of the BHE length. This extension will require a reasonable computational effort and will be performed shortly. Clearly, the whole study can be repeated for single U-tube BHEs.

For the evaluation of TRTs, one can transform the measured values of  $T_{ave}$  into values of  $T_m$  by the relation:

$$T_m = T_{ave} - \varphi \frac{\dot{V}_0}{\dot{V}} (T_{in} - T_{out}) \quad (6.17)$$

If only late-time data are employed, as is done when one applies the infinite line-source evaluation method,  $\varphi = \varphi_\infty$ .

For the hourly simulation of GCHPs, one needs to determine the outlet temperature  $T_{out}$  as a function of the mean fluid temperature  $T_m$  and of the difference  $T_{in} - T_{out}$ , which corresponds to the power exchanged between BHE and ground.

The relation between  $T_{out}$ ,  $T_m$  and  $T_{in} - T_{out}$  can be easily expressed through the coefficient  $f$  introduced by Beier and Spitler [79]. This method is extension of the method presented by Beier [78] to short times after a change in either heat input rate or fluid flow rate. They defined the dimensionless parameter  $f$  which allows to determine  $T_m$  through the relation:

$$T_m = f T_{in} + (1 - f) T_{out} \quad (6.18)$$

From equation (6.18), one obtains:

$$T_{out} = T_m - f (T_{in} - T_{out}) \quad (6.19)$$

Consider the identity:

$$\frac{T_{ave} - T_m}{T_{in} - T_{out}} + \frac{T_m - T_{out}}{T_{in} - T_{out}} = 0.5 \quad (6.20)$$

From equation (6.1), one has:

$$\frac{T_{ave} - T_m}{T_{in} - T_{out}} = \varphi \frac{\dot{V}_0}{\dot{V}} \quad (6.21)$$

The second term in the left hand side of equation (6.20) is equal to  $f$ . Therefore, equations (6.20) and (6.21) yield:

$$f = 0.5 - \phi \frac{\dot{V}_0}{\dot{V}} \quad (6.22)$$

By substituting equation (6.22) in equation (6.19) one has also

$$T_{out} = T_m - \left( 0.5 - \phi \frac{\dot{V}_0}{\dot{V}} \right) (T_{in} - T_{out}) \quad (6.23)$$

The values of  $\phi_{mean1}$ , obtainable from tables 6.1 and 6.2 and equation (6.23), allow to determine precise hourly mean values of  $T_{out}$  without enhancing the computation time.



## *Chapter 7*

---

*Effects of the temperature distribution on the thermal resistance*



## *Effects of the temperature distribution on the thermal resistance*<sup>3</sup>

---

Thermal resistance of the BHE can be calculated by knowledge of the bulk fluid temperature, the BHE external surface temperature, and the thermal power per unit length exchanged between BHE and ground. Two definitions of the BHE thermal resistance per unit length are usually considered in the literature. The first, that we denote by  $R_{b,2D}$ , refers to a BHE cross sections and is:

$$R_{b,2D} = \frac{T_f - T_s}{q_l} \quad (7.1)$$

where  $T_f$  is the bulk fluid temperature in a BHE cross section (averaged between tubes),  $T_s$  is the mean temperature of the BHE surface in the same section, and  $q_l$  is the thermal power per unit length exchanged between BHE and ground in the neighborhood of that section, positive if

---

<sup>3</sup> This chapter is based on the following publication [57]:  
- E. Zanchini, A. Jahanbin. Effects of the temperature distribution on the thermal resistance of double u-tube borehole heat exchangers. *Geothermics* 71 (2018) 46-54.



supplied to the ground. If the thermal conductivity of the grout is known,  $R_{b,2D}$  can be easily calculated by performing a 2D numerical simulation of the BHE cross section, or by employing approximate expressions cited in section 3.1.

The second definition, called *effective* thermal resistance, is given by:

$$R_{b,eff} = \frac{T_{f,ave} - T_{s,m}}{q_{l,m}} \quad (7.2)$$

where  $T_{f,ave}$  is the arithmetic mean of inlet and outlet fluid temperatures, and is defined as:

$$T_{f,ave} = \frac{T_{f,in} + T_{f,out}}{2} \quad (7.3)$$

$T_{s,m}$  is the mean temperature of the external surface of the BHE and  $q_{l,m}$  is the mean thermal power per unit length exchanged between BHE and ground, positive if supplied to the ground. As pointed out by Lamarche et al. [56], another possible definition is:

$$R_{b,3D} = \frac{T_{f,m} - T_{s,m}}{q_{l,m}} \quad (7.4)$$

where  $T_{f,m}$  is the real mean value of the bulk fluid temperature, namely:

$$T_{f,m} = \frac{1}{2L} \left( \int_0^L T_{f,d}(z) dz + \int_0^L T_{f,u}(z) dz \right) \quad (7.5)$$

where  $L$  is the BHE length,  $z$  is the vertical coordinate directed downwards,  $T_{f,d}$  is the local bulk temperature of the fluid going down (descending fluid), and  $T_{f,u}$  is the local bulk temperature of the fluid going up (ascending fluid). Although equation (7.4) would be the natural 3D extension of equation (7.1), it is usually replaced by equation (7.3), because  $T_{f,ave}$  can be easily measured.

Lamarche et al. [56] examined the accuracy of different methods to calculate  $R_{b,2D}$  for single U-tube BHEs, by employing finite element simulations, and showed that the temperature distribution on the BHE external surface has a relevant effect on  $R_{b,2D}$  for this kind of BHEs, for high values of the shank spacing. In addition, they compared different methods to determine the vertical distribution of the bulk fluid temperature and found a good agreement between their numerical results and those obtained through the method of Zeng et al. [70].

In this chapter, an analysis similar to that presented by Lamarche et al. [56] is performed, with reference to double U-tube BHEs, which are more widely used in Italy. First, the effects of the temperature distribution in a cross section on  $R_{b,2D}$  are investigated, by 2D finite element simulations. Then, the relations between  $R_{b,eff}$ ,  $R_{b,3D}$  and  $R_{b,2D}$  are investigated by 3D finite element simulations. The employed simulation code is that used in the previous chapter (Code II), and the

results of 3D simulations are validated by comparison with those yielded by the analytical method of Zeng et al. [70].

### 7.1 Thermal resistance of the cross section of a double U-tube BHE

In this section, we analyze the effects of the temperature distributions along the boundary surfaces on the thermal resistance  $R_{b,2D}$  of a typical double U-tube BHE in usual working conditions.

To clarify the problem, we briefly recall a rigorous definition of thermal resistance. As illustrated in figure 7.1, Let  $V$  be a portion of solid, under steady-state conditions, such that two boundary surfaces  $S_1$  and  $S_2$  of  $V$  are isothermal, and thus orthogonal to the heat flux density vector  $\mathbf{q}$ , while the other boundary surfaces are parallel to  $\mathbf{q}$ , and thus are not crossed by thermal power. Under these conditions,  $S_1$ ,  $S_2$  and any other surface in  $V$  which cuts all the flux lines of  $\mathbf{q}$  are crossed by the same thermal power  $q$ . If one denotes by  $T_1$  and  $T_2$  the temperatures of  $S_1$  to  $S_2$ , with  $T_1 > T_2$ , one can define the thermal resistance of  $V$  as:

$$R = \frac{T_1 - T_2}{q} \quad (7.6)$$

The thermal resistance defined by equation (7.6) is positive and depends only on the shape and size of  $V$  and on the thermal conductivity distribution in  $V$ .

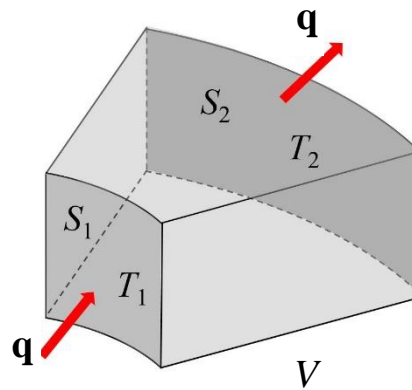


**Figure 7.1.** Illustration of the definition of thermal resistance: the lateral surfaces are tangent to the heat flux density vector  $\mathbf{q}$ .

If the state of  $V$  is stationary and the boundary surfaces other than  $S_1$  and  $S_2$  are tangent to the heat flux density vector, but  $S_1$  and  $S_2$  are non-isothermal, the definition of thermal resistance can be extended by replacing  $T_1$  and  $T_2$  with the mean values  $T_{m1}$  and  $T_{m2}$  on  $S_1$  and  $S_2$  respectively:

$$R = \frac{T_{m1} - T_{m2}}{q} \quad (7.7)$$

In equation (7.7), however,  $R$  depends on the temperature distributions on  $S_1$  and on  $S_2$ , as has been shown by Lamarche et al. [56] for  $R_{b,2D}$  of single U-tube BHEs. An analysis of this dependence for double U-tube BHEs is presented here.

Let us consider a double U-tube BHE with diameter  $D_b = 152$  mm, tubes in high-density polyethylene with external diameter  $D_e = 32$  mm, internal diameter  $D_i = 26$  mm, and thermal conductivity,  $k_p$ , equal to 0.4 W/(mK). Consider two values of the distance between the centers of opposite tubes, namely, shank spacing:  $d = 85$  mm and  $d = 120$  mm. The first is the most commonly used shank spacing in Italy; the second is the maximum possible one for the selected BHE diameter, and yields tubes touching the BHE external surface. Consider two values of the thermal conductivity of the sealing grout:  $k_{gt} = 0.9$  and  $k_{gt} = 1.6$  W/(mK), and three values of the thermal conductivity of ground:  $k_g = 1.4$ ,  $k_g = 1.8$  and  $k_g = 2.8$  W/(mK). The thermophysical properties and fluid flow characteristics are as presented in chapter 4 for Code II. The BHE cross section is sketched in figure 7.2, with lengths in mm.

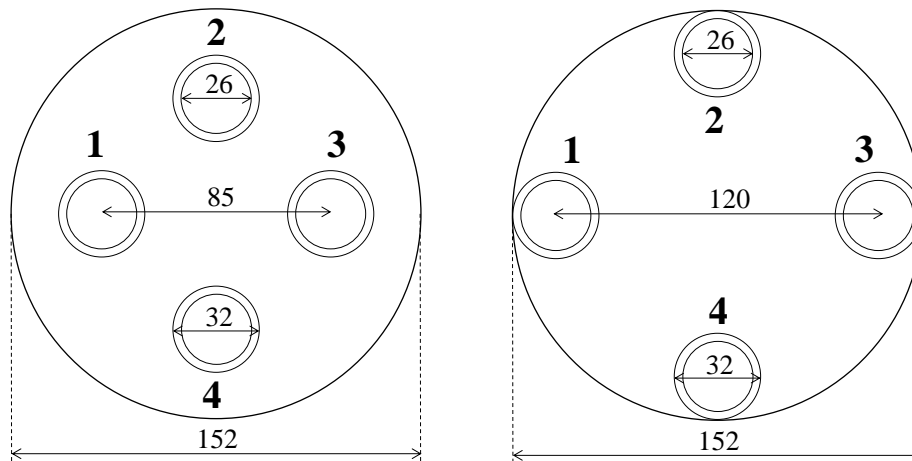


**Figure 7.2.** Cross section of the BHE considered, with shank spacing 85 mm (left) and 120 mm (right).

The thermal resistance  $R_{b,2D}$  of this BHE, with shank spacing 85 mm, has been determined with six different schemes. Schemes 1-4 consider steady-state conditions, and are as follows:

- 1) The flowing water has a bulk temperature equal to 30 °C in all tubes, and the external surface of the BHE is isothermal with  $T_2 = 20$  °C.
- 2) The flowing water has a bulk temperature equal to 32 °C in tubes 1 and 2, and equal to 28 °C in tubes 3 and 4, while the external surface of the BHE is isothermal with  $T_2 = 20$  °C.

- 3) The flowing water has a bulk temperature equal to 30 °C in all tubes, while the external surface is surrounded by a cylindrical ground layer with external radius 2 m and uniform external temperature equal to 14 °C.
- 4) The flowing water has a bulk temperature equal to 32 °C in tubes 1 and 2, and equal to 28 °C in tubes 3 and 4, while the external surface is surrounded by a cylindrical ground layer with external radius 2 m and uniform external temperature equal to 14 °C.

Schemes 5 and 6 consider unsteady heat transfer, with initial temperature 14 °C in the whole computational domain and duration 100 hours:

- 5) The flowing water has a bulk temperature equal to 30 °C in all tubes, while the external surface is surrounded by a cylindrical ground layer with external radius 10 m and adiabatic external surface.
- 6) The flowing water has a bulk temperature equal to 32 °C in tubes 1 and 2, and equal to 28 °C in tubes 3 and 4, while the external surface is surrounded by a cylindrical ground layer with external radius 10 m and adiabatic external surface.

Schemes 1 and 2 required two simulations each, with  $k_{gt} = 0.9$  W/(mK) and  $k_{gt} = 1.6$  W/(mK) respectively. Schemes 3-6 required 6 simulations each, with different combinations of  $k_{gt}$  and  $k_g$ . Simulations were performed through COMSOL Multiphysics, with unstructured meshes composed of triangular elements: 89 216 elements for schemes 1 and 2, 188 032 elements for schemes 3 and 4, 182 560 elements for schemes 5 and 6. The values of thermal resistance obtained by numerical simulations were compared with those obtained by applying the analytical expression proposed by Conti et al. [71] through line-source model and was presented in chapter 3, namely:

$$R_{b,2D,C} = \frac{1}{8\pi k_{gt}} \left[ \ln\left(\frac{D_b}{D_e}\right) + 2 \ln\left(\frac{D_b}{\sqrt{2}d}\right) + \ln\left(\frac{D_b}{2d}\right) - \frac{k_{gt} - k_g}{k_{gt} + k_g} \left(\frac{D_b^8 - d^8}{D_b^8}\right) \right] + \frac{R_p}{4} \quad (7.8)$$

where  $D_e$  is the external diameter of each polyethylene tube,  $d$  is the shank spacing, and  $R_p$  is the thermal resistance of each polyethylene tube. The latter is given by:

$$R_p = \frac{1}{2\pi k_p} \ln \frac{D_e}{D_i} + \frac{1}{h\pi D_i} \quad (7.9)$$

where  $D_i$  is the internal diameter of the tube.

The results are presented in table 7.1. They show that the temperature difference between pairs of tubes has completely no effect on  $R_{b,2D}$ . Indeed, the results obtained by scheme 1 coincide with those obtained by scheme 2, those obtained by scheme 3 coincide with those obtained by scheme 4, and those obtained by scheme 5 coincide with those obtained by scheme 6. A comparison between the results of scheme 3 and those of scheme 1 (or between those of scheme 4

and those of scheme 2) reveals that, in the case of shank spacing 85 mm, the non-uniform temperature distribution on the BHE external surface due to heat transfer with the ground yields a very small increase of  $R_{b,2D}$ : the highest increase, about 0.49%, is obtained for the pair of lowest conductivities, namely  $k_{gt} = 0.9$  W/(mK) and  $k_g = 1.4$  W/(mK).

**Table 7.1.** Values of the 2D thermal resistance for shank spacing 85 mm (figure 7.1, left), obtained by different calculation schemes.

$k_{gt}$	$k_g$	$R_{b,2D,C}$	Scheme	$T_s$	$q_l$	$R_{b,2D}$
0.9	----	----	1	20	97.848	0.1022
			2	20	97.848	0.1022
0.9	1.4	0.1072	3	26.536	33.719	0.1027
			4	26.536	33.719	0.1027
			5	----	----	0.1028
			6	----	----	0.1028
0.9	1.8	0.1072	3	25.808	40.835	0.1027
			4	25.808	40.835	0.1027
			5	---	---	0.1027
			6	---	---	0.1027
0.9	2.8	0.1071	3	24.312	55.477	0.1025
			4	24.312	55.476	0.1025
			5	---	---	0.1025
			6	---	---	0.1025
1.6	----	----	1	20	143.80	0.06954
			2	20	143.80	0.06954
1.6	1.4	0.07026	3	27.470	36.232	0.06983
			4	27.470	36.232	0.06983
			5	---	---	0.06983
			6	---	---	0.06983
1.6	1.8	0.07023	3	26.889	44.576	0.06979
			4	26.889	44.576	0.06979
			5	---	---	0.06980
			6	---	---	0.06980
1.6	2.8	0.07018	3	25.635	62.595	0.06973
			4	25.635	62.595	0.06973
			5	---	---	0.06974
			6	---	---	0.06974

A comparison between the results of scheme 5 and those of scheme 3 (or between those of scheme 6 and those of scheme 4) shows that a steady-state numerical simulation with BHE surrounded by a 2 m ground layer is sufficient to take into account the effects of the coupling between BHE and ground. The highest difference found between the results of these schemes is less than 1 unit in the fourth significant digit.

Finally, the values of  $R_{b,2D,c}$  reported in the third column of table 7.1 show that equation (7.8) yields an overestimation of about 4% of the 2D thermal resistance for  $k_{gt} = 0.9$  W/(mK), and is nearly exact (0.6% overestimation) for  $k_{gt} = 1.6$  W/(mK).

The 2D thermal resistance of the BHE in the limit case of shank spacing 120 mm has been analyzed with schemes 1, 3 and 5, and with equation (7.8). The computations with schemes 2, 4, 6 have not been carried out systematically, but some checks have confirmed that these schemes yield the same results as schemes 1, 3 and 5.

**Table 7.2.** Values of the 2D thermal resistance for shank spacing 120 mm (figure 7.1, right), obtained by schemes 1, 3, 5 and equation (7.8).

$k_{gt}$	$k_g$	$R_{b,2D,c}$	Scheme	$T_s$	$q_l$	$R_{b,2D}$
0.9	---	---	1	20	204.124	0.04899
0.9	1.4	0.05999	3	27.867	37.3051	0.05718
			5	---	---	0.05718
0.9	1.8	0.05915	3	27.403	46.3587	0.05602
			5	---	---	0.05602
0.9	2.8	0.05785	3	26.388	66.6562	0.05419
			5	---	---	0.05419
1.6	---	---	1	20	249.496	0.04008
1.6	1.4	0.04479	3	28.287	38.4318	0.04457
			5	---	---	0.04459
1.6	1.8	0.04428	3	27.885	48.0283	0.04404
			5	---	---	0.04405
1.6	2.8	0.04341	3	26.987	69.8722	0.04312
			5	---	---	0.04313

The results reported in table 7.2 show that, with this extreme value of the shank spacing, the non-uniform temperature distribution on the BHE boundary surface has a relevant effect on the 2D thermal resistance, especially in the case of low thermal conductivity of the ground. For  $k_g = 1.4$  W/(mK), considering the BHE boundary surface as isothermal (scheme 1) yields a 14%

underestimation of  $R_{b,2D}$  for  $k_{gt} = 0.9$  W/(mK) and a 10% underestimation for  $k_{gt} = 1.6$  W/(mK).

The increasing non-uniformity of the temperature distribution on the BHE surface, due to wider shank spacing, is illustrated in figure 7.3, for  $k_{gt} = 0.9$  W/(mK),  $k_g = 1.4$  W/(mK) and scheme 4.

The results obtained by scheme 3 are nearly identical with those obtained by scheme 5. The use of equations (7.8) yields an overestimation of the 2D thermal resistance between 5% and 7% for  $k_{gt} = 0.9$  W/(mK), and between 0.5% and 0.7% for  $k_{gt} = 1.6$  W/(mK).

The results of present analysis allow to conclude that scheme 3 is recommendable for the numerical calculations of  $R_{b,2D}$ , because it can be easily applied and yields accurate values of the BHE thermal resistance for every value of the shank spacing.

Equation (7.8) yields accurate results for high values of the thermal conductivity of the sealing grout and yields a slight overestimation of the BHE thermal resistance in case of low-conductivity grout.

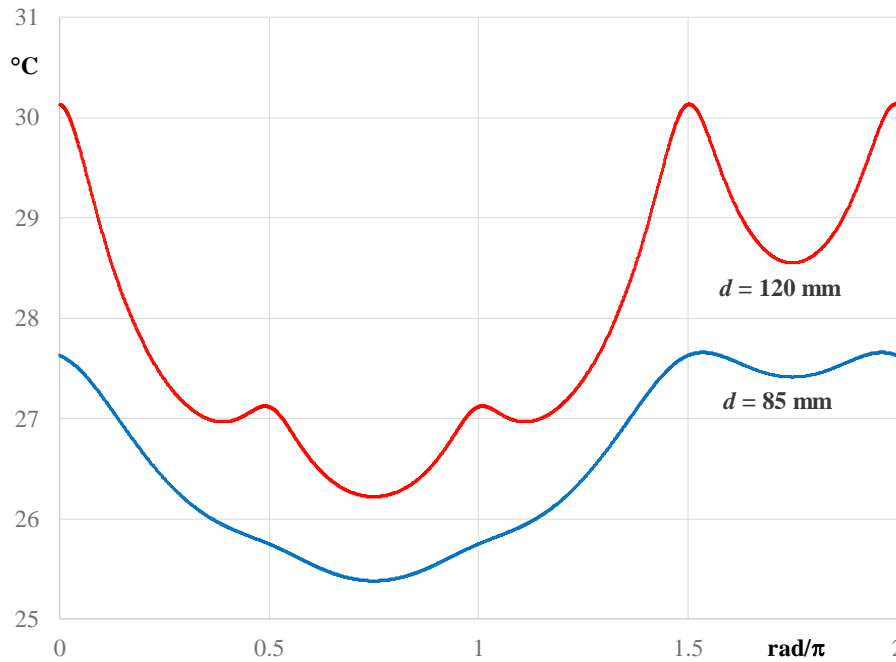


**Figure 7.3.** Temperature distribution on the BHE surface versus the angular distance from the upper point of figure 7.2, with  $d = 85$  mm and  $d = 120$  mm, for  $k_{gt} = 0.9$  W/(mK) and  $k_g = 1.4$  W/(mK), scheme 4.

## 7.2 Relations between $R_{b,eff}$ , $R_{b,3D}$ and $R_{b,2D}$ for double U-tube BHEs

In this section, we analyze the differences between the thermal resistances  $R_{b,eff}$ ,  $R_{b,3D}$  and  $R_{b,2D}$  for double U-tube BHEs in usual working conditions. While it is well known that  $R_{b,eff}$  is higher than  $R_{b,2D}$  (Hellström [62], Lamarche et al. [56]), the relation between  $R_{b,3D}$  and  $R_{b,2D}$  is not

discussed in the literature, maybe because these quantities are implicitly considered as coincident. However, since the non-uniform temperature distribution along the cross section boundary has an effect on  $R_{b,2D}$ , as shown by Lamarche et al. [56] for single U-tube BHEs and here in section 7.2 for double U-tube ones, the non-uniform axial temperature distribution could yield a difference between  $R_{b,3D}$  and  $R_{b,2D}$ .

In subsection 7.2.1 it is proved that, if the cross section thermal resistance  $R_{b,2D}$  is invariant along the BHE length, then  $R_{b,3D}$  is independent of the temperature distribution along the BHE axis and coincides with  $R_{b,2D}$ . In subsection 7.2.2, the results of our computational analysis of the relations between  $R_{b,eff}$ ,  $R_{b,3D}$  and  $R_{b,2D}$  are presented.

### 7.2.1 A theorem on the relation between $R_{b,3D}$ and $R_{b,2D}$

Consider a BHE with any number and distribution of tubes and length  $L$ . Suppose that the 2D thermal resistance  $R_{b,2D}$  is independent of the vertical coordinate  $z$ , and that the thermal power flowing from fluid to ground through the end horizontal surfaces can be neglected. Under these conditions,  $R_{b,3D}$  and  $R_{b,2D}$  are equal.

#### ❖ *Proof*

Denote by  $T_f(z)$  the bulk temperature of the fluid at a depth  $z$  (averaged between tubes) and by  $T_s(z)$  the mean temperature of the BHE external surface at the same depth. The 3D BHE thermal resistance per unit length is given by:

$$R_{b,3D} = \frac{T_{f,m} - T_{s,m}}{q/L} = \frac{L(T_{f,m} - T_{s,m})}{q} \quad (7.10)$$

where  $q$  is the total thermal power flowing from the fluid to the external lateral surface of the BHE. Clearly, one has:

$$q = \int_0^L q_l(z) dz \quad (7.11)$$

By definition of  $R_{b,2D}$ , one has

$$q_l(z) = \frac{T_f(z) - T_s(z)}{R_{b,2D}} \quad (7.12)$$

By substituting equation (7.12) in equation (7.11), one gets:



$$q = \frac{1}{R_{b,2D}} \left[ \int_0^L T_f(z) dz - \int_0^L T_s(z) dz \right] = \frac{1}{R_{b,2D}} (LT_{f,m} - LT_{s,m}) = \frac{L(T_{f,m} - T_{s,m})}{R_{b,2D}} \quad (7.13)$$

Equation (7.13) can be written as:

$$R_{b,2D} = \frac{L(T_{f,m} - T_{s,m})}{q} \quad (7.14)$$

Equations (7.10) and (7.14) yield:

$$R_{b,3D} = R_{b,2D} \quad (7.15)$$

## 7.2.2 Results of computational analysis

The 3D simulations allowed to determine, for each pair of values of grout thermal conductivity and volume flow rate, the time evolution of the outlet bulk fluid temperature  $T_{f,out}$ , of the mean bulk fluid temperature  $T_{f,m}$ , of the mean BHE surface temperature  $T_{s,m}$ , of the mean thermal power per unit length  $q_{l,m}$  flowing from the fluid to the BHE surface, of the effective BHE thermal resistance  $R_{b,eff}$ , and of the 3D BHE thermal resistance  $R_{b,3D}$ . Results have been reported for the time interval from 2 to 100 hours; for time values lower than 2 hours the heat transfer in the BHE is far from being stationary and the concept of BHE thermal resistance has a poor meaning.

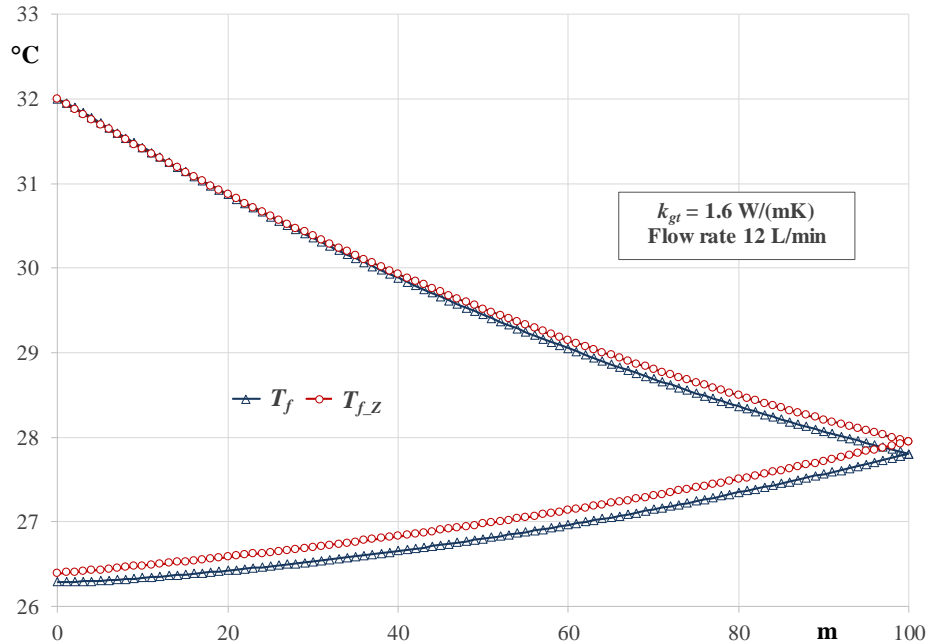


**Figure 7.4.** Plot of  $T_f$  versus the vertical coordinate  $z$ , compared with that yielded by the method of Zeng et al. [70],  $T_{f,Z}$ , for  $k_{gt} = 1.6 \text{ W/(mK)}$  and volume flow rate 12 L/min.

For each simulation run, the results for  $T_{f,out}$  and for  $R_{b,eff}$  were compared with those obtained by applying the analytical method proposed by Zeng et al. [70]. Again in this chapter the flow configuration considered is that denoted by Zeng et al. [70] as (1-3, 2-4).

The distributions of the bulk fluid temperature obtained by 3D simulations and by applying the method of Zeng et al. [70] are illustrated in figure 7.4, for the case  $k_{gt} = 1.6 \text{ W/(mK)}$  and volume flow rate 12 L/min. The figure shows that the temperature profile is far from being linear, due to the thermal short-circuiting between the fluid going down (upper part of the plot) and that coming up (lower part). The temperature decrease in the descending flow, where the fluid releases heat both to the ground and to the ascending flow, is much higher than that in the ascending flow, where the fluid is heated by the descending one. There is a fair agreement between the diagram of  $T_f(z)$  obtained by the 3D simulation and that obtained by applying the method of Zeng et al. [70]. With respect to simulations, the analytical method yields a slightly higher outlet temperature.

In figures 7.5-7.8, plots of the difference between inlet and outlet temperatures versus time obtained by 3D simulations are compared with those yielded by the method of Zeng et al. [70]. Figures 7.5 and 7.6 refer to  $k_{gt} = 0.9 \text{ W/(mK)}$ , and to volume flow rates 12 and 24 L/min respectively; figures 7.7 and 7.8 refer to  $k_{gt} = 1.6 \text{ W/(mK)}$ , and to volume flow rates 12 and 24 L/min respectively.

Values of  $T_{f,in} - T_{f,out}$  after 100 hours of operation are reported in table 7.3 and are compared with those yielded by the method of Zeng et al. [70].

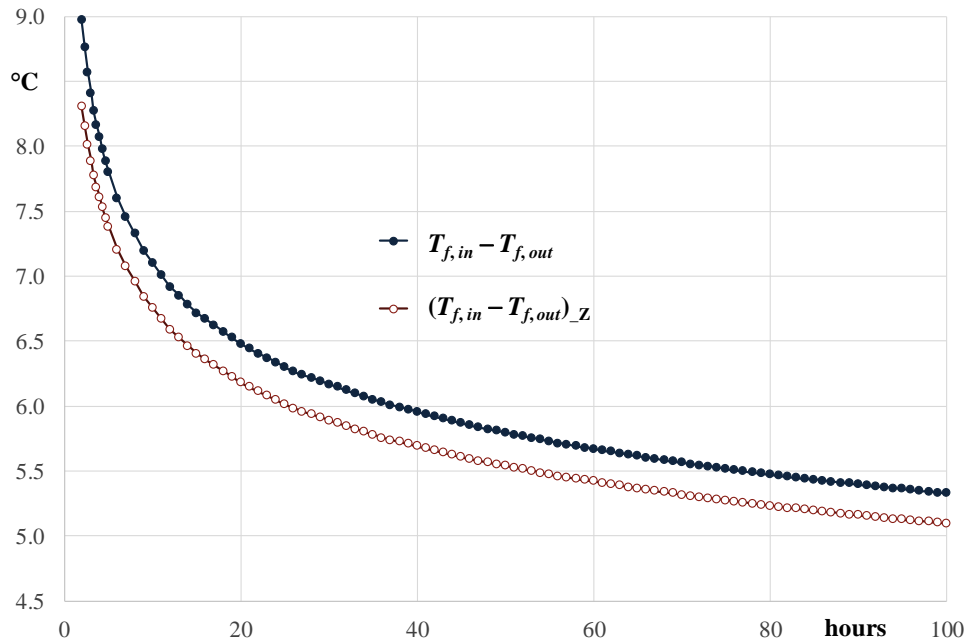


**Figure 7.5.** Plot of  $T_{f,in} - T_{f,out}$  versus time, compared with that yielded by the method of Zeng et al. [70],  $(T_{f,in} - T_{f,out})_Z$ , for  $k_{gt} = 0.9 \text{ W/(mK)}$  and volume flow rate 12 L/min.

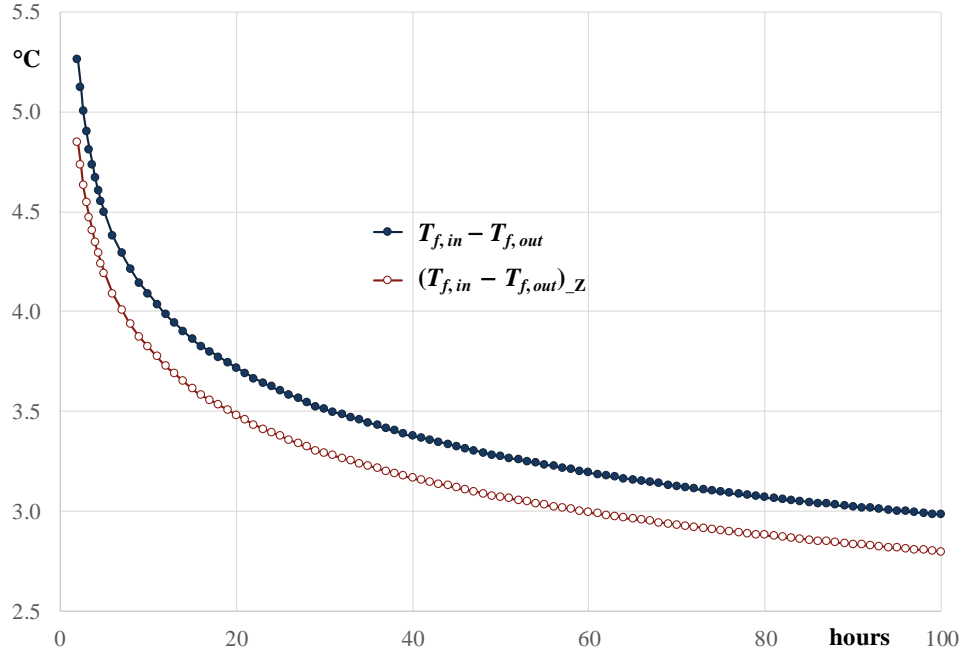


**Figure 7.6.** Plot of  $T_{f,in} - T_{f,out}$  versus time, compared with that yielded by the method of Zeng et al. [70],  $(T_{f,in} - T_{f,out})_Z$ , for  $k_{gt} = 0.9$  W/(mK) and volume flow rate 24 L/min.

Figures 7.5-7.8 and table 7.3 show an acceptable agreement between the results of numerical simulations and those obtained by the method of Zeng et al. [70]. In all cases, the analytical method yield a slight underestimation of the difference  $T_{f,in} - T_{f,out}$  with respect to the finite element simulations. The percent discrepancy in  $T_{f,in} - T_{f,out}$  after 100 hours of operation varies from 4.4% (flow rate 12 L/min) to 6.2% (flow rate 24 L/min) for a low conductivity grout ( $k_{gt} = 0.9$  W/(mK)), and from 1.6% (flow rate 12 L/min) to 3.3% (flow rate 24 L/min) for a high conductivity grout ( $k_{gt} = 1.6$  W/(mK)).

**Table 7.3.** Values of  $T_{f,in} - T_{f,out}$  after 100 hours of operation, compared with those yielded by the method of Zeng et al. [70].

$k_{gt}$	$\dot{V}$	$T_{f,in} - T_{f,out}$	$(T_{f,in} - T_{f,out})_Z$	% discrepancy
0.9	12	5.329	5.096	4.37
0.9	24	2.982	2.798	6.18
1.6	12	5.704	5.613	1.59
1.6	24	3.268	3.160	3.31

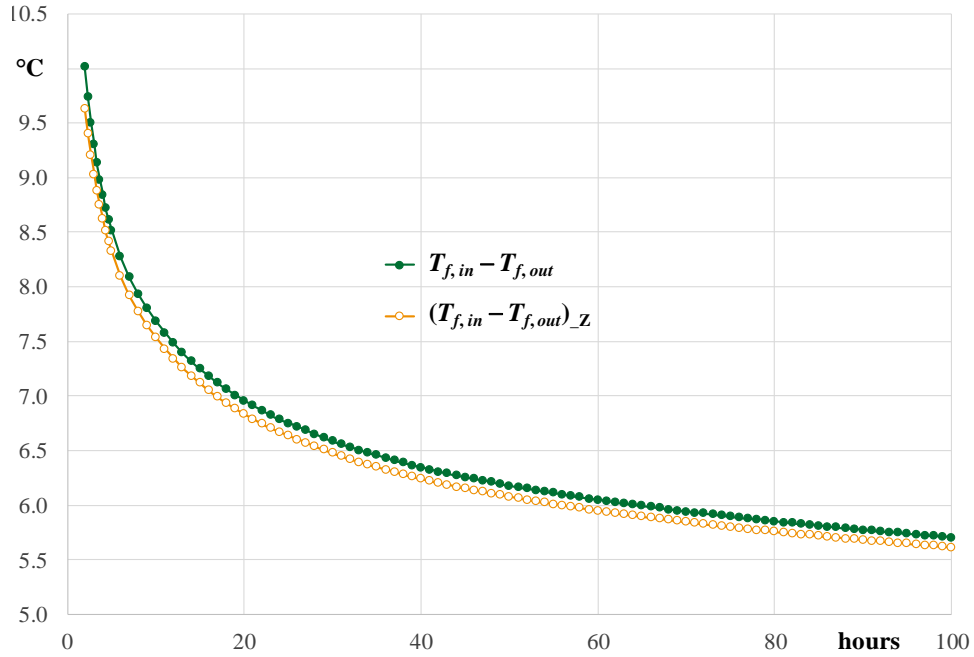


**Figure 7.7.** Plot of  $T_{f,in} - T_{f,out}$  versus time, compared with that yielded by the method of Zeng et al. [70],  $(T_{f,in} - T_{f,out})_Z$ , for  $k_{gt} = 1.6 \text{ W/(mK)}$  and volume flow rate  $12 \text{ L/min}$ .

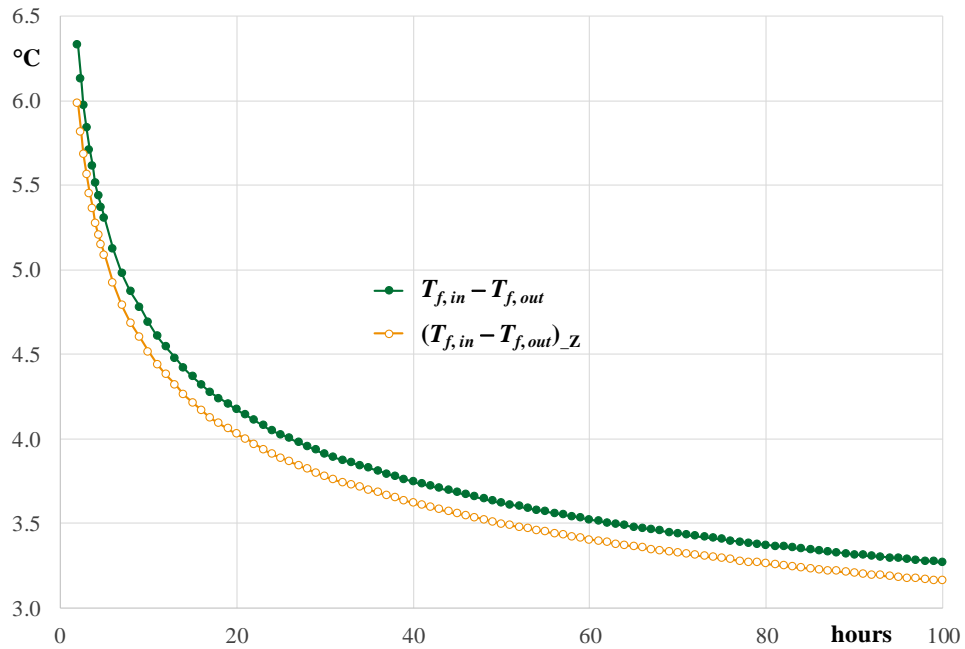


**Figure 7.8.** Plot of  $T_{f,in} - T_{f,out}$  versus time, compared with that yielded by the method of Zeng et al. [70],  $(T_{f,in} - T_{f,out})_Z$ , for  $k_{gt} = 1.6 \text{ W/(mK)}$  and volume flow rate  $24 \text{ L/min}$ .

Plots of the effective thermal resistance  $R_{b,eff}$  and of the 3D thermal resistance  $R_{b,3D}$  versus time, for volume flow rate 12 L/min, are reported in figures 7.9 and 7.10, and are compared with the constant value of  $R_{b,eff}$  yielded by the equation proposed by Zeng. et al. [70], denoted as  $(R_{b,eff})_Z$  in the figures. Figure 7.9 refers to  $k_{gt} = 0.9$  W/(mK), while figure 7.10 refers to  $k_{gt} = 1.6$  W/(mK).

The figures show that both  $R_{b,eff}$  and  $R_{b,3D}$  reach a time independent value in the time interval considered, and have a very small time dependence after the first 20 hours. The difference between  $R_{b,eff}$  and  $R_{b,3D}$  is relevant in both cases. The method of Zeng et al. [70] slightly overestimates  $R_{b,eff}$  for  $k_{gt} = 0.9$  W/(mK), and slightly underestimates it for  $k_{gt} = 1.6$  W/(mK).

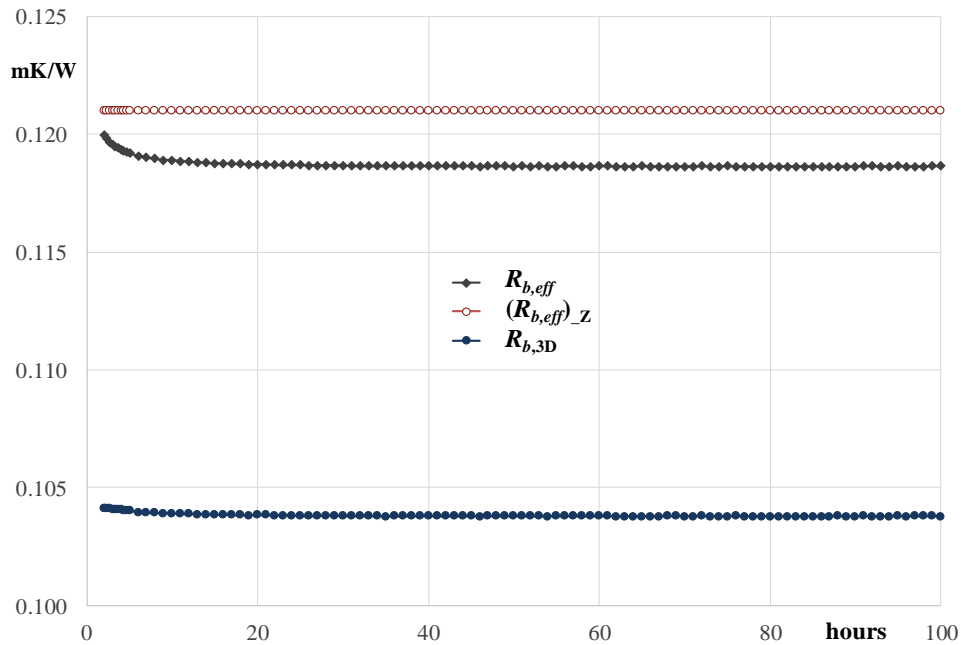


**Figure 7.9.** Plots of  $R_{b,eff}$  and of  $R_{b,3D}$  versus time, compared with the steady-state value  $(R_{b,eff})_Z$  yielded by the method of Zeng et al. [70], for  $k_{gt} = 0.9$  W/(mK) and volume flow rate 12 L/min.

Values of  $(R_{b,eff})_Z$ , of the time averages of  $R_{b,eff}$  and of  $R_{b,3D}$  between 90 and 100 hours of operation, and of  $R_{b,2D}$ , are reported in table 7.4. The values of  $R_{b,2D}$  have been obtained by steady-state simulations of the BHE cross section through scheme 3. The percent discrepancies between  $(R_{b,eff})_Z$  and  $R_{b,eff}$ , between  $R_{b,eff}$  and  $R_{b,3D}$ , and between  $R_{b,3D}$  and  $R_{b,2D}$ , are reported in table 7.5. Tables 7.4 and 7.5 show a fair agreement between the values of  $R_{b,eff}$  obtained by the analytical method of Zeng et al. [70] and those obtained by numerical simulations. The highest discrepancy is 3.54%, and occurs for  $k_{gt} = 0.9$  W/(mK) and flow rate 24 L/min.

The percent difference between  $R_{b,eff}$  and  $R_{b,3D}$  is important in the cases of low volume flow rate: 28.5% for  $k_{gt} = 1.6$  W/(mK) and 14.3% for  $k_{gt} = 0.9$  W/(mK); it is much smaller in the cases of high flow rate: 7.5% for  $k_{gt} = 1.6$  W/(mK) and 3.7% for  $k_{gt} = 0.9$  W/(mK).

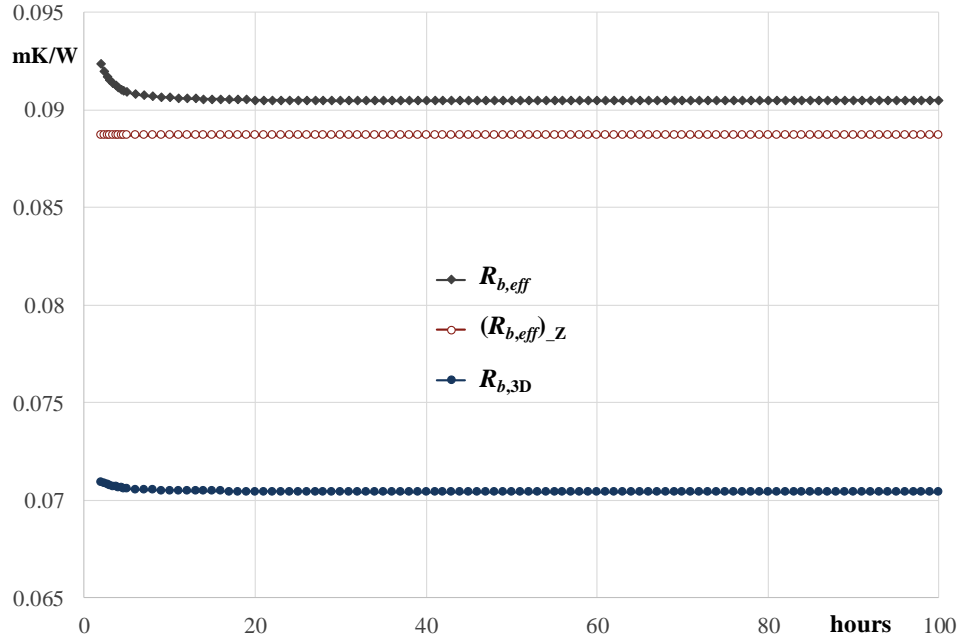


**Figure 7.10.** Plots of  $R_{b,eff}$  and of  $R_{b,3D}$  versus time, compared with the steady-state value  $(R_{b,eff})_Z$  yielded by the method of Zeng et al. [70], for  $k_{gt} = 1.6$  W/(mK) and volume flow rate 12 L/min.

Finally, the percent difference between  $R_{b,3D}$  and  $R_{b,2D}$  is nearly vanishing, and perhaps smaller than the precision that can be obtained by 3D simulations. Therefore, for double U-tube BHEs one can consider  $R_{b,3D}$  and  $R_{b,2D}$  as coincident.

**Table 7.4.** Values of  $(R_{b,eff})_Z$ , asymptotic values of  $R_{b,eff}$  and  $R_{b,3D}$ , and steady values of  $R_{b,2D}$ .

$k_{gt}$	$\dot{V}$	$(R_{b,eff})_Z$	$R_{b,eff}$	$R_{b,3D}$	$R_{b,2D}$
0.9	12	0.1210	0.1186	0.1038	0.1032
0.9	24	0.1101	0.1063	0.1025	0.1020
1.6	12	0.08866	0.09049	0.07042	0.07031
1.6	24	0.07441	0.07438	0.06921	0.06914

**Table 7.5.** Percent difference between  $(R_{b,eff})_Z$  and  $R_{b,eff}$ ,  $R_{b,eff}$  and  $R_{b,3D}$ ,  $R_{b,3D}$  and  $R_{b,2D}$ .

$k_{gt}$	$\dot{V}$	$\frac{(R_{b,eff})_Z - R_{b,eff}}{R_{b,eff}} \times 100$	$\frac{R_{b,eff} - R_{b,3D}}{R_{b,3D}} \times 100$	$\frac{R_{b,3D} - R_{b,2D}}{R_{b,2D}} \times 100$
0.9	12	2.02	14.26	0.58
0.9	24	3.57	3.71	0.49
1.6	12	-2.02	28.50	0.16
1.6	24	0.04	7.47	0.10

In the usual evaluation of TRTs by the infinite line-source method,  $T_{f,ave}$  is employed as mean fluid temperature and  $R_{b,eff}$  is determined. As already evidenced by some authors for single U-tube BHEs (Marcotte and Pasquier [66], Beier [78], Zhang et al. [76,77]) and confirmed here for double U-tube ones,  $R_{b,eff}$  is strongly dependent on the volume flow rate. Therefore, methods allowing to use  $T_{f,m}$  in the evaluation of TRTs (Beier [78], Zhang et al. [77], Beier and Spitler [79], Bauer et al. [55], and Zanchini and Jahanbin [95]) seem interesting. These methods allow an experimental evaluation of  $R_{b,3D}$ , which has a very small dependence on the volume flow rate and can be better employed in mathematical tools for the design and simulation of GCHP systems.

## *Chapter 8*

---

### *Conclusions & prospective*





---

## *Conclusions & prospective*

---

A series of 2D and 3D finite element simulations have been carried out, through the software COMSOL Multiphysics, to analyze the thermal performance and heat transfer processes in double U-tube borehole heat exchangers (BHEs). The developed numerical codes have been validated by comparing results with those of approximate analytical methods. The three main pillars of the present study have been as follows: analysis of the fluid temperature distribution, correlations to determine the mean fluid temperature, and effects of the temperature distribution on the thermal resistance.

First, a 3D numerical model has been developed and employed to determine the temperature distribution along the tubes of a double U-tube BHE, by taking into account the thermal short-circuiting effect between the descending fluid and the ascending fluid. The time evolution of the difference between the mean fluid temperature  $T_m$  and the arithmetic mean of inlet and outlet temperatures  $T_{ave}$  has been determined, in different working conditions. The results obtained have been compared with those yielded by the  $p$ -linear average model, proposed by Marcotte and Pasquier [66] for single U-tube BHEs. The comparison has revealed that the  $p$ -linear average model underestimates the magnitude of  $T_m - T_{ave}$  when applied to a typical double U-tube BHE, so that specific expressions for double U-tube BHEs are valuable.

Then, the 3D simulation model has been modified and employed to provide dimensionless correlations suitable to evaluate the difference  $T_m - T_{ave}$  for double U-tube BHEs. The results have

allowed determining quasi-stationary values and time evolution equations of a dimensionless coefficient  $\varphi$  that yields the mean fluid temperature  $T_m$  of a BHE as a function of inlet and outlet temperatures and volume flow rate. The results of 3D simulations have been validated by comparison with those obtained by applying the analytical method proposed by Zeng et al. [70]. Tables of the dimensionless coefficient  $\varphi$  that allow an immediate evaluation of  $T_m$  in any working condition have been provided, with reference to double U-tube BHEs with typical geometry (length 100 m and 85 mm distance between the axes of opposite tubes). The knowledge of  $T_m$  is important since it allows a more accurate estimation of the borehole thermal resistance by TRTs and a more accurate evaluation of the outlet temperature in dynamic simulations of GCHP systems.

It has been shown that the quasi-stationary values of  $\varphi$  can be considered as dependent only on the thermal conductivity of grout, and independent of the volume flow rate, of the thermal conductivity of ground, of the operative conditions and, for a fixed distance between the axes of opposite tubes (shank spacing), of the BHE diameter. The time evolution of  $\varphi$  during the first two hour depends also on the volume flow rate.

Three thermal resistances per unit length of a BHE have been considered: the 2D thermal resistance of a BHE cross section,  $R_{b,2D}$ ; the *effective* 3D thermal resistance  $R_{b,eff}$ , which refers to the arithmetic mean of inlet and outlet temperatures  $T_{f,ave}$ ; the 3D thermal resistance  $R_{b,3D}$ , which refers to the real mean fluid temperature  $T_{f,m}$ . The effects of the temperature distribution on  $R_{b,2D}$ ,  $R_{b,eff}$  and  $R_{b,3D}$  for double U-tube BHEs have been analyzed by 2D and 3D finite element simulations, with reference to 100 m long BHEs with a typical shank spacing and different values of material properties and volume flow rate. The 2D simulations have been repeated for the highest possible shank spacing, which yields tubes in contact with the ground. The results of 3D simulations have been validated by comparison with those obtained by the analytical method proposed by Zeng et al. [70], and a fair agreement has been found.

The results of 2D simulations have shown that the difference in bulk temperature between pairs of tubes has completely no effect on  $R_{b,2D}$ . On the contrary, the non-uniform temperature along the cross section boundary due to low values of grout and ground thermal conductivities has a non-negligible effect on  $R_{b,2D}$  for high shank spacing. We recommend calculating  $R_{b,2D}$  by a 2D stationary numerical simulation of the BHE cross section, which includes a 2 m thick ground layer with an isothermal external surface, and assuming that the bulk fluid temperature is the same in all tubes.

The results of 3D simulations have shown that the  $R_{b,eff}$  can be much higher than  $R_{b,3D}$ . The percent difference between  $R_{b,eff}$  and  $R_{b,3D}$  can exceed 28%, for high thermal conductivity grout (1.6 W/(mK)) and low volume flow rate (12 L/min). Higher percent differences would occur for longer BHEs with the same grout conductivity and volume flow rate. On the other hand, the difference between  $R_{b,3D}$  and  $R_{b,2D}$  is nearly vanishing, so that these quantities can be considered as coincident.

Since an accurate determination of  $T_m$  is important, both for a precise evaluation of the BHE thermal resistance in TRTs and for the dynamic simulation of GCHPs, the correlations for  $\varphi$  presented here will be extended to other values of the shank spacing and of the BHE length. The

extended correlations will allow a precise and immediate evaluation of  $T_m$  for any double U-tube BHE, both in quasi-stationary and in transient conditions, for any kind of operation (summer operation, winter operation, TRT).

Furthermore, an experimental setup allowing to perform accurate TRTs on four double U-tube BHEs will be installed soon at the Laboratory of Applied Thermal Engineering of the Department of Industrial Engineering of the University of Bologna. This setup will allow us to perform experimental validations of the 3D simulation models developed and to study new methods for the numerical evaluation of TRTs, based on 3D numerical simulations.



## *References*

---

- 
- [1] US Energy Information Administration (EIA), International Energy Statistics: <http://www.eia.gov/cfapps/ipdbproject/IEDIndex3.cfm#> .
- [2] UNDP, World energy assessment 2000 – energy and the challenge of sustainability. New York 2000.
- [3] I. Kralova, J. Sjöblom. Biofuels-renewable energy sources: a review. *Journal of Dispersion Science Technology* 31(3) (2010) 409-425.
- [4] N.Y. Amponsah, M. Troldborg, B. Kington, I. Aalders, R.L. Hough. Greenhouse gas emissions from renewable energy sources: A review of lifecycle considerations. *Renewable and Sustainable Energy Reviews* 39 (2014) 461-475.
- [5] European Commission portal for statistics (Eurostat): <http://ec.europa.eu/eurostat/data/database>.
- [6] Directive 2009/28/EC of the European Parliament and of the Council of 23 April 2009 on the promotion of the use of energy from renewable sources and amending and subsequently repealing Directives 2001/77/EC and 2003/30/EC, L 140/16. *Official Journal of the European Union*, 5 June 2009.
- [7] E. Bullard. *Basic theories (Geothermal energy; Review of research and development)*. UNESCO, Paris 1973.
- [8] [http://www.ucsusa.org/clean\\_energy/our-energy-choices/renewable-energy/how-geothermal-energy-works.html](http://www.ucsusa.org/clean_energy/our-energy-choices/renewable-energy/how-geothermal-energy-works.html).
- [9] S.P. Kavanaugh, K.D. Rafferty. *Ground-Source Heat Pumps – Design of geothermal systems for commercial and institutional buildings*. ASHRAE 1997.
- [10] US Energy Information Administration (EIA), *Geothermal Heat Pumps*: [https://www.eia.gov/energyexplained/index.cfm?page=geothermal\\_heat\\_pumps](https://www.eia.gov/energyexplained/index.cfm?page=geothermal_heat_pumps) .
- [11] M. Li, A.C.K. Lai. Review of analytical models for heat transfer by vertical ground heat exchangers (GHEs): A perspective of time and space scales. *Applied Energy* 151 (2015) 178-191.
- [12] <https://www.epa.gov/rhc/geothermal-heating-and-cooling-technologies> .
- [13] United States Environmental Protection Agency, *Space conditioning: the next frontier – the potential of advanced residential space conditioning technologies for reducing pollution and saving consumers money*. EPA 430-R-93-004, 1993.
- [14] S.J. Self, B.V. Reddy, M.A. Rosen. Geothermal heat pump systems: status review and comparison with other heating options. *Applied Energy* 101 (2013) 341-348.
- [15] J.W. Lund, T.L. Boyd. *Direct utilization of geothermal energy 2015 worldwide review*. *Geothermics* 60 (2016) 66-93.

- 
- [16] ASHRAE Handbook – HVAC Applications (SI), 2011.
- [17] S.P. Kavanaugh. Ground-coupled heat pumps for commercial building. ASHRAE Journal 34(9) (1992) 30-37.
- [18] S.P. Kavanaugh. Simulation and experimental verification of a vertical ground-coupled heat pump system. Ph.D. dissertation, Oklahoma State University, Stillwater, 1985.
- [19] C. Naldi. Development and applications of simulation codes for air-to-water and ground-coupled heat pump systems, Ph.D. Thesis, University of Bologna 2016.
- [20] H.S. Carslaw, J.C. Jaeger. Conduction of Heat in Solids, 2<sup>nd</sup> edition, Oxford University Press 1959.
- [21] L.R. Ingersoll, H.J. Plass. Theory of the ground pipe heat source for heat pump. ASHVE Transactions 54 (1948) 339-348.
- [22] B. Sanner, Erdgekoppelte Wärmepumpen: Geschichte, Systeme, Auslegung, Installation. IZW-Bereich 2/92, FIZ Karlsruhe 1992.
- [23] P. Mogensen. Fluid to duct wall heat transfer in duct system heat storage. In: Proceedings of the International Conference on Surface Heat Storage in Theory and Practice, Stockholm, Sweden, 1983, pp. 652-657.
- [24] E. Zanchini, B. Pulvirenti. An analytical solution for the temperature field around a cylindrical surface subjected to a time dependent heat flux. International Journal of Heat and Mass Transfer 66 (2013) 906-910.
- [25] L.R. Ingersoll, O.J. Zobel, A.C. Ingersoll. Heat conduction with engineering, geological, and other applications. McGraw-Hill, New York 1954.
- [26] P. Eskilson. Thermal analysis of heat extraction boreholes, PhD Thesis, Lund University 1987.
- [27] J. Claesson, P. Eskilson. Conductive heat extraction by a deep borehole. Analytical studies, Technical report, Lund University 1987.
- [28] E. Zanchini, S. Lazzari. Temperature distribution in a field of long Borehole Heat Exchangers (BHEs) subjected to a monthly averaged heat flux. Energy 59 (2013) 570-580.
- [29] H. Zeng, N. Diao, Z. Fang, A finite line-source model for boreholes in geothermal heat exchangers. Heat Transfer - Asian Research 31(7) (2002) 558-567.
- [30] L. Lamarche, B. Beauchamp. A new contribution to the finite line-source model for geothermal boreholes. Energy and Buildings 39 (2007) 188-198.



- 
- [31] T.V. Bandos, A. Montero, E. Fernandez, J.L.G. Santander, J.M. Isidro, J. Perez, P.J. Fernandez de Cordoba, J.F. Urchueguía. Finite line-source model for borehole heat exchangers: effect of vertical temperature variations. *Geothermics* 38 (2009) 263-270.
- [32] M. Fossa. The temperature penalty approach to the design of borehole heat exchangers for heat pump applications. *Energy and Buildings* 43 (2011) 1473-1479.
- [33] M. Fossa. A fast method for evaluating the performance of complex arrangements of borehole heat exchangers. *HVAC&R Research* 17(6) (2011) 948-958.
- [34] E. Zanchini, S. Lazzari. New g-functions for the hourly simulation of double U-tube borehole heat exchanger fields. *Energy* 70 (2014) 444-455.
- [35] C. Yavuzturk, J.D. Spitler, S.J. Rees. A Transient two-dimensional finite volume model for the simulation of vertical U-tube ground heat exchangers. *ASHRAE Transactions* 105(A) (1999) 465-474.
- [36] C. Yavuzturk, J.D. Spitler. Field validation of a short time step model for vertical ground-loop heat exchangers. *ASHRAE Transactions* 107(1) (2001) 617-625.
- [37] J.A. Shonder, J.V. Beck. Determining effective soil formation thermal properties from field data using a parameter estimation technique. *ASHRAE Transactions* 105(1) (1999) 458-466.
- [38] J. Claesson, P. Eskilson, G. Hellström. PC design model for heat extraction boreholes, *Proceedings of the 3rd WS on SAHPGCS Göteborg, CITη 1990:3, 1990*, pp. 99-102.
- [39] G. Hellström, B. Sanner, Software for dimensioning of deep boreholes for heat extraction, *Proceedings of the Conference "Calorstock 94", Espoo - Helsinki, 1994*, pp. 195-202.
- [40] Earth Energy Designer – EED version 4 user manuals, 2016.
- [41] G. Hellström. Duct ground heat storage model: Manual for computer code, Department of Mathematical Physics, Lund Institute of Technology 1989.
- [42] G. Hellström, L. Mazzarella, D. Pahud. Duct ground heat storage model, Lund – DST – TRNSYS 13.1 version January 1996, Department of Mathematical Physics, Lund University 1996.
- [43] M. Fossa, F. Minchio. The effect of borefield geometry and ground thermal load profile on hourly thermal response of geothermal heat pump systems. *Energy* 51 (2013) 323-329.
- [44] H. Yang, P. Cui, Z. Fang. Vertical-borehole ground-coupled heat pumps: A review of models and systems. *Applied Energy* 87 (2010) 16-27.
- [45] C. Yavuzturk, J. Spitler. A short time step response factor model for vertical ground loop heat exchangers. *ASHRAE Transactions* 105(2) (1999) 475-485.

- 
- [46] J.D. Spitler. GLHEPRO – A design tool for commercial building ground loop heat exchangers. In: Proceedings of the 4<sup>th</sup> international conference on heat pumps in cold climates, Aylmer, Québec 2000, p 1-16.
- [47] X. Liu. Enhanced design and energy analysis tool for geothermal water loop heat pump systems. In: Proceedings of 9<sup>th</sup> international energy agency heat pump conference, Zürich 2008.
- [48] M.H. Khan, A. Varanasi, J.D. Spitler, D.E. Fisher, R.D. Delahoussaye. Hybrid ground source heat pump system simulation using visual modeling tool for HVACSIM+. In: 8<sup>th</sup> international IBPSA conference, Eindhoven 2003.
- [49] M.Z. Yu, N.R. Diao, D.C. Su, Z.H. Fang. A pilot project of the closed-loop ground-source heat pump system in China. In: Proceeding of IEA 7<sup>th</sup> heat pump conference, Beijing 2002, pp. 356-64.
- [50] P. Cui, H.X. Yang, Z.H. Fang. The simulation model and design optimization of ground source heat pump systems. HKIE Transactions 14(1) (2007) 1-5.
- [51] N.K. Muraya, D.L. O’Nea, W.M. Heffington. Thermal interference of adjacent legs in a vertical U-tube heat exchanger for a ground-coupled heat pump. ASHRAE Transactions 102(2) (1996) 12-21.
- [52] Z. Li, M. Zheng. Development of a numerical model for the simulation of vertical U-tube ground heat exchangers. Applied Thermal Engineering 29(5-6) (2009) 920-924.
- [53] C.K. Lee, H.N. Lam. Computer simulation of borehole ground heat exchangers for geothermal heat pump systems. Renewable Energy 33 (2008) 1286-1296.
- [54] C.K. Lee. Effects of multiple ground layers on thermal response test analysis and ground-source heat pump simulation. Applied Energy 88(12) (2011) 4405-4410.
- [55] D. Bauer, W. Heidemann, H.-J.G. Diersch. Transient 3D analysis of borehole heat exchanger modeling, Geothermics 40 (2011) 250-260.
- [56] L. Lamarche, S. Kajl, B. Beauchamp. A review of methods to evaluate borehole thermal resistances in geothermal heat-pump systems. Geothermics 39 (2010) 187-200.
- [57] E. Zanchini, A. Jahanbin. Effects of the temperature distribution on the thermal resistance of double u-tube borehole heat exchangers. Geothermics 71 (2018) 46-54.
- [58] Y. Man, H. Yang, Z. Fang. Study on hybrid ground-coupled heat pump systems. Energy and Buildings 40(11) (2008) 2028-2036.
- [59] S.P. Kavanaugh. A design method for hybrid ground-source heat pumps. ASHRAE Transactions 104(2) (1998) 691-698.

- 
- [60] C. Yavuzturk, J.D. Spitler. Comparative study of operating and control strategies for hybrid ground-source heat pump systems using a short time step simulation model. *ASHRAE Transactions* 106 (2000) 192-209.
- [61] P. Cui, H. Yang, J.D. Spitler, Z. Fang. Simulation of hybrid ground-coupled heat pump with domestic hot water heating systems using HVACSIM+. *Energy and Buildings* 40(9) (2008) 1731-1736.
- [62] G. Hellström. Ground heat storage: thermal analysis of duct storage systems. Ph.D. Thesis, Lund University 1991.
- [63] Y. Gu, D.L. O'Neal. Development of an equivalent diameter expression for vertical U-tubes used in ground-coupled heat pumps. *ASHRAE Transactions* 104 (1998) 347-355.
- [64] J.A. Shonder, J.V. Beck. Field test of a new method for determining soil formation thermal conductivity and borehole resistance. *ASHRAE Transactions* 106 (1999) 843-850.
- [65] N.D. Paul. The effect of grout thermal conductivity on vertical geothermal heat exchanger design and performance. MSc Thesis, South Dakota University 1996.
- [66] D. Marcotte, P. Pasquier. On the estimation of thermal resistance in borehole thermal conductivity test. *Renewable Energy* 33 (2008) 2407-2415.
- [67] J. Bennet, J. Claesson, G. Hellström. Multipole method to compute the conductive heat transfer to and between pipes in a composite cylinder. *Notes on Heat Transfer* 3 (1987), Lund Institute of Technology.
- [68] J. Claesson, G. Hellström. Multipole method to calculate borehole thermal resistances in a borehole heat exchanger. *HVAC&R Research* 17(6) (2011) 895-911.
- [69] M.H. Sharqawy, E.M. Mokheimer, H.M. Badr. Effective pipe-to-borehole thermal resistance for vertical ground heat exchangers. *Geothermics* 38 (2009) 271-277.
- [70] H. Zeng, N. Diao, Z. Fang. Heat transfer analysis of boreholes in vertical ground heat exchangers. *International Journal of Heat and Mass Transfer* 46 (2003) 4467-4481.
- [71] P. Conti, D. Testi, W. Grassi. Revised heat transfer modeling of double-U vertical ground-coupled heat exchangers. *Applied Thermal Engineering* 106 (2016) 1257-1267.
- [72] D. Bauer, W. Heidemann, H. Müller-Steinhagen, H.-J. G. Diersch. Thermal resistance and capacity models for borehole heat exchangers. *International Journal of Energy Research* 35 (2011) 312-320.
- [73] S. Gehlin. Thermal Response Test: Method Development and Evaluation, Doctoral Thesis, Luleå University of Technology 2002.

- 
- [74] B. Sanner, G. Hellström, J. Spitler, S. Gehlin. Thermal response test current status and world-wide application. In: Proceedings World Geothermal Congress, Antalya, Turkey, 2005, pp. 1436-1445.
- [75] S. Signorelli, S. Bassetti, D. Pahud, T. Kohl. Numerical evaluation of thermal response tests. *Geothermics* 36 (2007) 141-166.
- [76] L. Zhang, Q. Zhang, G. Huang, Y. Du. A  $p(t)$ -linear average method to estimate the thermal parameters of the borehole heat exchangers for in situ thermal response tests. *Applied Energy* 131 (2014) 211-221.
- [77] L. Zhang, Q. Zhang, J. Acuña, X. Ma. Improved  $p(t)$ -linear average method for ground thermal properties estimation during in-situ thermal response test. *Procedia Engineering* 121 (2015) 726-734.
- [78] R.A. Beier. Vertical temperature profile in ground heat exchanger during in-situ test. *Renewable Energy* 36 (2011) 1578-1587.
- [79] R.A. Beier, J.D. Spitler. Weighted average of inlet and outlet temperatures in borehole heat exchangers. *Applied Energy* 174 (2016) 118-129.
- [80] W.M. Rohsenow, J.P. Hartnett, E.N. Ganic. Handbook of heat transfer fundamentals. 2<sup>nd</sup> edition, McGraw-Hill, New York 1985.
- [81] F. Kreith. Principles of Heat Transfer. 4<sup>th</sup> edition, Harper & Row, New York 1965.
- [82] G.P. Merker. Konvektive Wärmeübertragung. Springer Verlag, Berlin 1987.
- [83] A. Bejan. Convection heat transfer. 4<sup>th</sup> edition, John Wiley and Sons, Hoboken NJ 2013.
- [84] S.W. Churchill. Comprehensive correlating equations for heat, mass and momentum transfer in fully developed flow in smooth tubes. *Industrial & Engineering Chemistry Fundamentals* 16(1) (1977) 109-116.
- [85] M. Li, A.C.K. Lai. Thermodynamic optimization of ground heat exchangers with single U-tube by entropy generation minimization method. *Energy Conversion and Management* 65 (2013) 133-139.
- [86] J.N. Reddy. An introduction to the finite element method. 3<sup>rd</sup> edition, McGraw-Hill, New York 2006.
- [87] V. Wagner, P. Bayer, M. Kübert, P. Blum. Numerical sensitivity of thermal response tests. *Renewable Energy* 41 (2012) 245-253.
- [88] D. Marcotte, P. Pasquier. The effect of borehole inclination on fluid and ground temperature for GLHE systems. *Geothermics* 38 (2009) 392-398.

- [89] Heat Transfer Module user's guide. COMSOL 4.3, 2012.
- [90] <https://www.comsol.com/pipe-flow-module>.
- [91] NIST, Thermophysical properties of fluid systems. <http://webbook.nist.gov/chemistry/fluid/>.
- [92] E. Zanchini, S. Lazzari, A. Priarone. Improving the thermal performance of coaxial borehole heat exchangers. *Energy* 35 (2010) 657-666.
- [93] E. Zanchini, A. Jahanbin. Finite-element analysis of the fluid temperature distribution in double U-tube Borehole Heat Exchangers. *Journal of Physics: Conference Series* 745 (2016) 032003.
- [94] Y. Li, J. Mao, S. Geng, X. Han, H. Zhang. Evaluation of thermal short-circuiting and influence on thermal response test for borehole heat exchangers. *Geothermics* 50 (2014) 136-147.
- [95] E. Zanchini, A. Jahanbin. Correlations to determine the mean fluid temperature of double U-tube borehole heat exchangers with a typical geometry. *Applied Energy* 206 (2017) 1406-1415.
- [96] E. Zanchini, T. Terlizese. Finite element evaluation of thermal response tests performed on U-tube borehole heat exchangers. In: *Proceedings of the COMSOL Conference, Hannover 2008*.

# *Appendix*

---

## *List of publications*



- [1] A. Jahanbin, E. Zanchini - Effects of position and temperature-gradient direction on the performance of a thin plane radiator. *Applied Thermal Engineering* 105 (2016) 467-476.
- [2] E. Zanchini, A. Jahanbin - Finite-element analysis of the fluid temperature distribution in double U-tube Borehole Heat Exchangers. *Journal of Physics: Conference Series* 745 (2016) 032003.
- [3] E. Zanchini, A. Jahanbin - Correlations to determine the mean fluid temperature of double U-tube borehole heat exchangers with a typical geometry. *Applied Energy* 206 (2017) 1406-1415.
- [4] E. Zanchini, A. Jahanbin - Effects of temperature distribution on the thermal resistance of double U-tube borehole heat exchangers. *Geothermics* 71 (2018) 46-54.





